



DESIGN AND OPTIMIZATION OF LATTICE STRUCTURES FOR AEROSPACE APPLICATIONS

Enrico Stragiotti

François-Xavier Irisarri¹, Cédric Julien¹ and Joseph Morlier²

1: ONERA - The French Aerospace Lab
DMAS - Département matériaux et structures
92320 Châtillon, France
{francois-xavier.irisarri, cedric.julien}@onera.fr

2: ICA - Institut Clément Ader
ISAE - SUPAERO
31400 Toulouse, France
joseph.morlier@isae-supraero.fr
January 12, 2024

PhD manuscript

ONERA – ISAE Supaero

Colophon

This document was typeset with the help of KOMA-Script and L^AT_EX using the kaobook class.

ONERA – ISAE Supaero

CONTENTS

Contents	iii
List of Figures	v
List of Tables	vi
List of Abbreviations	vii
1 Literature review	1
1.1 An introduction to structural optimization	1
1.1.1 Optimizers	3
1.2 Ultra-lightweight structures optimization approaches	5
1.2.1 Density-based topology optimization	6
1.2.2 Feature-Mapping topology optimization	10
1.2.3 Truss topology optimization (TTO)	10
1.3 Modular structures and lattice materials	14
1.3.1 Modular structures and lattice materials optimization	17
1.3.2 Multi-scale structures optimization	18
1.3.3 Full-scale structures optimization	20
2 Evaluating discretization approaches for ultralight structure optimization	23
2.1 The formulation of a shared problem: volume minimization with stress constraints	23
2.1.1 Continuous topology optimization minimum volume formulation	23
2.1.2 Truss Topology Optimization (TTO) minimum volume formulation	30
2.2 Comparison between continuous topology optimization and TTO	32
2.2.1 Definition of a test case for the comparison	32
2.2.2 Numerical application	33
2.2.3 Discussion	40
2.3 Conclusion	43
Bibliography	45

LIST OF FIGURES

1.1	Visual representation of (a) size, (b) shape and (c) topology optimization [1].	1
1.2	The domain Ω is discretized using $N_e = N_x N_y$ continuous 4-nodes elements.	7
1.3	Comparison between SIMP model with the Hashin-Strikman upper bound, considering an isotropic material with a Poisson ratio of 1/3 mixed with void. The Hashin-Strikman upper bound is illustrated with microstructures approaching the specified bounds. [51].	8
1.4	Kernel of the 2D convolution operator.	8
1.5	Component (a) and density (b) plot of a short cantilever beam optimized using the component-based topology optimization method Generalized Geometry Projection (GGP) [72].	10
1.6	The TTO algorithm can be divided into 4 steps: (a) specification of the design space, loads, and boundary conditions; (b) discretization of the design space; (c) the ground structure is generated depending on the desired connectivity level; (d) resolution of the optimization problem and plot of the solution [77].	11
1.7	The domain Ω is discretized using a set of straight members connecting a set of nodes. This framework is known as the ground structure.	12
1.8	The optimal structures found by layout optimization tend at Michell-like structures, made up of a very large number of infinitesimal struts [85].	13
1.9	The natural evolution process frequently generates lattice materials and modular structures; (a) The spore-bearing gills of a Hypholoma fasciculare [97] (b) SEM image of a leaf microstructure [98] (c) cellular stucture of the wing of a dragonfly [99] (d) internal structure of a human bone [100].	14
1.10	Density versus yield strength Ashby chart. Exploiting the architecture of the material as a variable to design new metamaterials, empty spaces of the graph can be filled (see dots) [93].	15
1.11	The different length scales present in a moduar structure [107].	15
1.12	Vickers Wellingtons, bombers utilized during World War II, remained operational despite sustaining extensive damage, thanks to their lattice fuselage. When one of the ribs was damaged, the load was redistributed to the others, allowing the structure to remain functional [117].	16
1.13	A stretch-dominated and a bending-dominated Representative Volume Element (RVE). Bending-dominated structure act as a mechanism if the joints cannot withstand moments. The scaling laws are different for the two structure families [93].	17
1.14	Graphical representation of the asymptotic homogenization method used to retrieve the equivalent mechanical properties of a periodic cell [134].	18
1.15	In the study of Zhang <i>et al.</i> [106] the same test case is optimized using a different number of microstructures. Here we show the multi-scale optimized structures using 3 and 19 differnt microstructures.	19

1.16 Three structures with the same volume are optimized for compliance minimization using three different methods: on the left, a classic mono-scale topology optimization algorithm. Middle: the variable linking method is used to enforce the pattern repetition on the structure. On the right an optimized structure with local volume constraints. The algorithms used to optimize the last two structures belong to the family of <i>full-scale</i> methods. [122].	20
2.1 A four-node quadrilateral element. GP is the Gaussian integration point for which the equivalent stress is evaluated.	25
2.2 On the left, plot of the L-shape beam test case, on the right the graphical representations of the two discretizations used, the continuous (above) composed of 600×600 quadrilateral elements, and the truss-like (below) discretized using 33×33 nodes and a fully connected ground structure. The images represent a coarser discretization for visual clarity.	33
2.3 (a-d) Topology of the optimized structures for different values of the material allowable $\sigma_L = 10.00, 2.00, 0.40$, and 0.25 , showing a volume fraction of $V_f = 1.60\%, 4.04\%, 18.03\%$ and 34.71% , respectively. (e-h) Von Mises stress distribution for the optimized structures.	34
2.4 The intermediate resulting structure for $\sigma_L = 0.2$ with $V_f = 48.08\%$ after 7500 optimization iterations.	36
2.6 Linear (a) and logarithmic (b) plot of the volume fraction V_f and the compliance C with respect to the maximum material allowable σ_L for the continuous mesh structures. Areas in red represent the zones outside the domains of applicability of the applied method.	37
2.5 The optimized structure for $\sigma_L = 10.0$ with $V_f = 1.60\%$. Some of the structure's features present not even a fully-dense element in their thickness.	37
2.7 Topology (a) and stress distribution (b) plot for the Truss Topology Optimization (TTO) optimized structure of the L-shape beam test case with varying values of the material allowable σ_L on a 33×33 nodes ground structure. The structure topology is invariant with respect to the value of σ_L	38
2.8 Optimized structure obtained using a fully connected ground structure with 13×13 nodes and 7705 candidates.	38
2.9 Linear (a) and logarithmic (b) plot of the volume fraction V_f and the compliance C with respect to the value of the maximum material allowable σ_L for the TTO optimized structures. Areas in red represent the zones outside the domains of applicability of the truss discretization.	39
2.10 Compliance C versus maximum material allowable σ_L plot for the continuous topology optimization and the TTO algorithms.	40
2.11 Maximum material allowable σ_L versus volume fraction V_f plot for the continuous topology optimization and the TTO algorithms.	41
2.12 Compliance C versus volume fraction V_f plot for the continuous topology optimization and the TTO algorithms.	41
2.13 Computational time t versus volume fraction V_f plot for the continuous topology optimization and the TTO algorithms.	42

LIST OF TABLES

2.1	Material data used for the optimizations. The value of the maximum material allowable σ_L is used as the parameter to generate multiple optimized topologies.	33
2.2	Numerical results of the topology optimization method of the L-shape beam load case with varying material allowable σ_L on a 600×600 elements mesh. Numbers in red highlight the results that have not converged.	36
2.3	Numerical results of the TTO method of the L-shape beam test case with varying values of the material allowable σ_L on a 33×33 nodes ground structure. Numbers in red highlight the results that lie outside the domains of applicability of the optimization method. . .	38

LIST OF ABBREVIATIONS

AD	Alternate Directions
AI	Artificial Intelligence
BESO	Bi-directional ESO
CONLIN	CONvex LINearization
DOFs	Degrees Of Freedom
ESO	Evolutionary Structural Optimization
FEM	Finite Element Method
GA	Genetic Algorithm
GBMMA	Gradient Based MMA
GCMMA	Globally Convergent MMA
GGP	Generalized Geometry Projection
GP	Geometry Projection
HS	Hashin-Shtrikman
KS	Kreisselmeier-Steinhauser
LP	Linear Programming
MIP	Mixed-Integer Programming
MMA	Method of Moving Asymptotes
MMC	Moving Morphable Components
MPVCs	Mathematical Programs with Vanishing Constraints
NAND	Nested Analysis and Design
OC	Optimality Criteria
RVE	Representative Volume Element
SAND	Simultaneous Analysis and Design
SIMP	Solid Isotropic Material with Penalization Method
SLP	Sequential Linear Programming
SLSQP	Sequential Least Square Quadratic Programming
SQP	Sequential Quadratic Programming
TTO	Truss Topology Optimization

LITERATURE REVIEW

This thesis focuses on the numerical optimization in the structural engineering domain. As such, one needs familiarity with existing optimization methods and contemporary engineering practices. The purpose of this chapter is to provide the reader with a non-exhaustive historical overview of structural optimization, particularly in the context of ultralight and modular structures. Additionally, we introduce crucial concepts and terminology that will be employed consistently throughout the document.

1.1 AN INTRODUCTION TO STRUCTURAL OPTIMIZATION	1
1.2 ULTRA-LIGHTWEIGHT STRUCTURES OPTIMIZATION APPROACHES	5
1.3 MODULAR STRUCTURES AND LATTICE MATERIALS	14

1.1 AN INTRODUCTION TO STRUCTURAL OPTIMIZATION

Structural optimization is a multidisciplinary field within engineering that aims to systematically improve the performance—considering factors like mass, stiffness, and dynamic response—by optimizing their shape, material distribution, and overall design. Historically, structural optimization algorithms are categorized into three families: sizing, shape, and topology optimization. Sizing optimization concentrates on determining the optimal distribution of variables, where both the design and state variable domains are known *a priori* and remain constant during optimization. In contrast, shape optimization aims to discover the optimal shape of a predefined domain, treating the domain itself as a design variable allowing for flexibility in shaping the structure. Topology optimization goes further, involving the determination of features like the number, location, and shape of holes, as well as the connectivity of the structural domain. This approach offers a more comprehensive exploration of possibilities in structural design. A visual representation of the three families is provided in Fig. 1.1.

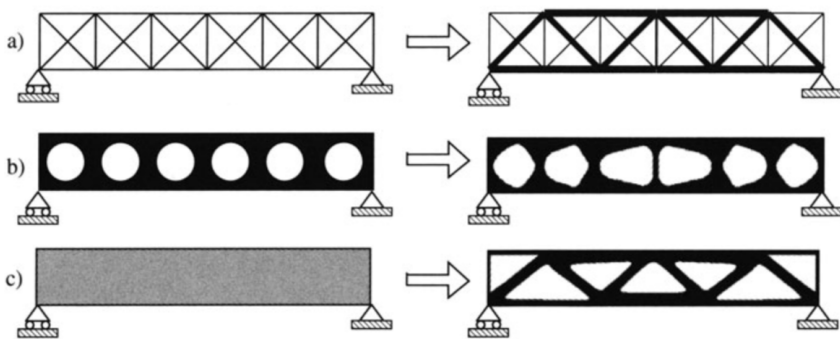


Figure 1.1: Visual representation of (a) size, (b) shape and (c) topology optimization [1].

Structural optimization involves using mathematical algorithms, computational models, and iterative analyses to explore and refine design solutions. For that reason, we introduce now the basic concepts and terminology behind numerical optimization. In numerical optimization, algorithms are employed to minimize or maximize a specific function by adjusting various design variables. The problem may or may not be subject to constraints. Formulating an optimization problem is a crucial step to prevent common conceptual errors, such as confusing constraints with objective functions. An incorrect problem formulation can lead to a failed solution or yield a mathematical optimum that lacks feasibility from an engineering perspective.

The most general formulation of an optimization problem is written as:

$$\begin{aligned} \min_x \quad & f(x) \\ \text{by varying} \quad & x \in [l^-, l^+] \\ \text{s.t.} \quad & g_e(x) = 0 \\ & g_i(x) > 0, \end{aligned} \tag{1.1}$$

where $f(x)$ is the objective function to minimize, x is the vector of design variables bounded between l^- and l^+ , and g_e and g_i represent the equality and inequality constraints, respectively.

OBJECTIVE FUNCTION In numerical optimization, the objective function $f(x)$ represents the scalar that we aim to minimize. Should the goal be to maximize a function, one can achieve this by minimizing the opposite of that function, maintaining adherence to the convention. Common objective functions in structural design include the minimization of volume or structural compliance. The objective function can take the form of an explicit function or result from a highly complex computational procedure. The selection of the objective function is crucial to propose a design that is feasible from an engineering perspective, regardless of the precision of the optimization scheme employed.

Optimization problems are categorized in the literature based on how the objective function is with respect to design variables, whether linear, quadratic, or generally non-linear. It is possible to concurrently optimize multiple objective functions, but this usually results in a family of optimum designs with differing emphases on the various objectives called Pareto front. When possible, it is more straightforward to convert these diverse objectives into constraints [2].

². Martins et al. (2021), 'Engineering Design Optimization'

DESIGN VARIABLES The design variables x are the parameters that the optimizer algorithm can change to minimize the objective function. Design variables could be continuous or discrete if only some distinct values are allowed (for example, only a certain size for a hole in a

structural analysis). The optimization problem formulation allows for the lower and upper boundary for each design variable known in the literature as variable bounds.

CONSTRAINTS The constraints are functions used to restrict the design variables in some way. They serve the purpose of preventing the algorithm from converging to a numerical minimum that is not feasible due to physical and engineering constraints. Similar to the objective function, constraint functions can take on linear, quadratic, or generally non-linear forms, and different algorithms must be applied accordingly.

Constraint functions can be further classified into two types: equality constraints (g_e), which arise when the design variables are restricted to be equal to a fixed quantity, and inequality constraints (g_i), which come into play when the design variables are required to be greater than or equal to a certain quantity.

1.1.1 OPTIMIZERS

The field of numerical optimizers is extensive. For that reason, our focus here will be specifically on algorithms employed in structural optimization. Various algorithm types have been applied to address structural optimization problems, predominantly categorized into three main families: optimality criteria, metaheuristic algorithms, and gradient-based strategies.

Optimality Criteria (OC) refer to mathematical conditions or rules used to assess and guide the modification of a design or structure to achieve the desired performance [3, 4]. In the context of topology optimization, OC are primarily applied in compliance minimization problems, as each element contributes independently to the overall compliance. Bendsøe used OC to seek the stiffest plate i.e. compliance minimization—that can be made of a given amount of material and, together with Kikuchi [5], they used OC to obtain optimal shape design of structural elements based on boundary variations without the use of remeshing. Later, Bendsøe and Sigmund [6, 7] introduced a heuristic update scheme for isotropic materials, while Allaire *et al.* [8] demonstrated the convergence proof for both isotropic and anisotropic materials using the Alternate Directions (AD) approach. In both methods mechanical analysis provides essential information for solving closed-form conditions, allowing iterative updates of variables until convergence is achieved. Recently, OC methods gained interest again thanks to their reduced calculation time [9, 10] thanks to a modified Anderson acceleration strategy [11].

Metaheuristic (or gradient-free) algorithms offer a broader range of options compared to their gradient-based counterparts. While gradient-based algorithms typically conduct local searches, possess

3. Prager et al. (1968), 'Problems of Optimal Structural Design'
4. Prager (1968), 'Optimality Criteria in Structural Design'
5. Bendsøe et al. (1988), 'Generating optimal topologies in structural design using a homogenization method'
6. Bendsøe (1995), 'Optimization of Structural Topology, Shape, and Material'
7. Sigmund (2001), 'A 99 line topology optimization code written in Matlab'
8. Allaire et al. (1996), 'The homogenization method for topology and shape optimization. Single and multiple loads case'
9. Li et al. (2020), 'Accelerated fixed-point formulation of topology optimization'
10. Ferrari et al. (2020), 'A new generation 99 line Matlab code for compliance topology optimization and its extension to 3D'
11. Anderson (1965), 'Iterative Procedures for Nonlinear Integral Equations'

- 12. Conn et al. (2009), 'Introduction to Derivative-Free Optimization'
- 13. Audet et al. (2017), 'Derivative-Free and Blackbox Optimization'
- 14. Simon (2013), 'Evolutionary optimization algorithms'
- 15. Balamurugan et al. (2011), 'A two phase approach based on skeleton convergence and geometric variables for topology optimization using genetic algorithm'
- 16. Sigmund (2011), 'On the usefulness of non-gradient approaches in topology optimization'
- 17. Luh et al. (2009), 'Structural topology optimization using ant colony optimization algorithm'
- 18. Luh et al. (2011), 'A binary particle swarm optimization for continuum structural topology optimization'
- 19. Stolpe (2004), 'Global optimization of minimum weight truss topology problems with stress, displacement, and local buckling constraints using branch-and-bound'
- 20. Mattheck et al. (1990), 'A new method of structural shape optimization based on biological growth'
- 21. Xie et al. (1993), 'A simple evolutionary procedure for structural optimization'
- 22. Manickarajah et al. (1998), 'An evolutionary method for optimization of plate buckling resistance'
- 23. Young et al. (1999), '3D and multiple load case bi-directional evolutionary structural optimization (BESO)'

mathematical justification, and operate deterministically, metaheuristic algorithms are simpler and usually take much less developer time to use, and are perfect candidates for smaller problems. They find very diverse application cases and are useful when the design space is discrete, with multiple objective functions, or highly non-linear with many local minima (multimodal). The works authored by Conn *et al.* [12] and Audet and Hare [13] offer a comprehensive exploration of gradient-free optimization algorithms. Evolutionary algorithms, a prominent category, simulate natural selection by retaining the fittest solutions in each generation while introducing mutations or crossovers for improvement. A review on these optimization methods is given in the following reference [14]. These algorithms, also called Genetic Algorithm (GA), are employed for example by Balamurugan *et al.* [15] for compliance minimization, showcase versatility but face challenges with combinatorial considerations as the number of design variables increases [16]. Particle swarm and ant colony algorithms, inspired by nature, provide alternative strategies with randomness and new search directions. However, these non-gradient methods require regularization schemes for topology optimization, as outlined by Luh, Lin, and others [17, 18]. Targeting the resolution of Mixed-Integer Programming (MIP) problems, branch-and-bound algorithms divide the feasible set of the original problem into subsets through a process known as branching. These subsets are then further segmented to refine the partition of the feasible set. For each subset, lower bounds and optionally upper bounds on the objective function value are determined, a process referred to as bounding. Typically, the lower bounding problems are convex problems that can be efficiently solved to global optimality. Stolpe [19] addresses a volume minimization problem on a truss using a continuous branch-and-bound method, ensuring convergence to a globally optimal solution. The Evolutionary Structural Optimization (ESO) framework, initially a metaheuristic, removes less solicited elements iteratively [20, 21]. These methods offer freedom in optimization and improved convergence to local minima, especially in handling various optimization problems like buckling [22]. The ESO algorithm has been enhanced by the Bi-directional ESO (BESO) framework [23], which allows both removal and addition of elements.

Gradient-based algorithms in optimization leverage local information at a trial point to comprehend the shape of the local objective function in the neighborhood. This insight is crucial for determining the optimal direction to minimize the objective function. Typically, only the Jacobian (first derivative) is utilized, though more advanced algorithms incorporate the Hessian (second derivative). The computational demand for gradient calculation often constitutes the most resource-intensive aspect of the optimization loop. When constraints are present, solving the problem directly on the analytic response surface of the objective function becomes impractical. Consequently,

the approach involves creating local approximations of the problem at the current design point using gradient information. These approximations are designed so that specialized algorithms can efficiently solve them. The categorization of gradient-based algorithms is often based on how this local approximation is constructed.

The most used approximations in structural optimization includes among others Sequential Linear Programming (SLP), Sequential Quadratic Programming (SQP) and Sequential Least Square Quadratic Programming (SLSQP) [24], Method of Moving Asymptotes (MMA) [25] and its amelioration Globally Convergent MMA (GCMMA) [26] and Gradient Based MMA (GBMMA) [27], and CONvex LINearization (CONLIN) [28]. Specialized algorithms for solving the approximated problems are, among others, the primal-dual method and interior-point method.

An interior-point method is a numerical optimization algorithm used to solve constrained optimization problems. The key idea behind interior-point methods is to transform the constrained optimization problem into a sequence of unconstrained problems, allowing for efficient iterative solutions. The method introduces a barrier function that penalizes points outside the feasible region, effectively creating a "barrier" against leaving that region. This barrier function is incorporated into the objective function, and as the optimization progresses, it guides the search towards the interior of the feasible region. The term "interior-point" originated from early methods that relied on interior penalty techniques, assuming the initial point was feasible. Nevertheless, contemporary interior-point methods as the open source IPOPT [29] are more versatile and can start from infeasible points. Rojas Labanda and Stolpe conducted a benchmark of various optimization algorithms and structural optimization formulations using a compliance minimization problem. Their findings highlight the efficacy of employing interior-point algorithms such as IPOPT in topology optimization problems [30].

1.2 ULTRA-LIGHTWEIGHT STRUCTURES OPTIMIZATION APPROACHES

Two of the most frequently employed formulations for structural optimization are the minimization of volume while adhering to stress constraints and the minimization of compliance under volume constraints. Historically, the volume minimization formulation has been used in the first works of structural optimization of truss structures [31–33]. The problem was initially formulated in terms of member forces, ignoring the kinematic compatibility to obtain a Linear Programming (LP) problem. The formulation was modeled using the Simultaneous Analysis and Design (SAND) approach, in which the equations of nodal equilibrium are treated as equality constraints, and

24. Kraft (1988), 'A software package for sequential quadratic programming'

25. Svanberg (1987), 'The method of moving asymptotes—a new method for structural optimization'

26. Svanberg (2002), 'A Class of Globally Convergent Optimization Methods Based on Conservative Convex Separable Approximations'

27. Bruyneel et al. (2002), 'A family of MMA approximations for structural optimization'

28. Fleury et al. (1986), 'Structural optimization'

29. Wächter et al. (2006), 'On the implementation of an interior-point filter line-search algorithm for large-scale nonlinear programming'

30. Rojas Labanda et al. (2015), 'Benchmarking optimization solvers for structural topology optimization'

31. Dorn et al. (1964), 'Automatic design of optimal structures'

32. Chan (1964), 'Optimum structural design and linear programming'

33. Hemp (1973), 'Optimum Structures'

34. Sankaranarayanan et al. (1994), 'Truss topology optimization with simultaneous analysis and design'

5. Bendsøe et al. (1988), 'Generating optimal topologies in structural design using a homogenization method'

35. Bendsøe (1989), 'Optimal shape design as a material distribution problem'

36. Sigmund (1994), 'Materials with prescribed constitutive parameters'

37. Zhang et al. (2006), 'Scale-related topology optimization of cellular materials and structures'

38. Collet et al. (2018), 'Topology optimization for microstructural design under stress constraints'

39. Borrvall et al. (2003), 'Topology optimization of fluids in Stokes flow'

40. Bruyneel et al. (2005), 'Note on topology optimization of continuum structures including self-weight'

41. Sigmund (2009), 'Manufacturing tolerant topology optimization'

42. Brackett et al. (2011), 'Topology Optimization for Additive Manufacturing'

43. Sigmund (1997), 'On the Design of Compliant Mechanisms Using Topology Optimization*

44. Bruns et al. (2001), 'Topology optimization of non-linear elastic structures and compliant mechanisms'

45. Wang et al. (2020), 'Space-time topology optimization for additive manufacturing'

46. Allaire et al. (2002), 'A level-set method for shape optimization'

47. Wang et al. (2003), 'A level set method for structural topology optimization'

48. Allaire et al. (2004), 'Structural optimization using sensitivity analysis and a level-set method'

1: This proposition holds when referring to the end of the 1980s when computational power was scarce compared to what we have today.

2. Martins et al. (2021), 'Engineering Design Optimization'

49. Tortorelli et al. (1994), 'Design sensitivity analysis'

1. Bendsøe et al. (2004), 'Topology Optimization'

where both nodal displacements and the cross-sectional areas of truss members serve as design variables [34]. These methods are known in the literature as layout optimization or Truss Topology Optimization (TTO).

However, to attain greater design freedom, the structure optimization field later transitioned from truss structures to continuous discretization (also called density methods). While truss structures offered simplicity and ease of analysis, they imposed limitations on design due to their discrete member configurations and their inability to transmit moments, handle torsional effects, and represent complex structural elements such as plates or volumes. The continuum mesh offered instead more versatility [5, 35], and has since been used for multiple different applications, e.g. the design of optimized repetitive metamaterials [36–38], fluids optimization [39], modelization of self-weight of the structure [40], the simulation of advanced manufacturing constraints [41, 42], the design of compliant mechanism [43, 44], or the optimization for additive manufacturing [45]. Other than the density methods, other ways to deal with topology optimization exist, like level-set methods [46–48]. The SAND approach is, however, incompatible with continuum meshes due to its excessive number of variables¹. Given this limitation, a new approach was required to better handle the complexity of continuum meshes.

In density-based Nested Analysis and Design (NAND) approach, the nodal displacement (state) variables are eliminated from the optimization problem through a process where the structural equilibrium equation is solved every iteration instead of being used as a constraint of the optimization. This results in an independent nested phase where the state equation of structural equilibrium is solved separately from the optimization algorithm. This creates a dense coupling between displacement and material density variables, necessitating a computationally expensive sensitivity analysis within the nested algorithm, typically employing the adjoint method (more information about the adjoint method on the following resources [2, 49]). Nevertheless, if the problem is reformulated as a compliance minimization with volume constraints, the problem is self-adjoint and the adjoint algorithm is no longer necessary to evaluate the gradient sensitivities [1], and this reduces considerably the computational times.

Both the TTO methods based on the ground structure and the density-based topology optimization approaches are good candidate for the optimization of ultra-light structures. We review here their main characteristics and numerical properties, starting from density-based approaches.

1.2.1 DENSITY-BASED TOPOLOGY OPTIMIZATION

Let $\Omega \in \mathbb{R}^2$ be a rectangular domain in of dimensions X and Y , containing respectively N_x and N_y linear 4-nodes elements, for a total

of $N_e = N_x N_y$ elements and M nodes (see Fig. 1.2). The objective of the optimization is the minimization of the compliance C of the structure, equivalent to finding the structure with the least possible nodal displacement with respect to a defined set of boundary conditions.

COMPLIANCE MINIMIZATION FORMULATION The Problem \mathbb{T}_0 is stated in terms of the design variables ρ as follows:

$$\begin{aligned} \min_{\rho} \quad & C = \sum_i \mathbf{u}_{e,i}^T \mathbf{K}_{e,i} \mathbf{u}_{e,i} = \mathbf{f}^T \mathbf{u} \quad \forall i \in [0, \dots, N_e] \\ \text{s.t.} \quad & \frac{\sum_i (\bar{\rho}_i v_i) / V_0}{V_p} - 1 \leq 0 \quad \forall i \in [0, \dots, N_e] \quad (\mathbb{T}_0) \\ & \mathbf{K}\mathbf{u} = \mathbf{f} \\ & 0 \leq \rho_i \leq 1. \quad \forall i \in [0, \dots, N_e] \end{aligned}$$

The design variables ρ are defined for every element of the structure as $\rho = [\rho_1, \rho_2, \dots, \rho_{N_e}]^T$, with $\rho_i \in [0, 1]$, $\forall i \in [0, \dots, N_e]$. The physical densities $\bar{\rho}$ are related to the design variable ρ through density filtering and threshold projection [50], as explained later in the document. V_p is the prescribed volume fraction that acts as the constraint of the minimization problem, while v_i represents the area of the i -th element and V_0 is the total area of the domain Ω . $\mathbf{K}\mathbf{u} = \mathbf{f}$ is the state equation of the problem and defines the elastic response of the structure to an external nodal load $\mathbf{f} = [f_1, f_2, \dots, f_{2M}]^T$. The global stiffness matrix \mathbf{K} is assembled from the element stiffness matrix $\mathbf{K}_{e,i}$ and $\mathbf{K}_{e,i} = E_i \mathbf{K}_{e,0}$ where $\mathbf{K}_{e,0}$ represents the element stiffness matrix relative to the chosen type of element (linear or quadratic) and $E_i(\bar{\rho}_i)$ the Young's modulus of the i -th element.

The material scheme used to interpolate between void and full material is the well-known Solid Isotropic Material with Penalization Method (SIMP) [35, 51] approach. It is governed by the equation:

$$E_i(\bar{\rho}_i) = E_{\min} + \bar{\rho}_i^p (E_0 - E_{\min}), \quad (1.2)$$

where the parameter p penalizes the intermediate densities and pushes the result to a black-and-white result. E_0 is the Young's modulus of the dense material and E_{\min} is a small value used to avoid the global stiffness matrix \mathbf{K} from being singular when $\bar{\rho}_i = 0$.

The SIMP exponent p is constrained to be greater than or equal to 1. From a physical perspective, the extreme case of $p = 1$ makes sense only in a two-dimensional optimization context, where it becomes equivalent to optimizing membrane thickness. When $p > 1$, the interpolation results in an equivalent homogenized stiffness tensor for intermediate densities, determined by the material-to-void ratio ρ . This mirrors microstructures conforming to the Hashin-Shtrikman

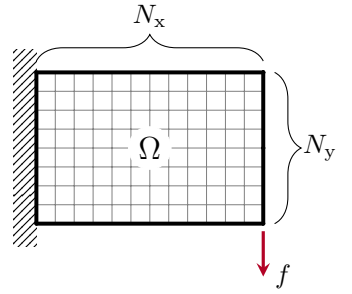


Figure 1.2: The domain Ω is discretized using $N_e = N_x N_y$ continuous 4-nodes elements.

50. Wang et al. (2011), 'On projection methods, convergence and robust formulations in topology optimization'

35. Bendsøe (1989), 'Optimal shape design as a material distribution problem'

51. Bendsøe et al. (1999), 'Material interpolation schemes in topology optimization'

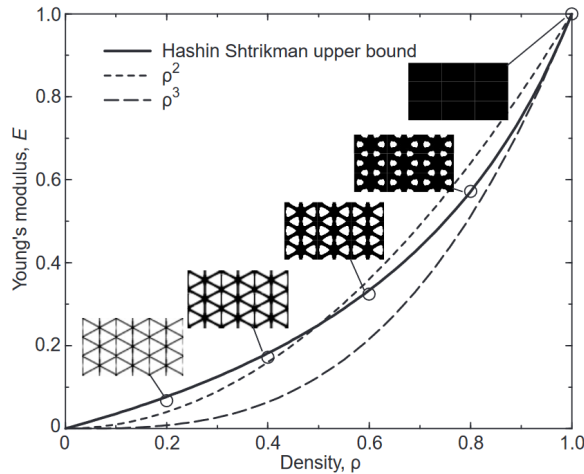


Figure 1.3: Comparison between SIMP model with the Hashin-Shtrikman upper bound, considering an isotropic material with a Poisson ratio of 1/3 mixed with void. The Hashin-Shtrikman upper bound is illustrated with microstructures approaching the specified bounds. [51].

52. Hashin et al. (1963), 'A variational approach to the theory of the elastic behaviour of multiphase materials'

51. Bendsøe et al. (1999), 'Material interpolation schemes in topology optimization'

(HS) conditions, which estimate the theoretical lower and upper bounds for the elastic modulus of a homogeneous, isotropic mixture of different materials based on their elastic modulus and volume fractions [52]. If the exponent p exceeds 3, Bendsøe [51] mathematically proves that the equivalent homogenized stiffness tensor adheres to the upper bound of the HS conditions (refer to Fig. 1.2). It is important to note that in the single-scale topology optimization context, deviating from the HS bounds for intermediate densities is allowed. The objective is to drive the density distribution towards a black-and-white result with minimal intermediate densities, without concerning ourselves with whether the equivalent homogenized stiffness tensor can be replicated by a real microstructure.

53. Díaz et al. (1995), 'Checkerboard patterns in layout optimization'

43. Sigmund (1997), 'On the Design of Compliant Mechanisms Using Topology Optimization'

54. Sigmund (1994), 'Design of Material Structures using Topology Optimization'

55. Sigmund (2007), 'Morphology-based black and white filters for topology optimization'

SPATIAL FILTERING AND PROJECTION Multiple approaches have been developed to solve the problems linked to mesh discretization, such as mesh dependence or the checkerboard problem [53]. Filtering the sensitivity information of the optimization problem proved to be an effective approach to guarantee independence from mesh resolution [43, 54]. Another possibility is instead to directly filter the density field ρ using the 2D convolution operator [55]. The weight function w (or kernel) of the convolution is defined as:

$$w(d_j) = R - d_j, \quad j \in \mathbb{N}_{i,R} \quad (1.3)$$

where $\mathbb{N}_{i,R}$ represent the set of elements lying within a circle of radius R centered on the i -th element and d_j is the distance of the j -th element to the center of the filter (see Fig. 1.4).

The filtered values of the design variable are calculated as:

$$\tilde{\rho}_i = \frac{\sum_{j \in \mathbb{N}_{i,R}} w(d_j) v_j \rho_j}{\sum_{j \in \mathbb{N}_{i,R}} w(d_j) v_j}. \quad (1.4)$$

As the filtering phase produces a large number of gray elements,

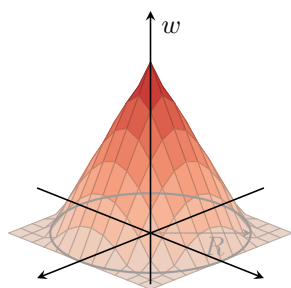


Figure 1.4: Kernel of the 2D convolution operator.

a smooth projection technique based on the *tanh* function is implemented [50]:

$$\bar{\bar{\rho}}_j = \frac{\tanh(\beta\eta) + \tanh(\beta(\bar{\rho}_j - \eta))}{\tanh(\beta\eta) + \tanh(\beta(1 - \eta))}, \quad (1.5)$$

where β is a parameter that defines the slope of this approximation function: the larger the value of β , the less intermediate elements are present in the structure topology. η is the threshold value of the projection.

In the domain of structural topology optimization, it is a widely adopted strategy to employ continuation methods. Introduced in the 90s [56, 57], they are used to converge towards more optimized structures. These methods solve a sequence of problems with increasing values of the SIMP material penalization parameter p . Many researchers such as Bendsøe and Sigmund [1] and Rozvany [58] consider, among others, continuation methods as a standard procedure in topology optimization. However, this approach comes at the expense of an increased number of iterations and, consequently, augmented computational time [59]. In an effort to mitigate this drawback, Rojas Labanda and Stolpe [60] have derived an automatic penalization scheme. This innovative scheme aims to reduce both the objective function value and the number of iterations, providing an improvement over the classical formulation with a fixed penalty parameter. While the literature is predominantly focused on the continuation scheme on the SIMP material penalization parameter p , it is worth noting that similar techniques could be employed for other optimization parameters e.g. the filter radius R or the projection parameter β .

While density-based topology optimization offers tremendous benefits in terms of weight reduction and structural efficiency, it is important to acknowledge the challenges associated with manufacturing such designs. The intricate and complex geometries generated through the optimization can pose difficulties in the fabrication process, often requiring advanced manufacturing techniques, specialized equipment, and specific constraints in the optimization [42, 61, 62]. Additionally, the computational time required for generating such optimized designs, particularly for low volume fractions typical of the aerospace domain, can be significant [63], impacting the overall efficiency of the design process. This remains true even with the use of adaptive meshes [64, 65]. Even if the freedom of the design space offered by continuum meshes is high, it is known that at very low volume fractions (e.g. ultralight structures), and, especially if buckling constraints and manufacturing considerations (e.g. minimum length scale), are taken into account, the optimal topology resemble to a truss-like structure [66]. As a result, a distinct branch of continuous topology optimization has emerged specifically tailored for optimizing truss-like structures, known as feature-Mapping topology optimization (also

50. Wang et al. (2011), 'On projection methods, convergence and robust formulations in topology optimization'

56. Allaire et al. (1993), 'A Numerical Algorithm for Topology and Shape Optimization'

57. Allaire et al. (1993), 'Topology Optimization and Optimal Shape Design Using Homogenization'

58. Rozvany (2009), 'A critical review of established methods of structural topology optimization'

59. Petersson et al. (1998), 'Slope constrained topology optimization'

60. Rojas-Labanda et al. (2015), 'Automatic penalty continuation in structural topology optimization'

42. Brackett et al. (2011), 'Topology Optimization for Additive Manufacturing'

61. Zhou et al. (2002), 'Progress in Topology Optimization with Manufacturing Constraints'

62. Liu et al. (2018), 'Current and future trends in topology optimization for additive manufacturing'

63. Aage et al. (2017), 'Giga-voxel computational morphogenesis for structural design'

64. Salazar de Troya et al. (2018), 'Adaptive mesh refinement in stress-constrained topology optimization'

65. Zhang et al. (2020), 'Adaptive mesh refinement for topology optimization with discrete geometric components'

66. Sigmund et al. (2016), 'On the (non-)optimality of Michell structures'

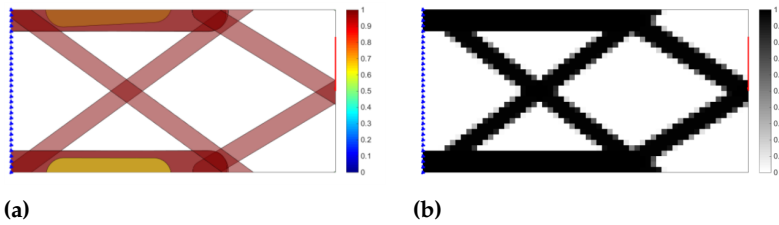


Figure 1.5: Component (a) and density (b) plot of a short cantilever beam optimized using the component-based topology optimization method GGP [72].

called topology optimization with explicitly defined components).

1.2.2 FEATURE-MAPPING TOPOLOGY OPTIMIZATION

Topology optimization methods using explicitly defined components have been developed to permit an easier interpretation of the solution, finding the optimal shape, size, and connectivity of components projected over a finite element continuum mesh (see Fig. 1.5). Two main feature-mapping methods applied to topology optimization have been developed [67], the Moving Morphable Components (MMC) approach [68, 69] and the Geometry Projection (GP) approach [70, 71], later combined in a unique methodology called Generalized Geometry Projection (GGP) [72]. Recently, the GP approach has been used to optimize light lattice structures, proving the effectiveness of the method to provide easy-to-interpret solutions [73]. Nevertheless, the optimization is still based on a density field projected on a continuum mesh, that needs to be refined to correctly discretize low volume fraction structures. Additionally, truss structure design naturally depends on constraints on maximum allowable stress and buckling which are all known for being difficult to implement on topology optimization using the Nested Analysis and Design (NAND) formulation. This is principally due to the singular optima (or topologies) phenomenon [74, 75] and the pseudo-modes of buckling of low-density elements [76].

- 67. Wein et al. (2020), 'A review on feature-mapping methods for structural optimization'
- 68. Guo et al. (2014), 'Doing Topology Optimization Explicitly and Geometrically—A New Moving Morphable Components Based Framework'
- 69. Zhang et al. (2017), 'A new three-dimensional topology optimization method based on moving morphable components (MMCs)'
- 70. Norato et al. (2015), 'A geometry projection method for continuum-based topology optimization with discrete elements'
- 71. Zhang et al. (2016), 'A geometry projection method for the topology optimization of plate structures'
- 72. Coniglio et al. (2020), 'Generalized Geometry Projection'
- 73. Kazemi et al. (2020), 'Multi-material topology optimization of lattice structures using geometry projection'
- 74. Cheng et al. (1997), ' ε -relaxed approach in structural topology optimization'
- 75. Rozvany (2001), 'On design-dependent constraints and singular topologies'
- 76. Gao et al. (2015), 'Topology optimization of continuum structures under buckling constraints'
- 31. Dorn et al. (1964), 'Automatic design of optimal structures'
- 33. Hemp (1973), 'Optimum Structures'

1.2.3 TRUSS TOPOLOGY OPTIMIZATION (TTO)

Truss Topology Optimization (TTO) focuses on optimizing the topology of the truss structure itself, instead of operating on a continuous mesh. It involves selecting the cross-sectional areas and the connectivity of a discrete and dense mesh called ground structure, aiming to minimize weight while satisfying structural constraints. The process is graphically presented in Fig. 1.6.

In the early works, the TTO problem was formulated in terms of member forces [31, 33] with plastic material modelization, ignoring the kinematic compatibility to obtain a LP problem. Formulated using the SAND approach, the equations of structural mechanics of the problem are imposed as constraints of the optimization and, contrary to NAND approaches, are not explicitly solved. Formulated that way, it is trivial to add maximum stress constraints compared to an equivalent NAND formulation. However, the SAND formulation with plastic

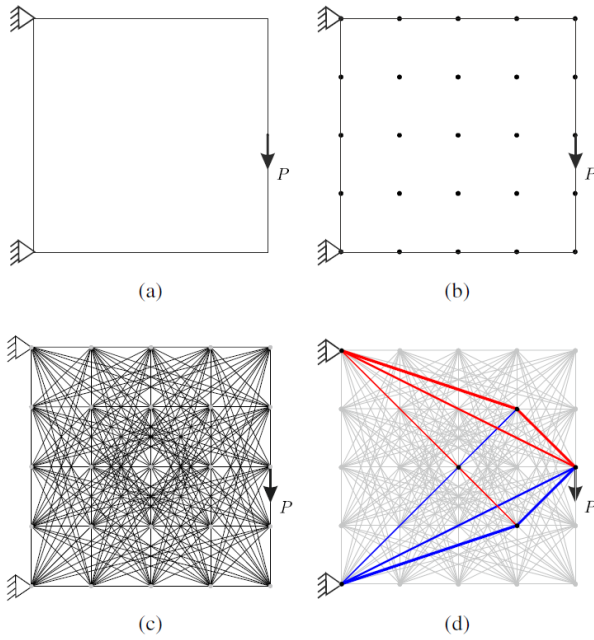


Figure 1.6: The TTO algorithm can be divided into 4 steps: (a) specification of the design space, loads, and boundary conditions; (b) discretization of the design space; (c) the ground structure is generated depending on the desired connectivity level; (d) resolution of the optimization problem and plot of the solution [77].

material modelization only correctly predicts the mechanical behavior of statically determinate structures or mechanisms [78, 79]. Moreover, adding local buckling constraints to the optimization formulation is fundamental, as ultralight truss structures are often dominated by this mode of failure [66]. Multiple works in the field of truss structure optimization have focused on addressing these two crucial challenges [80–82].

CLASSICAL MICHELL STRUCTURES The characteristics of these class of truss structures are described by some simple criteria that date to the end of the 19th and the beginning of the 20th century. When a structure is statically determinate — i.e. the structure is not a mechanism, and it is not over-constrained by the supports — the Maxwell theorem [83] states that:

$$\sum_{\forall i|q_i>0} \ell_i q_i + \sum_{\forall i|q_i<0} \ell_i q_i = \text{const.} \quad (1.6)$$

where ℓ_i and q_i represent the length and the axial force of the i -th member, respectively. The constant value at the right of Equation 1.6 depends on the nature of the boundary conditions and the material used. The Maxwell theorem dictates that any increment in compression forces must be counterbalanced by an equivalent increase in tension forces when the structure remains topologically unchanged. So for statically determinate structures the structure layout is not influenced by the ratio between σ_c and σ_t , Young's modulus E of the material, nor the force magnitude.

Starting from Maxwell's findings, Michell theorized two further criteria for optimal truss structures [84] valid when the maximum allowable stress is equal in tension and compression ($\sigma_t = \sigma_c$) and

- 78. Kirsch (1989), 'Optimal topologies of truss structures'
- 79. Rozvany et al. (1995), 'Layout Optimization of Structures'
- 66. Sigmund et al. (2016), 'On the (non-)optimality of Michell structures'
- 80. Kirsch (1980), 'Optimal design of trusses by approximate compatibility'
- 81. Cheng (1995), 'Some aspects of truss topology optimization'
- 82. Achtziger (1999), 'Local stability of trusses in the context of topology optimization Part I'
- 83. Maxwell (1870), 'I.—On Reciprocal Figures, Frames, and Diagrams of Forces'
- 84. Michell (1904), 'The limits of economy of material in frame-structures'

[33.](#) Hemp (1973), 'Optimum Structures'

when the supports of the structure are statically determinate. The first one states that all the members of an optimal structure should present internal stress equal in magnitude to the maximum allowable value of the material – i.e. the structure is *fully stressed*. The second criterion asserts that the strain of all the members of the structure should be equal and there should be no other point having a strain higher than this value. As formulated, these two criteria are known as the Michell criteria. The second criterion was later generalized by Hemp [33] as:

$$-\frac{1}{\sigma_c} \leq \varepsilon \leq \frac{1}{\sigma_t}. \quad (1.7)$$

Compared to the second Michell criterion, Equation 1.7 permits to correct identification of the minimum volume structure even when different strength values for compression and tension and different support types are taken. These criteria are known as the Michell-Hemp criteria.

[31.](#) Dorn et al. (1964), 'Automatic design of optimal structures'

[32.](#) Chan (1964), 'Optimum structural design and linear programming'

[33.](#) Hemp (1973), 'Optimum Structures'

PLASTIC MATERIAL FORMULATION The rigid-plastic formulation characterizes the material as entirely rigid up to the point of reaching the yield stress, denoted as σ_y , and subsequently assumes a constant stress level of σ_y once that threshold is exceeded. This formulation is a clear consequence of the application of the Michell-Hemp criteria and has thus been used in the very first work of TTO [31–33].

THE GROUND STRUCTURE APPROACH The ground structure is a framework composed of various structural members that connect specified points or nodes in two- or three-dimensional space (see Fig. 1.7). These members can take the form of beams, columns, wires, or bars elements, depending on the specific structural requirements. In this thesis, we will deal with trusses, and so the chosen element is the bar. Since the nodes within the ground structure are considered pin-joints, all straight members exclusively face either tension or compression loads.

Depending on how the connectivity of the grid of nodes is, we can experience very different ground structures. In a fully connected ground structure, every node within the system is linked to every other node, resulting in a dense and redundant structural configuration. The number of bars N_{el} of a fully connected ground structure can be determined using the following formula:

$$N_{el} = \frac{M \cdot (M - 1)}{2}, \quad (1.8)$$

where M represents the number of nodes of the structure.

In classic works, the ground structure is used as the start of the optimization, where the optimized structure is obtained as a subset of

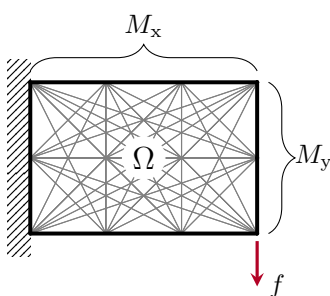


Figure 1.7: The domain Ω is discretized using a set of straight members connecting a set of nodes. This framework is known as the ground structure.

the initial ground structure, but multiple alternative approaches have been proposed since then, e.g. starting from a very coarse ground structure that is enriched during the analysis [85], or giving the nodes of a coarse ground structure the possibility to move, during [86–88], or after the optimization, simultaneously reducing the number of active members of the solution [89, 90]. Recently, a hybrid method based on the projection of explicitly defined components on a discrete ground structure has been proposed, easing the interpretation of the stiffening pattern of the optimized truss [91].

OPTIMIZATION FORMULATION The volume minimization formulation with maximum stress constraints is stated in terms of members' cross-sectional areas α and member forces q as follows:

$$\begin{aligned} \min_{\alpha, q} \quad & V = \ell^T \alpha \quad (\text{Volume minimization}) \\ \text{s.t.} \quad & \mathbf{B}q = f \quad (g_{\text{eq}}) \\ & -\sigma_c \alpha \leq q \leq \sigma_t \alpha \quad (g_{\text{st,c}}, g_{\text{st,t}}) \\ & \alpha \geq 0, \end{aligned} \quad (\mathbb{P}_0)$$

where \mathbf{B} is a $N_{\text{dof}} \times N_{\text{el}}$ matrix containing the direction cosines of the i -th member with respect to the i -th degree of freedom to calculate the nodal force equilibrium constraints g_{eq} , and where N_{dof} is the number of Degrees Of Freedom (DOFs), equal to $2M$ or $3M$ for a two- or a three-dimensional load case, respectively. $q = [q_1, q_2, \dots, q_{N_{\text{el}}}]^T$ is the vector containing the internal member forces, with a positive sign when in tension, caused by the external load $f = [f_1, f_2, \dots, f_{N_{\text{dof}}}]^T$. The state variable $\alpha = [\alpha_1, \alpha_2, \dots, \alpha_{N_{\text{el}}}]^T$ represents the cross-sectional area of the N_{el} members of the structure. σ_c and σ_t are the compressive and tensile maximum allowable stresses of the material, respectively, used in the stress constraints $g_{\text{st,c}}$ and $g_{\text{st,t}}$. This formulation takes into account only the linear behavior of the structure and is equivalent to the original and well-studied member force formulation [1, 31].

The resolution of Problem \mathbb{P}_0 frequently produces complex structures made up of a multitude of small members that tend to the shapes of Michell structures (see Fig 1.8) [84]. While it is known that these structures are nearly optimal, one would want to limit the complexity of the resulting structure. Substituting ℓ with $\tilde{\ell} = [\ell_1 + s, \ell_2 + s, \dots, \ell_{N_{\text{el}}} + s]^T$ in the objective function of \mathbb{P}_0 , one would penalize the appearance of small members [92]. $\tilde{\ell}$ is called augmented member length and s the joint cost. This approach mimics the mesh-independency regularization filter of topology optimization, avoiding the inevitable apparition of structures with tiny features when a fine mesh is adopted.

- 85. Gilbert et al. (2003), 'Layout optimization of large-scale pin-jointed frames'
- 86. Pedersen (1973), 'Optimal Joint Positions for Space Trusses'
- 87. Achtziger (2007), 'On simultaneous optimization of truss geometry and topology'
- 88. Descamps et al. (2013), 'A lower-bound formulation for the geometry and topology optimization of truss structures under multiple loading'
- 89. He et al. (2015), 'Rationalization of trusses generated via layout optimization'
- 90. Lu et al. (2023), 'Reducing the number of different members in truss layout optimization'
- 91. Savine et al. (2021), 'A component-based method for the optimization of stiffener layout on large cylindrical rib-stiffened shell structures'

- 1. Bendsøe et al. (2004), 'Topology Optimization'
- 31. Dorn et al. (1964), 'Automatic design of optimal structures'
- 84. Michell (1904), 'The limits of economy of material in frame-structures'
- 92. Parkes (1975), 'Joints in optimum frameworks'

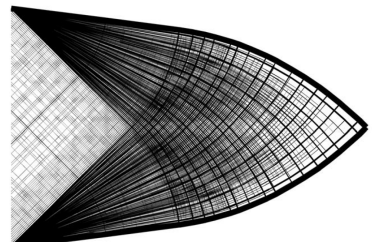


Figure 1.8: The optimal structures found by layout optimization tend at Michell-like structures, made up of a very large number of infinitesimal struts [85].

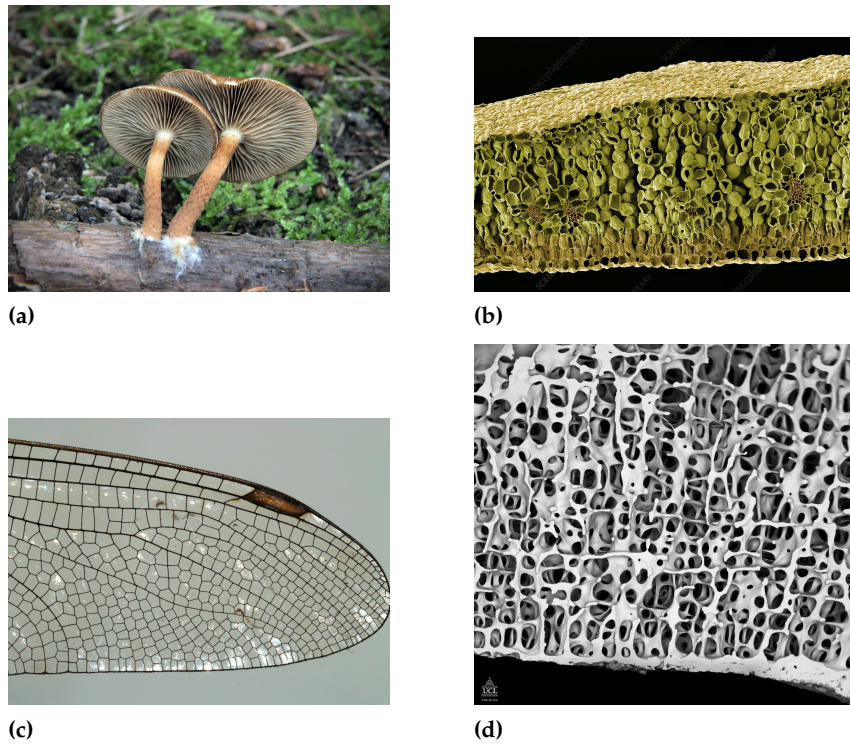


Figure 1.9: The natural evolution process frequently generates lattice materials and modular structures; (a) The spore-bearing gills of a *Hypholoma fasciculare* [97] (b) SEM image of a leaf microstructure [98] (c) cellular stucture of the wing of a dragonfly [99] (d) internal structure of a human bone [100].

1.3 MODULAR STRUCTURES AND LATTICE MATERIALS

93. Schaedler et al. (2016), 'Architected Cellular Materials'

Historically, material properties were modified by manipulating chemical composition, microstructure, and production processes [93]. Another possible way for enhancing material properties involves tailoring the spatial arrangement of solid and voids within the material. Referred to as architected materials, this concept has gained significant traction in research, particularly with recent advancements in additive manufacturing. These materials, often observed in natural structures like bone microstructures or birds' beaks (refer to Fig. 1.9 for additional examples), have garnered interest due to the recognition that optimal structures exhibit stiffness across multiple scales [94, 95]. Additionally, Fleck noted [96] that one reason for structural hierarchy in engineering is to augment buckling strength. In fact, local buckling strength scales with the strut length l following l^{-2} , indicating that finer length scales contribute to higher buckling strength.

94. Kohn et al. (1986), 'Optimal design and relaxation of variational problems'

95. Allaire et al. (1999), 'On optimal microstructures for a plane shape optimization problem'

96. Fleck et al. (2010), 'Microarchitected materials'

101. Ashby (1999), 'Materials selection in mechanical design'

2: The HS bounds are the tightest bounds possible from the range of composite moduli for a two-phase isotropic mixture. In lattices, usually, the second material is void.

If we observe the Ashby material chart [101] shown in Fig. 1.10, where the material yield strength is plotted against density, it becomes evident that numerous empty spaces exist. Besides some unattainable areas delineated by the HS bounds², these empty spaces can be filled by architected structures, extending the property space of actual materials.

A highly interesting class of architected materials and structures is represented by lattices, alternatively referred to in the literature

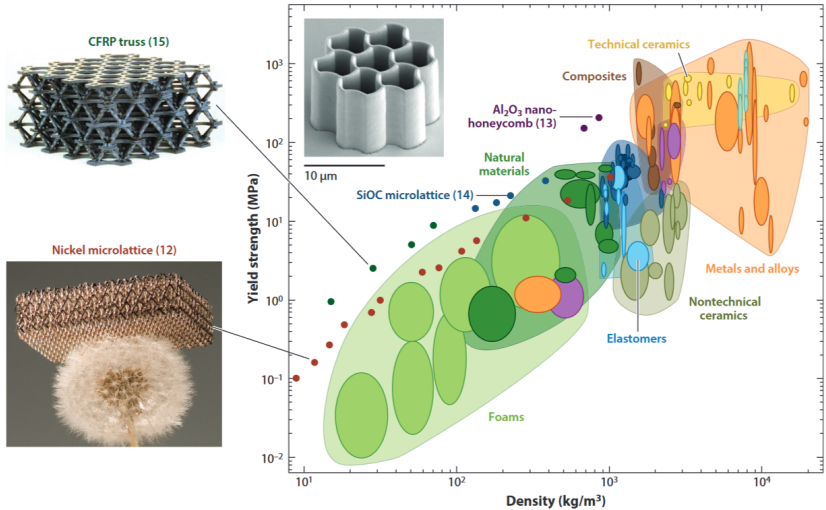


Figure 1.10: Density versus yield strength Ashby chart. Exploiting the architecture of the material as a variable to design new metamaterials, empty spaces of the graph can be filled (see dots) [93].

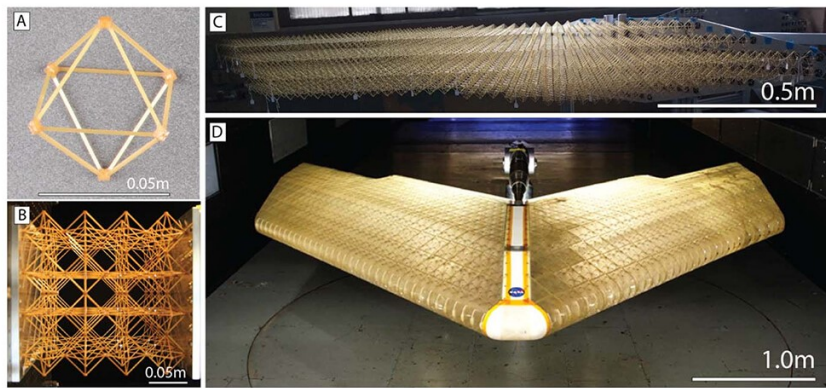


Figure 1.11: The different length scales present in a modular structure [107].

as cellular architected or modular materials and structures. The defining feature of lattices is to exhibit a repetitive Representative Volume Element (RVE) (also commonly called module or cell) that is replicated throughout space. This characteristic allows for the establishment of a systematic and reproducible unit that captures the essential structural and material properties of the lattice. The study of the repetitive nature of the RVE permits a comprehensive understanding of the lattice's behavior, enabling researchers to analyze and predict its mechanical, thermal, and other pertinent properties with a high degree of accuracy [102]. It is possible to differentiate between a lattice material and a lattice structure based on the size of the RVE with respect to the considered structure. In a lattice structure, there is no clear physical scale separation between the RVE and the macrostructure, indicating that the lattice's characteristics are manifested at both the micro and macro scales (see Fig. 1.11). However, defining a specific threshold to distinctly categorize the two is challenging, as the transition from lattice material to lattice structure can be gradual and context-dependent [103–106].

Lattice structures and materials exhibit a wide range of promising applications. They showcase notable energy-absorbing properties, particularly when designed as bending-dominated structures [108–

102. Bensoussan et al. (1978), 'Asymptotic analysis for periodic structures'

103. Dai et al. (2008), 'Size effects of basic cell in static analysis of sandwich beams'

104. Kalamkarov et al. (2009), 'Asymptotic Homogenization of Composite Materials and Structures'

105. Coelho et al. (2016), 'Scale-size effects analysis of optimal periodic material microstructures designed by the inverse homogenization method'

106. Zhang et al. (2018), 'Multiscale concurrent topology optimization for cellular structures with multiple microstructures based on ordered SIMP interpolation'

- 108. Evans et al. (2010), 'Concepts for Enhanced Energy Absorption Using Hollow Micro-Lattices'
- 109. Schaedler et al. (2014), 'Designing Metallic Microlattices for Energy Absorber Applications'
- 110. Ozdemir et al. (2016), 'Energy absorption in lattice structures in dynamics'
- 107. Cramer et al. (2019), 'Elastic shape morphing of ultralight structures by programmable assembly'
- 111. Opgenoord et al. (2018), 'Aeroelastic Tailoring using Additively Manufactured Lattice Structures'
- 112. Hutmacher (2000), 'Scaffolds in tissue engineering bone and cartilage'
- 113. Mota et al. (2015), 'Additive manufacturing techniques for the production of tissue engineering constructs'
- 114. Nikolova et al. (2019), 'Recent advances in biomaterials for 3D scaffolds'
- 115. Lu et al. (1998), 'Heat transfer in open-cell metal foams'
- 116. Wadley et al. (2007), 'Thermal Applications of Cellular Lattice Structures'



Figure 1.12: Vickers Wellingtons, bombers utilized during World War II, remained operational despite sustaining extensive damage, thanks to their lattice fuselage. When one of the ribs was damaged, the load was redistributed to the others, allowing the structure to remain functional [117].

[110]. This quality positions lattice structures as potential candidates for a novel design schemes in aerodynamics, thanks to their remarkable aeroelastic properties [107, 111]. Additionally, lattices have proven to be compelling choices for constructing biomedical scaffolds [112–114]. Furthermore, lattice materials demonstrate excellent heat exchanger properties, attributed to their high surface-to-volume ratio and the turbulent mixing flow they induce when a fluid passes through [115, 116].

Lattices show additional captivating properties that demonstrate their versatility. Firstly, cellular structures can be purposefully designed for reversible assembly, introducing the concept of rapid assembly and easily repairable structures. Various approaches, such as utilizing fasteners [107, 118, 119], or incorporating snap-fit joints [120], have been proposed to realize this idea. Furthermore, lattice structures inherently exhibit damage tolerance [121, 122]. In a skin-lattice design, the skin is non-load-bearing, ensuring that skin damage does not lead to progressive structural failure. Additionally, in cases of rib damage, the affected rib can be isolated from the load without compromising the integrity of the entire structure (refer to Fig. 1.12). Lastly, lattice structures pave the way for extensive utilization of robotics in both the manufacturing [123] and assembly phases [124–127].

Lattices can be categorized as open- or closed-wall structures based on the topology of the repeating RVE. Despite closed-wall lattices potentially resulting in stiffer structures, the preference for open-cell configurations is well-articulated by Sigmund *et al.* [66]. They emphasize that the outcome of minimum compliance-type continuum topology optimization studies should inherently be of sheet type unless explicit constraints favoring Michell-like structures are specified. These constraints include considerations of structural and microstructural stability, where the load required to initiate buckling in a slender strut of an open-cell lattice is significantly higher than that of a comparable closed-cell lattice [128]. Consequently, open-cell structures are less prone to buckling. Additionally, the porosity of open-wall cells allows for the passage of flow, making them suitable for applications such as heat exchangers or promoting bone regrowth in biomedical scaffolds. From a manufacturing perspective, open-cell designs are preferable, as very thin walls are challenging to manufacture. The transparency inherent in open-cell structures is advantageous for tasks such as repair and health monitoring. Finally, an open-cell design is considered elegant and aesthetic, as it embodies Michell-like structures, which are described "inarguably beautiful" and "look elegant and efficient" by Sigmund *et al.* [66].

Lattice structures are further categorized into stretching- and bending-dominated based on the RVE topology. A stretching-dominated structure is characterized as a lattice in which its constitutive struts exclusively experience tension and compression loads. In such a structure,

the nodal stiffness does not contribute to the overall structural stiffness, and the truss undergoes collapse primarily through the stretching of its struts. Desphande *et al.* [128] noted that freezing the joints of a stretching-dominated truss has minimal impact on its macroscopic stiffness or strength. Despite the bending of the struts, the frame remains stretching-dominated, and the collapse load is predominantly determined by the axial strength of the struts. Consequently, if an open-cell structure is stretching-dominated, it can effectively be treated as a connected set of pin-jointed struts.

The relative density of the lattice is defined as:

$$\bar{\rho} = \frac{\rho_l}{\rho} \quad (1.9)$$

where ρ_l and ρ represent the density of the lattice and of the dense material, respectively [129]. A stretching-dominated structure exhibits approximately 10 times greater stiffness and 3 times greater strength than a bending-dominated structure at $\bar{\rho} = 0.1$, as illustrated in Figure 1.13 [128]. Nevertheless, when subjected to compression, stretching-dominated structures display a softening post-yield response attributed to the buckling of struts, rendering them less suitable for energy absorption tasks. In contrast, bending-dominated lattices showcase a more favorable energy-absorbing behavior, characterized by a plateau-like response.

1.3.1 MODULAR STRUCTURES AND LATTICE MATERIALS OPTIMIZATION

The initial density-based topology optimization method, as seen in Bendsøe and Kikuchi's foundational work [5], employed numerical homogenization to model a meta-material consisting of infinitesimally small square cells with square holes. Notably, this marked the advent of multi-scale optimization, driven by the fact that optimal stiffness for a structure encompasses various scales [94, 95].

In the 1990s, the focus shifted from homogenization algorithms to mono-scale algorithms, where the optimization involved a homogeneous distribution of an isotropic material [35, 130]. This shift was primarily caused by the manufacturing challenges associated with producing multi-scale meta-materials. Subsequently, these approaches evolved into what is now known as density-based topology optimization. Mono-scale methods, where the design domain discretization results in structures at a single scale, can achieve theoretical stiffness-optimal structures spanning multiple scales with fine mesh discretization and careful continuation techniques, provided there is no regularization for mesh independence. Bendsøe and Kikuchi original work and homogenization-based algorithms has gained recently more interest due to the advances in additive manufacturing technologies. Contemporary studies are combining asymptotic ho-

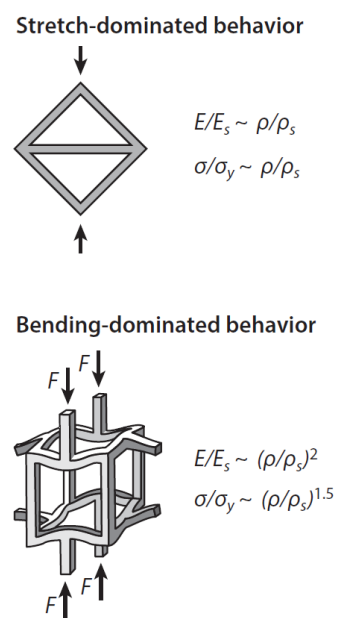


Figure 1.13: A stretch-dominated and a bending-dominated RVE. Bending-dominated structure act as a mechanism if the joints cannot withstand moments. The scaling laws are different for the two structure families [93].

107. Cramer et al. (2019), 'Elastic shape morphing of ultralight structures by programmable assembly'

118. Cheung et al. (2013), 'Reversibly Assembled Cellular Composite Materials'

119. Jenett et al. (2017), 'Digital Morphing Wing: Active Wing Shaping Concept Using Composite Lattice-Based Cellular Structures'

120. Dong et al. (2015), 'Mechanical response of Ti-6Al-4V octet-truss lattice structures'

121. Stolpe (2019), 'Fail-safe truss topology optimization'

122. Wu et al. (2021), 'Topology optimization of multi-scale structures'

123. Hunt et al. (2019), 'WrapToR composite truss structures'

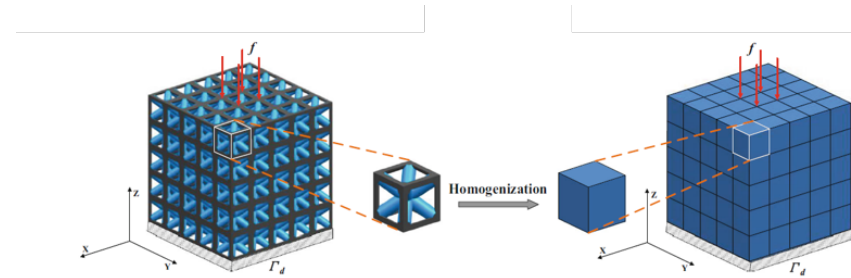


Figure 1.14: Graphical representation of the asymptotic homogenization method used to retrieve the equivalent mechanical properties of a periodic cell [134].

- 124. Gershenfeld et al. (2015), 'Macro-fabrication with Digital Materials'
- 125. Jenett et al. (2017), 'BILL-E: Robotic Platform for Locomotion and Manipulation of Lightweight Space Structures'
- 126. Costa et al. (2020), 'Algorithmic Approaches to Reconfigurable Assembly Systems'
- 127. Niehs et al. (2020), 'Recognition and Reconfiguration of Lattice-Based Cellular Structures by Simple Robots'
- 66. Sigmund et al. (2016), 'On the (non-)optimality of Michell structures'
- 128. Deshpande et al. (2001), 'Foam topology'
- 129. Ashby (2006), 'The properties of foams and lattices'
- 5. Bendsøe et al. (1988), 'Generating optimal topologies in structural design using a homogenization method'
- 94. Kohn et al. (1986), 'Optimal design and relaxation of variational problems'
- 95. Allaire et al. (1999), 'On optimal microstructures for a plane shape optimization problem'
- 35. Bendsøe (1989), 'Optimal shape design as a material distribution problem'
- 130. Zhou et al. (1991), 'The COC algorithm, Part II'
- 122. Wu et al. (2021), 'Topology optimization of multi-scale structures'
- 131. Rodrigues et al. (2002), 'Hierarchical optimization of material and structure'
- 132. Pantz et al. (2008), 'A Post-Treatment of the Homogenization Method for Shape Optimization'
- 133. Groen et al. (2018), 'Homogenization-based topology optimization for high-resolution manufacturable microstructures'

mogenization and topology optimization to optimize multi-scale structures.

Lattice structures are optimized through either a multi-scale or a full-scale approach. Multi-scale algorithms operate on structures with different physical scales between the micro- and macro-levels, assuming periodic boundary conditions for the RVE. Doing that allows for the use of a material model with micro-structure properties evaluated using asymptotic homogenization. In contrast, full-scale methods represent mono-scale approaches where optimization is achieved by directly controlling the layout locally. In these full-scale approaches, both analysis and optimization are conducted at the full resolution of the domain. For a more in-depth exploration and comparison of full-scale and multi-scale approaches, interested readers can refer to the comprehensive review by Wu *et al.* [122].

1.3.2 MULTI-SCALE STRUCTURES OPTIMIZATION

Multi-scale topology optimization approaches aim to speed up computations for optimizing structures at full resolution. Optimal structures span multiple scales, and using a finer mesh allows for detailed geometric improvements, potentially enhancing optimized structures. However, higher resolution mono-scale approaches come with increased computational costs. To tackle this, multi-scale approaches like the hierarchical method by Rodrigues *et al.* [131] and de-homogenization techniques [132, 133] have been introduced.

The hierarchical optimization framework consists of a master problem addressing the global spatial distribution of material and an inner problem tackling the optimal choice of material at the local level. This approach shifts the focus from a specific composite's material distribution problem to a more comprehensive challenge involving both topology and material optimal design. The idea is to use the homogenized micro-scale cell as the base material of the macro-scale topology optimization. Fig. 1.14 gives a graphical representation of how asymptotic homogenization works. The equivalent elastic tensor \mathbf{D}^H is calculated using the following formula [135]:

$$\mathbf{D}^H = \frac{1}{|\Omega_m|} \int_{\Omega_m} (\varepsilon_m^0 - \varepsilon_m) \mathbf{D} (\varepsilon_m^0 - \varepsilon_m) d\Omega_m \quad (1.10)$$

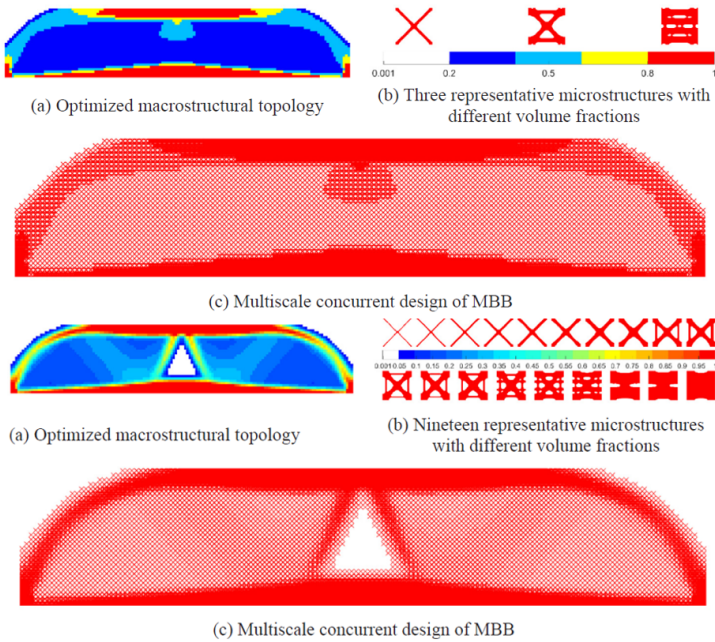


Figure 1.15: In the study of Zhang *et al.* [106] the same test case is optimized using a different number of microstructures. Here we show the multi-scale optimized structures using 3 and 19 different microstructures.

where \mathbf{D}^H is the homogenized elastic tensor, Ω_m represents the RVE volume, \mathbf{D} is the base material elastic tensor and ε_m^0 are called unit test strain and are defined as $\varepsilon^{11} = (1, 0, 0)^T$, $\varepsilon^{22} = (0, 1, 0)^T$, $\varepsilon^{12} = (0, 0, 1)^T$. An example of the results obtained using a hierarchical method is presented in Fig. 1.15.

De-homogenization is an approach where the optimization problem is initially solved solely on the macroscopic level using a homogenization method. Subsequently, an additional phase is introduced to obtain connected and physically realizable microstructures based on the obtained macroscopic result. In the macroscale optimization, multiple additional parameters are typically optimized concurrently with the density of the Representative Volume Element (RVE). These parameters may include microstructure orientation, contributing to the creation of a smooth mapping function [133, 136–138]. An alternative approach involves approximating the material behavior through a reduced database model, as demonstrated by Xia and Breitkopf [139]. In this method, microstructural computations are performed offline, only once. Precomputed databases are then employed to obtain the full design for the parametrized lattice RVE, often using a polynomial model to interpolate between the database microstructures [140, 141]. Recent approaches are now using Artificial Intelligence (AI) and deep learning to speed up the de-homogenization phase [142–145].

In conclusion, despite maintaining the separation of the two physical scales during the optimization process, it is imperative to conduct a full-scale validation for all multi-scale methods, as highlighted in various studies [122, 133, 146, 147]. Additionally, in the multi-scale optimization approaches in which the microstructure is aligned to local stress fields without constraints imposed by cell geometry or

135. Guedes *et al.* (1990), ‘Preprocessing and postprocessing for materials based on the homogenization method with adaptive finite element methods’

133. Groen *et al.* (2018), ‘Homogenization-based topology optimization for high-resolution manufacturable microstructures’

136. Allaire *et al.* (2019), ‘Topology optimization of modulated and oriented periodic microstructures by the homogenization method’

137. Geoffroy-Donders *et al.* (2020), ‘3-d topology optimization of modulated and oriented periodic microstructures by the homogenization method’

138. Kumar *et al.* (2020), ‘A density-and-strain-based K-clustering approach to microstructural topology optimization’

139. Xia *et al.* (2015), ‘Multiscale structural topology optimization with an approximate constitutive model for local material microstructure’

140. Wang *et al.* (2018), ‘Concurrent topology optimization design of structures and non-uniform parameterized lattice microstructures’

141. Imediegwu *et al.* (2019), ‘Multiscale structural optimization towards three-dimensional printable structures’

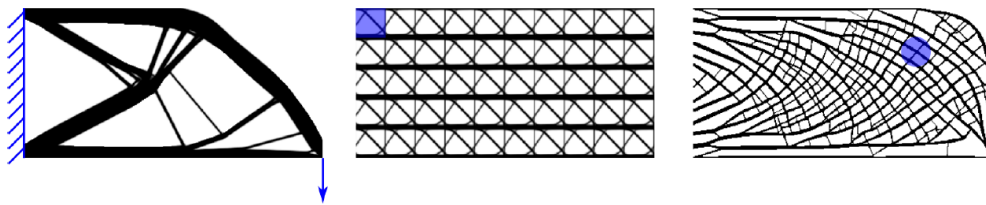


Figure 1.16: Three structures with the same volume are optimized for compliance minimization using three different methods: on the left, a classic mono-scale topology optimization algorithm. Middle: the variable linking method is used to enforce the pattern repetition on the structure. On the right an optimized structure with local volume constraints. The algorithms used to optimize the last two structures belong to the family of *full-scale* methods. [122].

142. Kim et al. (2021), 'Machine learning-combined topology optimization for functionary graded composite structure design'

143. White et al. (2019), 'Multiscale topology optimization using neural network surrogate models'

144. Chandrasekhar et al. (2021), 'Multi-Material Topology Optimization Using Neural Networks'

145. Wang et al. (2021), 'Enhancing Data-driven Multiscale Topology Optimization with Generalized De-homogenization'

122. Wu et al. (2021), 'Topology optimization of multi-scale structures'

133. Groen et al. (2018), 'Homogenization-based topology optimization for high-resolution manufacturable microstructures'

146. Duriez et al. (2021), 'A well connected, locally-oriented and efficient multi-scale topology optimization (EMTO) strategy'

147. Sigmund (2022), 'On benchmarking and good scientific practise in topology optimization'

105. Coelho et al. (2016), 'Scale-size effects analysis of optimal periodic material microstructures designed by the inverse homogenization method'

148. Cheng et al. (2019), 'Functionally graded lattice structure topology optimization for the design of additive manufactured components with stress constraints'

102. Bensoussan et al. (1978), 'Asymptotic analysis for periodic structures'

104. Kalamkarov et al. (2009), 'Asymptotic Homogenization of Composite Materials and Structures'

37. Zhang et al. (2006), 'Scale-related topology optimization of cellular materials and structures'

orientation [133], delivers good performance even for structures with less periodicity compared to a bulk distribution.

1.3.3 FULL-SCALE STRUCTURES OPTIMIZATION

Recent studies have focused on assessing homogenization predictions compared to mechanical responses, revealing up to a 20 % variation in the effective components of the stiffness tensor for a $6 \times 6 \times 6$ cube when compared to homogenized models [105, 148]. This variability is attributed to the "boundary layer phenomenon" observed in the late 70s, challenging the assumptions of periodic boundary conditions and scale separability inherent in homogenization [102, 104]. To address these limitations, a new family of methodologies, known as full-scale approaches, has emerged. Unlike homogenization-based methods, full-scale approaches, such as pattern repetition and local volume constraints, avoid reliance on homogenization. In pattern repetition, the initial design space is partitioned into repetitive domains that are optimized constrained to ensure their uniformity [37]. In contrast, local volume constraints method imposes an upper limit on the solid elements' fraction in a neighborhood radius centered in each point within the design domain. The objective is to generate porous structures aligned with principal stress directions. While experiencing a modest stiffness reduction compared to mono-scale designs, these structures demonstrate heightened resilience against variations in load angle, local material failure, and buckling. [structures wu_infill_2018].

Variable linking approach faces a common limitation, leading to compromised structural performance due to topological periodicity [37, 149]. This limitation arises as the design converges toward solutions influenced by the region with the highest compliance, resulting in suboptimal solutions for other regions where the same module design is applied [150]. To address this, Bakker [151] identified two key approaches. The first involves extending the solution space by introducing additional module properties as design variables. For instance, allowing module rotations has proven effective, as it modifies the local material distribution and enhances structural performance [152]. Another extension involves allowing the module unit to resize, providing flexibility in adapting to different regions within

the global domain [153, 154]. These strategies offer ways to overcome the challenges associated with topological periodicity and achieve more optimal solutions for diverse regions within the structure.

structures wu_infill_2018

37. Zhang et al. (2006), 'Scale-related topology optimization of cellular materials and structures'

149. Huang et al. (2008), 'Optimal design of periodic structures using evolutionary topology optimization'

150. Tugilimana et al. (2019), 'An integrated design methodology for modular trusses including dynamic grouping, module spatial orientation, and topology optimization'

151. Bakker et al. (2021), 'Simultaneous optimization of topology and layout of modular stiffeners on shells and plates'

152. Tugilimana et al. (2017), 'Spatial orientation and topology optimization of modular trusses'

153. Stromberg et al. (2011), 'Application of layout and topology optimization using pattern gradation for the conceptual design of buildings'

154. Wu et al. (2016), 'A System for High-Resolution Topology Optimization'

EVALUATING DISCRETIZATION APPROACHES FOR ULTRALIGHT STRUCTURE OPTIMIZATION

2

check buchi fatti dallo spostamento IMPORTANTE, sostituisci continuous con density based add equations that are in precedent chapter, virgole e peunti The process of topology optimization for a structure involves the selection and sizing of optimal elements within a predetermined set. As discussed in the previous chapter, in our context this set could be composed of either continuum elements (shell or volumetric) or truss-like elements. Based on the discretization choice we distinguish between continuous topology optimization and Truss Topology Optimization (TTO). This chapter aims to assess the suitability and the inherent advantages and disadvantages of both methods when optimizing ultralight structures i.e. structures that exhibit a low volume fraction, typically below 5%.

For this purpose, we initially formulate a volume minimization problem subject to maximum stress constraints for both discretizations in Section 2.1. Later, a two-dimensional test case, featuring identical dimensions, loads, and material properties is optimized using the continuous topology optimization and the TTO algorithms. The outcomes of the comparison of both optimization approaches are presented and discussed in Section 2.2.

2.1 THE FORMULATION OF A SHARED PROBLEM: VOLUME MINIMIZATION WITH STRESS CONSTRAINTS

Instead of focusing on the commonly used compliance minimization formulation in continuous topology optimization, our emphasis on the aerospace sector leans towards the volume minimization problem. Prioritizing volume minimization, directly linked to the more crucial mass minimization objective, is driven by economic, environmental, and performance considerations within the aerospace industry. This strategic approach supports industry goals of sustainability, efficiency, and technological advancement. Therefore, we have chosen to adopt the volume minimization optimization formulation for our study, and we will now implement it on both continuum and truss-like meshes.

2.1.1 CONTINUOUS TOPOLOGY OPTIMIZATION MINIMUM VOLUME FORMULATION

This section introduces the Nested Analysis and Design (NAND) volume minimization formulation for topology optimization on continuum meshes. We will begin by explaining important notations and concepts that are essential for developing the volume minimization formulation.

2.1 THE FORMULATION OF A SHARED PROBLEM: VOLUME MINIMIZATION WITH STRESS CONSTRAINTS	23
2.2 COMPARISON BETWEEN CONTINUOUS TOPOLOGY OPTIMIZATION AND TTO	32
2.3 CONCLUSION	43

Part of the content presented in this chapter has been published and showcased during a conference as: Stragiotti, E. et al. (2021) "Towards manufactured lattice structures: a comparison between layout and topology optimization", in *AeroBest 2021 International Conference on Multidisciplinary Design Optimization of Aerospace Systems*. Book of proceedings. Lisbon, Portugal: ECCOMAS [155].

OBJECTIVE AND CONSTRAINT FUNCTIONS The goal of the optimization is to minimize the volume fraction occupied by a structure under a specified load case. In this thesis, as we deal with two- and three-dimensional structures, we should differentiate between area and volume, but for the sake of generality, we talk about volume. The volume fraction of the structure, denoted as V_f , is expressed as the ratio between the structural volume $V = \sum_{i \in \Omega} \bar{\rho}_i v_i$ and the total volume V_0 of the domain Ω :

$$V_f = \frac{V}{V_0} = \frac{1}{V_0} \sum_{i \in \Omega} \bar{\rho}_i v_i. \quad (2.1)$$

We assume that the elementary volume v_i occupied by the i -th element is equal for all the elements, and thus Equation 2.1 is simplified as follows:

$$V_f = \frac{1}{N_e} \sum_{i \in \Omega} \bar{\rho}_i. \quad (2.2)$$

The normalized local stress constraint g_{st} is formulated as:

$$g_{st} := \frac{\sigma_{VM,i}}{\sigma_L} - 1 \leq 0, \quad \forall i \in \Omega_{mat}(\rho) \quad (2.3)$$

where $\Omega_{mat}(\rho) \subseteq \Omega$ represents the design-dependent set of elements with a non-zero density i.e., stress constraints are defined only for the active elements, $\sigma_{VM,i}$ is the equivalent Von Mises stress for the i -th element, and σ_L is the maximum allowable of the material.

The first difficulty that arises using this formulation is that the stress constraints are defined only for the elements where $\bar{\rho}_i > 0$, while $\bar{\rho}_i \in [0, 1]$. Thus, the set of constraints changes during the optimization. This class of problems is called Mathematical Programs with Vanishing Constraints (MPVCs) [156] and is known for being difficult to solve with a gradient descent optimization algorithm. The original set of constraints g_{st} is then reformulated into an equivalent design-independent set of constraints \bar{g}_{st} as follows [157]:

$$\bar{g}_{st} := \bar{\rho}_i \left(\frac{\sigma_{VM,i}}{\sigma_L} - 1 \right) \leq 0, \quad \forall i \in \Omega. \quad (2.4)$$

156. Achtziger et al. (2008), 'Mathematical programs with vanishing constraints'

157. Cheng et al. (1992), 'Study on Topology Optimization with Stress Constraints'

VON MISES STRESS EVALUATION The evaluation of the equivalent stress of a two-dimensional element follows the formulation proposed by Von Mises. Let us take a four-node quadrilateral linear element with a single integration (or Gauss) point in the center and four $2a$ equal-length sides (see Fig. 2.1). If bilinear shape functions are used to interpolate the displacement field, we can evaluate the deformations

at the integration point as:

$$\begin{pmatrix} \varepsilon_x \\ \varepsilon_y \\ \gamma_{xy} \end{pmatrix} = \mathbf{B}_s \mathbf{q}_s, \text{ with } \mathbf{B}_s = \frac{1}{4a} \begin{pmatrix} -1 & 1 & 1 & -1 & 0 & 0 & 0 & 0 \\ 0 & 0 & 0 & 0 & -1 & -1 & 1 & 1 \\ -1 & -1 & 1 & 1 & -1 & 1 & 1 & -1 \end{pmatrix}, \quad (2.5)$$

where $\mathbf{q}_s = (u_1, u_2, u_3, u_4, v_1, v_2, v_3, v_4)^T$ represents the vector of the displacement degrees of freedom of the element.

The stress tensor is evaluated using the elasticity Hooke's law in 2D as follows:

$$\begin{pmatrix} \sigma_x \\ \sigma_y \\ \tau_{xy} \end{pmatrix} = \mathbf{C}_e \begin{pmatrix} \varepsilon_x \\ \varepsilon_y \\ \gamma_{xy} \end{pmatrix} \quad \text{with} \quad \mathbf{C}_e = \frac{E}{1-\nu^2} \begin{pmatrix} 1 & \nu & 0 \\ \nu & 1 & 0 \\ 0 & 0 & G \end{pmatrix}. \quad (2.6)$$

The equivalent Von Mises stress of the element can then be written as:

$$\langle \sigma_{VM} \rangle = \sqrt{\sigma_x^2 + \sigma_y^2 - \sigma_x \sigma_y + 3\tau_{xy}} \quad (2.7)$$

$$= \sqrt{(\sigma_x \ \sigma_y \ \tau_{xy}) \begin{pmatrix} 1 & -1/2 & 0 \\ -1/2 & 1 & 0 \\ 0 & 0 & 3 \end{pmatrix} \begin{pmatrix} \sigma_x \\ \sigma_y \\ \tau_{xy} \end{pmatrix}} \quad (2.8)$$

$$= \sqrt{\mathbf{q}_s^T \mathbf{B}_s^T \mathbf{C}_e^T \mathbf{D}_{VM} \mathbf{C}_e \mathbf{B}_s \mathbf{q}_s}, \text{ with } \mathbf{D}_{VM} = \begin{pmatrix} 1 & -1/2 & 0 \\ -1/2 & 1 & 0 \\ 0 & 0 & 3 \end{pmatrix} \quad (2.9)$$

$$\langle \sigma_{VM} \rangle = \sqrt{\mathbf{q}_s^T \mathbf{S} \mathbf{q}_s}, \quad \text{with } \mathbf{S} = \mathbf{B}_s^T \mathbf{C}_e^T \mathbf{D}_{VM} \mathbf{C}_e \mathbf{B}_s. \quad (2.10)$$

in which we used the notation introduced by Verbart [158] $\langle \dots \rangle$ to represent macroscopic (or homogenized) variables.

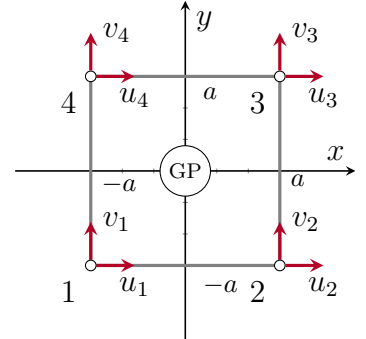


Figure 2.1: A four-node quadrilateral element. GP is the Gaussian integration point for which the equivalent stress is evaluated.

158. Verbart et al. (2017), 'A unified aggregation and relaxation approach for stress-constrained topology optimization'

MICROSCOPIC AND MACROSCOPIC STRESS In stress-constrained topology optimization, the element stress is usually evaluated using the microscopic stress formulation, assuming that there is no direct correlation between stress and density [159]. Indeed, the use of the macroscopic stress in volume minimization optimization problems creates an all-void design [160]. The properties that the microscopic stress should present are:

- (i) The stress criterion should be mathematically as simple as possible, as the relationship between Young's modulus and density. This permits a simple numerical implementation.
- (ii) To mimic the real physical behavior, the microscopic stress should be inversely proportional to density.

159. Duysinx et al. (1998), 'Topology optimization of continuum structures with local stress constraints'

160. Le et al. (2010), 'Stress-based topology optimization for continua'

158. Verbart et al. (2017), 'A unified aggregation and relaxation approach for stress-constrained topology optimization'

Equation 1.2 reads as follows:

$$E_i(\bar{\rho}_i) = E_{\min} + \bar{\rho}_i^p (E_0 - E_{\min})$$

where the parameter p is called SIMP penalization parameter, and it is used to reduce the quantity of intermediate densities, pushing the result to a black-and-white result.

158. Verbart et al. (2017), 'A unified aggregation and relaxation approach for stress-constrained topology optimization'

160. Le et al. (2010), 'Stress-based topology optimization for continua'

161. Holmberg et al. (2013), 'Stress constrained topology optimization'

162. Silva et al. (2019), 'Stress-constrained topology optimization considering uniform manufacturing uncertainties'

75. Rozvany (2001), 'On design-dependent constraints and singular topologies'

163. Stolpe (2003), 'On Models and Methods for Global Optimization of Structural Topology'

164. Sved et al. (1968), 'Structural optimization under multiple loading'

74. Cheng et al. (1997), ' ε -relaxed approach in structural topology optimization'

- (iii) The microscopic stress should converge to a non-zero value at zero density. This requisite is deduced from investigations into the asymptotic stress behavior in thin layers [158].

The relation between stress and displacement is written as:

$$\langle \sigma_{VM} \rangle = C_e(\langle E \rangle) \langle \varepsilon \rangle, \quad (2.11)$$

where the variables between angular brackets $\langle \dots \rangle$ represent macroscopic variables.

Combining (i) and (ii) with Equations 1.2, and 2.11, the microscopic stress can be written as:

$$\sigma_{VM} = \frac{\langle \sigma_{VM} \rangle}{\rho_e^q} = \rho_e^{p-q} C_e(E_0) \langle \varepsilon \rangle, \quad (2.12)$$

where the exponent q is a number greater than 1.

One possible choice that satisfy all the requirements is $q = p$ [158, 160–162]. Thus, the microscopic stress is defined as:

$$\sigma_{VM} = C_e(E_0) \langle \varepsilon \rangle. \quad (2.13)$$

The significance of microscopic stress becomes evident when considering an element with intermediate density, that is physically realized by a porous microstructure. The microscopic stress presented in Equation 2.13 measures the stress in the material of the microstructure. It is grounded in the assumption that the macroscopic deformations of the homogenized element generate within the microstructure of the element a stress state that remains unaffected by the density of the element itself.

CONSTRAINTS AGGREGATION AND RELAXATION When optimizing a structure with stress constraints using a NAND formulation, two primary challenges commonly arise:

- (i) Is it known in the literature [75, 163] that stress-based topology optimization suffers from the *singular minima* (or *singularity*) problem: firstly observed on truss structure optimization [164], these *minima* are almost inaccessible to a standard gradient-based optimizer, often preventing it to reach the global optimum of the optimization [75]. This is because achieving the optimal solution to a problem using continuous design variables may necessitate passing through a state where the optimization constraints are violated, i.e. the *minimum* is on a lower dimension compared to the design space. This problem is often solved using a technique called *constraints relaxation* [74].
- (ii) The stress is a local measure, and thus a large set of constraints is generated when a reasonably fine mesh is used (one element,

one constraint). This problem is often solved using a technique called *constraints aggregation* or *global constraints* [165].

Following the work developed by Verbart *et al.* [158], the lower bound Kreisselmeier-Steinhaus (KS) function [166] is used to approximate the local relaxed stress constraint maximum. The authors showed that employing lower-bound KS aggregation functions to approximate the maximum operator in stress-constrained topology optimization ensures the relaxation and the aggregation of the constraints simultaneously. The KS aggregated stress constraint function is defined as follows:

$$G_{\text{KS}}^{\text{L}} = \frac{1}{P} \ln \left(\frac{1}{N_e} \sum_{i \in \Omega} e^{P \bar{g}_i} \right). \quad (2.14)$$

Its main advantage over other different formulations is that it uses a single hyperparameter P to control the aggregation and the relaxation of the constraints simultaneously.

165. Silva et al. (2021), 'Local versus global stress constraint strategies in topology optimization'

158. Verbart et al. (2017), 'A unified aggregation and relaxation approach for stress-constrained topology optimization'

166. Kreisselmeier et al. (1979), 'Systematic Control Design by Optimizing a Vector Performance Index'

MINIMUM VOLUME FORMULATION The NAND minimum volume formulation for continuous discretization is written combining Equations 2.2, and 2.14 as:

$$\begin{aligned} \min_{\rho} \quad & V = \frac{1}{N_e} \sum_{i \in \Omega} \bar{\rho}_i, && \text{(Volume minimization)} \\ \text{s.t.} \quad & G_{\text{KS}}^{\text{L}} = \frac{1}{P} \ln \left(\frac{1}{N_e} \sum_{i \in \Omega} e^{P \bar{g}_i} \right) \leq 0 && \text{(Stress constraints)} \quad (\mathbb{T}_1) \\ & \mathbf{Ku} = \mathbf{F} && \text{(FEM equation)} \\ & 0 \leq \rho_i \leq 1, \end{aligned}$$

The optimization is carried out using a gradient descent optimization algorithm for which the sensitivities are given in analytical form. Using analytic gradients is in general more efficient than finite differences as it avoids the need for multiple function evaluations, making the optimization process faster and more precise.

SENSITIVITY ANALYSIS OF THE OBJECTIVE FUNCTION Deriving Equation 2.2 with respect to $\bar{\rho}$ we obtain:

$$\frac{\partial V}{\partial \bar{\rho}_i} = \frac{1}{N_e}. \quad (2.15)$$

The sensitivity of the objective function can then be evaluated using Equation 2.15 as follows:

$$\frac{dV}{d\rho_i} = \sum_{j \in \mathbb{N}_{i,R}} \frac{\partial V}{\partial \bar{\rho}_j} \frac{\partial \bar{\rho}_j}{\partial \bar{\rho}_i} \frac{\partial \bar{\rho}_i}{\partial \rho_i}. \quad (2.16)$$

Equation 1.4 reads:

$$\tilde{\rho}_i = \frac{\sum_{j \in \mathbb{N}_{i,R}} w(d_j) v_j \rho_j}{\sum_{j \in \mathbb{N}_{i,R}} w(d_j) v_j}.$$

Equation 1.5 reads:

$$\bar{\tilde{\rho}}_j = \frac{\tanh(\beta\eta) + \tanh(\beta(\tilde{\rho}_j - \eta))}{\tanh(\beta\eta) + \tanh(\beta(1 - \eta))}.$$

in which the derivative of the filtered density $\tilde{\rho}$ with respect to the design variable ρ is written deriving Equation 1.4:

$$\frac{\partial \tilde{\rho}_i}{\partial \rho_j} = \frac{w(d_j) v_j}{\sum_{j \in \mathbb{N}_{i,R}} w(d_j) v_j}. \quad (2.17)$$

The sensitivity of the physical densities $\bar{\tilde{\rho}}$ with respect to the filtered $\tilde{\rho}$ can be written deriving Equation 1.5 as:

$$\frac{\partial \bar{\tilde{\rho}}_j}{\partial \tilde{\rho}_j} = \beta \frac{1 - \tanh^2(\beta(\tilde{\rho}_j - \eta))}{\tanh(\beta\eta) + \tanh(\beta(1 - \eta))}. \quad (2.18)$$

Using the chain rule it is possible to write:

$$\frac{\partial h}{\partial \rho_i} = \sum_{j \in \mathbb{N}_{i,R}} \frac{\partial h}{\partial \bar{\tilde{\rho}}_j} \frac{\partial \bar{\tilde{\rho}}_j}{\partial \tilde{\rho}_j} \frac{\partial \tilde{\rho}_j}{\partial \rho_i}, \quad (2.19)$$

where h represents a generic function.

SENSITIVITY ANALYSIS OF THE CONSTRAINT FUNCTION The sensitivity of the aggregated constraint function G_{KS}^L with respect to the design variable ρ is evaluated using:

$$\frac{dG_{KS}^L}{d\rho_i} = \sum_{j \in \mathbb{N}_{i,R}} \frac{\partial G_{KS}^L}{\partial \bar{\tilde{\rho}}_j} \frac{\partial \bar{\tilde{\rho}}_j}{\partial \tilde{\rho}_j} \frac{\partial \tilde{\rho}_j}{\partial \rho_i}. \quad (2.20)$$

As the constraint function $G_{KS}^L = G(\bar{\tilde{\rho}}, \mathbf{u}(\bar{\tilde{\rho}}))$ is explicitly and implicitly (via the relationship with \mathbf{u}) depending on $\bar{\tilde{\rho}}$, the first-order derivative is evaluated using the total derivative formula:

$$\frac{dG}{d\bar{\tilde{\rho}}_j} = \frac{\partial G}{\partial \bar{\tilde{\rho}}_j} + \frac{\partial G}{\partial \mathbf{u}} \frac{\partial \mathbf{u}}{\partial \bar{\tilde{\rho}}_j}. \quad (2.21)$$

As function G_{KS}^L depends on \mathbf{u} via the stresses σ_i , it is possible to write:

$$\frac{\partial G}{\partial \mathbf{u}} = \sum_{i \in \Omega} \left(\frac{\partial G}{\partial \sigma_i} \frac{\partial \sigma_i}{\partial \mathbf{u}} \right). \quad (2.22)$$

Combining Eq. 2.21 with Eq. 2.22, we obtain:

$$\frac{dG}{d\bar{\tilde{\rho}}_j} = \underbrace{\frac{\partial G}{\partial \bar{\tilde{\rho}}_j}}_A + \sum_{i \in \Omega} \left(\underbrace{\frac{\partial G}{\partial \sigma_i}}_B \underbrace{\frac{\partial \sigma_i}{\partial \mathbf{u}}}_C \right) \underbrace{\frac{\partial \mathbf{u}}{\partial \bar{\tilde{\rho}}_j}}_D. \quad (2.23)$$

We compute the four factors separately:

A – The first term represents the explicit relationship of G to the physical densities and its calculation is straightforward:

$$\frac{\partial G}{\partial \bar{\rho}_j} = \frac{1}{P} \frac{\left(\frac{\sigma_{VM,j}}{\sigma_L} - 1 \right) \frac{1}{N_e} P e^{P \bar{g}_j}}{\frac{1}{N_e} \sum_k e^{P \bar{g}_k}} = \left(\frac{\sigma_{VM,j}}{\sigma_L} - 1 \right) \frac{e^{P \bar{g}_j}}{\sum_k e^{P \bar{g}_k}}. \quad (2.24)$$

B – The second term can be calculated using the chain rule:

$$\frac{\partial G}{\partial \sigma_i} = \frac{\partial G}{\partial \bar{g}_i} \frac{\partial \bar{g}_i}{\partial \sigma_i} = \frac{1}{P} \frac{\frac{1}{N_e} P e^{P \bar{g}_i}}{\frac{1}{N_e} \sum_k e^{P \bar{g}_k}} \frac{\bar{\rho}_i}{\sigma_L} = \frac{\bar{\rho}_i}{\sigma_L} \frac{e^{P \bar{g}_i}}{\sum_k e^{P \bar{g}_k}}. \quad (2.25)$$

C – We reformulate Equation 2.10 to be written in global coordinates instead of local:

$$\sigma_i^2 = \mathbf{q}_s^T \mathbf{S} \mathbf{q}_s = \mathbf{u}^T \mathbf{S}_g \mathbf{u}, \quad (2.26)$$

where \mathbf{S}_g represents the matrix \mathbf{S} of Equation 2.10 written on global coordinates¹. We can now differentiate Equation 2.26 with respect of the displacement field in global coordinates \mathbf{u} to obtain:

$$\frac{\partial \sigma_i}{\partial \mathbf{u}} = \frac{\mathbf{S}_g \mathbf{u}}{\sigma_i}. \quad (2.27)$$

Equations 2.25, and 2.27 are now combined to obtain the result of the product of the \mathbf{B} and \mathbf{C} terms. As a result, the derivatives of G with respect to \mathbf{u} , are written as:

$$\frac{\partial G}{\partial \mathbf{u}} = \frac{\bar{\rho}_j}{\sigma_L \sigma_j} e^{P \bar{g}_i} |S_j|_g \mathbf{u}. \quad (2.28)$$

D – To calculate the last term, we take the static equilibrium equation $\mathbf{K}\mathbf{u} = \mathbf{f}$ and differentiate it with respect to the physical densities $\bar{\rho}_j$, obtaining:

$$\frac{\partial \mathbf{K}}{\partial \bar{\rho}_j} \mathbf{u} + \mathbf{K} \frac{\partial \mathbf{u}}{\partial \bar{\rho}_j} = 0 \iff \frac{\partial \mathbf{u}}{\partial \bar{\rho}_j} = -\mathbf{K}^{-1} \frac{\partial \mathbf{K}}{\partial \bar{\rho}_j} \mathbf{u}, \quad (2.29)$$

where

$$\frac{\partial \mathbf{K}}{\partial \bar{\rho}_j} = (E_0 - E_{\min}) p \bar{\rho}_j^{p-1} \mathbf{K}_{e,j}. \quad (2.30)$$

Equation 2.30 represent the well-known first-derivative term of the global stiffness matrix \mathbf{K} with respect to the physical densities $\bar{\rho}_j$ when using Solid Isotropic Material with Penalization Method (SIMP) material scheme [1]. We obtain the last term:

$$\frac{\partial \mathbf{u}}{\partial \bar{\rho}_j} = -\mathbf{K}^{-1} \left((E_0 - E_{\min}) p \bar{\rho}_j^{p-1} \mathbf{K}_e \right) \mathbf{u}. \quad (2.31)$$

1: The matrix \mathbf{S}_g can be calculated using the very same assembling approach used for the stiffness matrix \mathbf{K} starting from the elemental stiffness matrix \mathbf{K}_e . As the global stiffness matrix \mathbf{K} , \mathbf{S}_g is symmetric and sparse.

[1] Bendsøe et al. (2004), 'Topology Optimization'

Combining Eq. 2.23, Eq. 2.24, Eq. 2.28, and Eq. 2.31, we finally obtain:

$$\frac{\partial G_{KS}^L}{\partial \bar{\rho}_j} = \left(\frac{\sigma_{VM,j}}{\sigma_L} - 1 \right) \frac{e^{P\bar{g}_j}}{\sum_k e^{P\bar{g}_k}} - K^{-1} \frac{\partial G}{\partial u} \left(\frac{\partial K}{\partial \bar{\rho}_j} \right) u. \quad (2.32)$$

2: More information about the adjoint method used to analytically calculate the first-order derivatives can be found on the Martins *et al.* book [2].

To avoid the explicit calculation of K^{-1} we use the *adjoint method*². Here is the linear system that, once solved, permits to calculate ψ :

$$K\psi = \frac{\partial G}{\partial u} \iff \psi = K^{-1} \frac{\partial G}{\partial u}. \quad (2.33)$$

This formula is called *adjoint equation*. This equation is solved for ψ and the result used to evaluate:

$$\frac{\partial G_{KS}^L}{\partial \bar{\rho}_j} = \left(\frac{\sigma_{VM,j}}{\sigma_L} - 1 \right) \frac{e^{P\bar{g}_j}}{\sum_k e^{P\bar{g}_k}} - \psi \left(\frac{\partial K}{\partial \bar{\rho}_j} \right) u. \quad (2.34)$$

Solving linear system 2.33 instead of directly calculating the inverse matrix of K is more efficient from a performance perspective. The cost of solving a system using the Cholesky decomposition is $\mathcal{O}(N^3/3)$, while a matrix inversion is $\mathcal{O}(N^3)$.

where N represents the size of the square matrix describing the linear system. Equation 2.34 represents the first-order derivative equation used to evaluate the sensitivity of the constraint function G_{KS}^L with respect to the physical densities $\bar{\rho}$. The value of ψ is calculated every iteration solving the linear system 2.33.

2.1.2 TRUSS TOPOLOGY OPTIMIZATION (TTO) MINIMUM VOLUME FORMULATION

We are now shifting our focus from continuous structures to discrete truss systems, describing the Truss Topology Optimization (TTO) (also known in early literature as layout optimization), a structure optimization method that focuses on discrete structures. In his most used formulation, TTO aims at reducing structural volume while meeting stress criteria using a Simultaneous Analysis and Design (SAND) approach. The problem is already well-posed for the comparison with continuous discretization.

OBJECTIVE AND CONSTRAINT FUNCTIONS The goal of the optimization is to minimize the volume occupied by a structure under a specified load case. For a truss structure, we can write:

$$V = \ell^T a \quad (2.35)$$

in which $\ell = [\ell_1, \ell_2, \dots, \ell_{Nel}]^T$ is the length vector of the member of the ground structure. The volume fraction is evaluated as the ratio $V_f = \frac{V}{V_0}$, where V_0 represents the total volume of the design domain Ω .

As the volume minimization problem is stated using the SAND approach, both the members' cross-sectional areas a and member

forces \mathbf{q} are design variables of the problem. For that reason the stress constraints in tension and compression ($g_{st,t}$ and $g_{st,c}$) can be trivially written as:

$$-\sigma_c \mathbf{a} \leq \mathbf{q} \leq \sigma_t \mathbf{a} \quad (2.36)$$

in which σ_c and σ_t are the compressive and tensile maximum allowable stresses of the material.

MINIMUM VOLUME FORMULATION We recall the full volume minimization formulation here, stated in terms of members' cross-sectional areas \mathbf{a} and member forces \mathbf{q} as follows:

$$\begin{aligned} \min_{\mathbf{a}, \mathbf{q}} \quad & V = \tilde{\ell}^T \mathbf{a} \quad (\text{Volume minimization}) \\ \text{s.t.} \quad & \mathbf{B}\mathbf{q} = \mathbf{f} \quad (g_{eq}) \\ & -\sigma_c \mathbf{a} \leq \mathbf{q} \leq \sigma_t \mathbf{a} \quad (g_{st,c}, g_{st,t}) \\ & \mathbf{a} \geq 0, \end{aligned} \quad (\mathbb{P}_0)$$

where $\tilde{\ell} = [\ell_1 + s, \ell_2 + s, \dots, \ell_{Nel} + s]^T$ is called augmented member length and s the joint cost, used to penalize the appearance of small members [92]. The listing and explanation of the others parameters is given in Section 1.2.3. This formulation takes into account only the linear behavior of the structure and is equivalent to the original and well-studied member force formulation [1, 31].

Is it worth listing the key distinctions of the TTO formulation compared to the continuous topology optimization formulation described earlier in this chapter. Firstly, the TTO problem is formulated using the SAND approach, in which the equations of structural mechanics are treated as constraints in the optimization. Unlike NAND approaches, these equations are not explicitly solved. Consequently, concerns about the singularity of the stiffness matrix \mathbf{K} are avoided, and bars can potentially vanish from the structure during the optimization ($\mathbf{a} = 0$). Secondly, the TTO problem is expressed in terms of members' cross-sectional areas \mathbf{a} and member forces \mathbf{q} with a plastic material model, disregarding kinematic compatibility to formulate a Linear Programming (LP) problem. Due to its linearity, this optimization problem is convex, ensuring that the solutions found are global optima. Moreover, the linear nature of the formulation \mathbb{P}_0 makes it computationally efficient, even with a large number of design variables, when employing modern interior point optimizers. However, the SAND formulation with a plastic material model accurately predicts the mechanical behavior of only statically determinate structures or mechanisms [78, 79]. When dealing with more complex structures, such as those that are statically indeterminate due to symmetry or multiple load cases, explicit consideration of the linear kinematic constraints is necessary, leading to a loss of the linear property of the formulation.

92. Parkes (1975), 'Joints in optimum frameworks'

1. Bendsøe et al. (2004), 'Topology Optimization'

31. Dorn et al. (1964), 'Automatic design of optimal structures'

78. Kirsch (1989), 'Optimal topologies of truss structures'

79. Rozvany et al. (1995), 'Layout Optimization of Structures'

2.2 COMPARISON BETWEEN CONTINUOUS TOPOLOGY OPTIMIZATION AND TTO

In the upcoming discussion, we will be comparing the optimized structures obtained using the continuous topology optimization and the TTO optimization algorithms. Our primary objective in this comparison is to choose the most appropriate method for our study by understanding the application limits inherent in these two structural discretization methods. If, indeed, we identify such limitations, the aim is to discern and define them. Such discussions have already been briefly addressed in the literature [35, 167], but treating the problem without providing numerical results as a basis for making the choice.

Since our interest is in ultralight structures, we are willing to compare the results of both optimization methods when dealing with different volume fractions on a common load case. The volume minimization formulation with stress constraints we use cannot, however, directly control the volume of the optimized structure. For that reason, we decided to adjust the material strength σ_L to influence the volume fraction of the optimized structure i.e. employing a more resistant material results in a lower volume fraction and *vice versa*. For this comparative analysis, we have selected three key performance metrics: the volume fraction V_f , the structural compliance C , and the maximum material allowable – or strength σ_L . Among these, we classify stress limit as the active metric used to influence the optimization, while volume and compliance are the objective of the optimization and a passive metric, respectively. In addition to the aforementioned performance metrics, we will also track the execution time of the algorithms.

2.2.1 DEFINITION OF A TEST CASE FOR THE COMPARISON

The L-shape beam is one of the most used load case benchmarks for stress-based topology optimization [159, 160]. This choice is driven by the distinctive geometry of the problem, which generates a stress concentration at the sharp corner in the case of linear elasticity—a phenomenon approaching infinity. Consequently, optimized solutions often feature a large fillet, mitigating the intensity of the stress singularity. The geometric description of the test case is given in Fig. 2.2. The beam with dimensions $L \times L$ presents a fixed support on the nodes in the top part and a load on the right extremity.

To permit the methods' comparison, the design domain Ω is discretized using two distinct meshes: in the continuous case, we employ a mesh consisting of 600×600 quadrilateral elements, totaling 270 000 elements. For this mesh, the load is distributed over multiple elements (5% of L) to avoid local stress concentrations. Additionally, the stress constraints are not evaluated on the corresponding elements, and this

³⁵. Bendsøe (1989), 'Optimal shape design as a material distribution problem'

¹⁶⁷. Watts et al. (2019), 'Simple, accurate surrogate models of the elastic response of three-dimensional open truss micro-architectures with applications to multiscale topology design'

¹⁵⁹. Duysinx et al. (1998), 'Topology optimization of continuum structures with local stress constraints'
¹⁶⁰. Le et al. (2010), 'Stress-based topology optimization for continua'

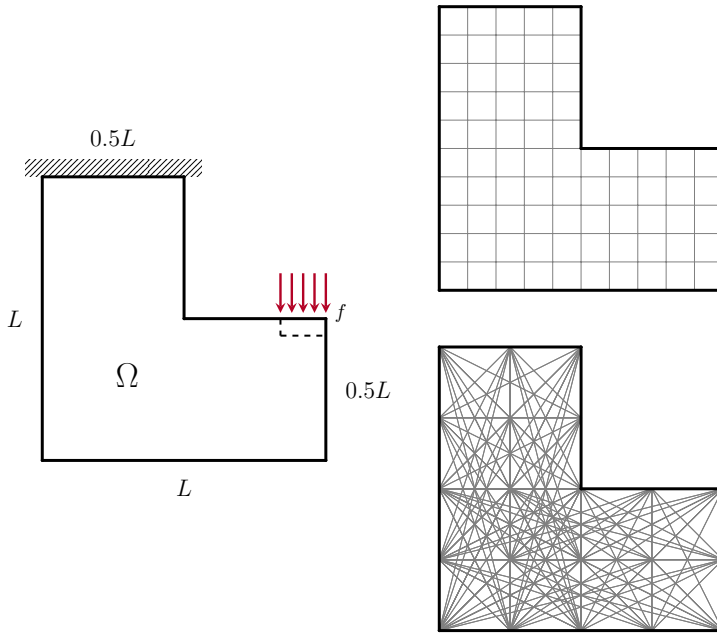


Figure 2.2: On the left, plot of the L-shape beam test case, on the right the graphical representations of the two discretizations used, the continuous (above) composed of 600×600 quadrilateral elements, and the truss-like (below) discretized using 33×33 nodes and a fully connected ground structure. The images represent a coarser discretization for visual clarity.

zone is considered outside of the design domain Ω . Concerning the truss discretization for the TTO algorithm, we employ a mesh with 33×33 nodes and a fully connected ground structure, comprising a total of 305 728 candidates. The load is applied only on one single node.

We employ the same isotropic material and structure dimensions for the two optimizations, and the complete data is resumed in Table 2.1. The value of the maximum material allowable σ_L is used to control, although not directly, the volume fraction of the solutions. For simplicity, all numeric values are assumed normalized and dimensionless.

2.2.2 NUMERICAL APPLICATION

The continuous topology optimization and the TTO have both been implemented using Python, employing different optimization algorithms. For continuous topology optimization, the chosen optimization algorithm is the Method of Moving Asymptotes (MMA), developed by Svanberg [25]. The parameter called *movelimit*³ is set to 0.1 while the other algorithm's parameters are set to their default value. We chose to filter the density field ρ using the 2D convolution operator [55] and the projection technique based on the \tanh function [50]. The radius of the filter is set to $R = 5$ elements. Using the projection Equation 1.5 is not volume conservative for all values of η , and to stay conservative we use a volume-increasing filter [10]. The value of $\eta = 0.4$ is then chosen. A continuation scheme for the projection parameter β is set to increase by one every 200 iterations and starting from 1, the number of maximum iteration is set to 7500, the stopping criteria is calculated as $\|\Delta x\|_2 / \sqrt{N_e}$ [10] on the absolute difference between two successive iterations of the physical densities

Parameter	Value
E	1
ν	0.3
L	100
σ_L	[0.20, 20]

Table 2.1: Material data used for the optimizations. The value of the maximum material allowable σ_L is used as the parameter to generate multiple optimized topologies.

25. Svanberg (1987), 'The method of moving asymptotes—a new method for structural optimization'

3: More information on the implementation of the *movelimit* parameter can be found on the paper by Verbart [158].

55. Sigmund (2007), 'Morphology-based black and white filters for topology optimization'

50. Wang et al. (2011), 'On projection methods, convergence and robust formulations in topology optimization'

Equation 1.5 reads:

$$\tilde{\bar{\rho}}_j = \frac{\tanh(\beta\eta) + \tanh(\beta(\tilde{\rho}_j - \eta))}{\tanh(\beta\eta) + \tanh(\beta(1 - \eta))}.$$

10. Ferrari et al. (2020), 'A new generation 99 line Matlab code for compliance topology optimization and its extension to 3D'

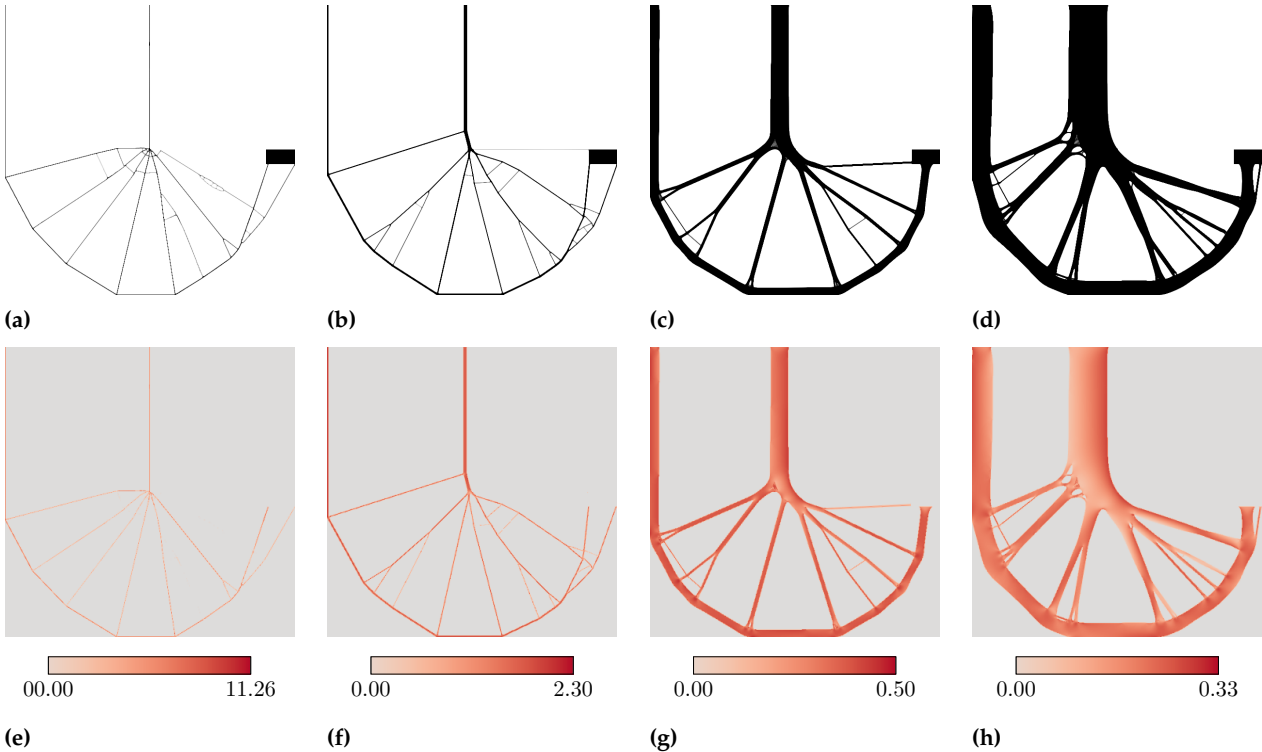


Figure 2.3: (a-d) Topology of the optimized structures for different values of the material allowable $\sigma_L = 10.00, 2.00, 0.40$, and 0.25 , showing a volume fraction of $V_f = 1.60\%, 4.04\%, 18.03\%$ and 34.71% , respectively. (e-h) Von Mises stress distribution for the optimized structures.

[51.](#) Bendsoe et al. (1999), 'Material interpolation schemes in topology optimization'
[52.](#) Hashin et al. (1963), 'A variational approach to the theory of the elastic behaviour of multiphase materials'
[168.](#) Johnson (2007), 'The NLopt nonlinear-optimization package'
[169.](#) Diamond et al. (2016), 'CVXPY: A Python-Embedded Modeling Language for Convex Optimization'
[170.](#) Domahidi et al. (2013), 'ECOS: An SOCP solver for embedded systems'

$\bar{\rho}$, and it is set to 10^{-4} . The aggregation parameter P of the aggregation function G_{KS}^L is set to 32. The SIMP parameters of Equation 1.2 are set to $E_0 = 1$, and $E_{\min} = 10^{-9}$. The value of the penalization parameter p is selected as $p = 3$ because in that way intermediate densities respect the Hashin-Shtrikman (HS) bounds [51, 52]. The optimization is carried out using the NLopt Python optimization package [168], analytically evaluating the sensitivity using Equations 2.15, and 2.23.

The volume minimization TTO problem as formulated in \mathbb{P}_0 represents a LP problem that can be efficiently solved by modern algorithms. In this work, we used the Python package CVXPY 1.2.2 [169] with the ECOS 2.0.7 [170] solver. The joint cost s is set to 0.001 and the stopping criterion is chosen as $\|\Delta x\|_\infty \leq 10^{-8}$. As the formulation is linear, no sensitivity calculation is carried out.

The optimizations presented in this section are performed using a single core on a cluster equipped with an Intel® Xeon® CPU E5-2650 @ 2.20 GHz and using 8 GB of RAM.

CONTINUOUS TOPOLOGY OPTIMIZATION RESULTS We generate multiple optimized structures with different volume fractions V_f by launching

the optimization code for continuous mesh with different values of the material allowable σ_L spanning from 0.2 to 20.

The results obtained for $\sigma_L = 10.00, 2.00, 0.40$ and 0.25 are shown in Fig. 2.3. In the upper part of the figure (a-d), we see the topology of the optimized structures with an increasing volume fraction V_f . Interestingly, the topology of the solution remains almost unchanged, varying principally in the thickness of its members. We notice the classic large fillet around the corner that alleviates the local stress concentration. As the volume decreases, the optimized structure tends to a solution that resembles a truss-like structure, with a reducing fillet radius. In those cases, we know that the topology optimization algorithm acts as a method for the layout of truss-like structures [5]. This effect is caused by the combination of different factors, such as the regularization filter, the mesh size, and the low volume fraction [66].

A summary of the numerical results is presented in Table 2.2. Firstly, we can observe how we successfully controlled the volume fraction V_f by modifying the material resistance σ_L , obtaining results that perfectly follow a monotonically decreasing function. Additionally, as expected, a more voluminous solution also exhibits a lower value of structural compliance. Next, we notice that the optimization processes exhibit long execution times, especially when dealing with extreme cases like low-material resistance and high-volume fractions. This effect is caused by the very fine mesh used to discretize the design domain Ω , the sensitivity calculation using the adjoint method, and the increasing difficulty of satisfying the stress constraints. Furthermore, it is observed that the maximum stress exceeds the material allowable σ_L . This is because we are employing an aggregation function for the stress constraints that estimates the maximum value of the constraint across a group of elements. However, these aggregation methods do not perfectly align with the exact maximum value, which is a recognized limitation.

On top of volume fraction, compliance, and stress, we evaluate an additional metric specific to continuous meshes called the *greyness level* or *measure of non-discreteness* [55] to evaluate the quality of the solutions. It is defined as:

$$M_{nd} = \frac{\sum_e 4\bar{\rho}_e(1 - \bar{\rho}_e)}{n} \times 100\%, \quad (2.37)$$

where results near zero mean a completely black-and-white design. Observing the M_{nd} values in Table 2.2, we notice that all the optimized structures converged to nearly black-and-white solutions, confirming the correct numerical implementation of the problem.

In the lower part of Fig. 2.3 (e-f), we plot the equivalent Von Mises stress for every element of the solution with physical density $\bar{\rho} > 0.5$. Multiple interesting observations can be made. First, we notice that the

5. Bendsøe et al. (1988), 'Generating optimal topologies in structural design using a homogenization method'

66. Sigmund et al. (2016), 'On the (non-)optimality of Michell structures'

55. Sigmund (2007), 'Morphology-based black and white filters for topology optimization'

Table 2.2: Numerical results of the topology optimization method of the L-shape beam load case with varying material allowable σ_L on a 600×600 elements mesh. Numbers in red highlight the results that have not converged.

σ_L	max σ_L	V_f	C	M_{nd}	It.	Time
20.00	23.51	1.18 %	6992	1.91 %	1142	8 h 11 m
10.00	11.26	1.60 %	3837	2.19 %	1147	7 h 55 m
8.00	8.78	1.74 %	2766	1.95 %	792	5 h 39 m
6.00	7.15	1.89 %	2243	1.81 %	806	5 h 35 m
5.00	5.81	2.17 %	1823	1.81 %	849	5 h 53 m
4.00	4.69	2.67 %	1424	2.02 %	894	6 h 12 m
3.00	3.47	3.00 %	1133	1.64 %	993	6 h 45 m
2.00	2.30	4.04 %	781	1.45 %	1189	8 h 20 m
1.00	1.18	7.28 %	404	1.35 %	1621	11 h 41 m
0.90	1.06	8.09 %	365	1.31 %	1656	11 h 36 m
0.80	0.96	8.82 %	332	1.21 %	1937	15 h 21 m
0.70	0.84	10.05 %	292	1.09 %	1827	13 h 21 m
0.60	0.73	11.80 %	250	1.19 %	1955	14 h 21 m
0.50	0.61	14.18 %	213	1.06 %	2032	15 h 39 m
0.40	0.50	18.03 %	170	1.08 %	2259	17 h 6 m
0.35	0.44	21.12 %	148	1.15 %	2421	19 h 29 m
0.30	0.38	26.21 %	126	1.50 %	3100	24 h 46 m
0.25	0.33	34.71 %	104	1.04 %	3484	27 h 39 m
0.20	0.27	48.08 %	77	1.26 %	7500	91 h 46 m

Michell theorized two criteria for optimal truss structures [84] valid when the maximum allowable stress is equal in tension and compression ($\sigma_t = \sigma_c$) and when the supports of the structure are statically determinate. The first one states that all the members of an optimal structure should present internal stress equal in magnitude to the maximum allowable value of the material – i.e. the structure is *fully stressed*. The second criterion asserts that the strain of all the members of the structure should be equal and there should be no other point having a strain higher than this value.

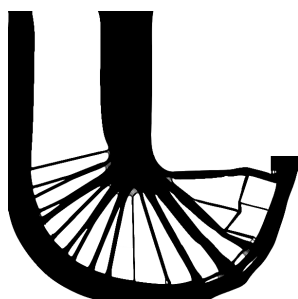


Figure 2.4: The intermediate resulting structure for $\sigma_L = 0.2$ with $V_f = 48.08\%$ after 7500 optimization iterations.

stress distribution is almost uniform in the structure, and it tends to the value of the material allowable σ_L – i.e. we approach a *fully stressed* structure. Even if the geometric support of the theory is different, it looks like the topology-optimized structures follow the Michell criteria presented in Section 1.2.3 for optimal truss structures.

As previously mentioned, our focus lies in exploring the method's limits, particularly at the volume fraction boundaries. When dealing with low-resistance materials – i.e. materials that show a low σ_L , we encounter a scenario where no solution can be attained since no distribution can fulfill the imposed constraints. Throughout our research with this specific test case and mesh size, we did not produce any solutions with a volume fraction exceeding 50%, suggesting we have encountered a limitation of the problem. With this combination of material properties, loading conditions, geometry, and mesh, it appears that there is no feasible solution for $V_f > 50\%$. We notice that the calculation time has significantly increased with the increase of V_f because the algorithm faces greater difficulty in satisfying the stress constraints. Fig. 2.4 shows the topology of the non-converged solution with $\sigma_L = 0.2$, $V_f = 48.08\%$ and over five days of optimization.

Conversely, when dealing with excessively strong material – i.e. materials that show a high σ_L , the optimal scenario would demand such minimal material usage that certain sections of the structure become thinner than the width of a single element. In this case, the mesh used for discretization is too coarse to accurately represent the solution, and finer meshing becomes essential to capture the details of the optimized design. Fig. 2.5 shows the limit case when $\sigma_L = 10.0$ and $V_f = 1.60\%$.

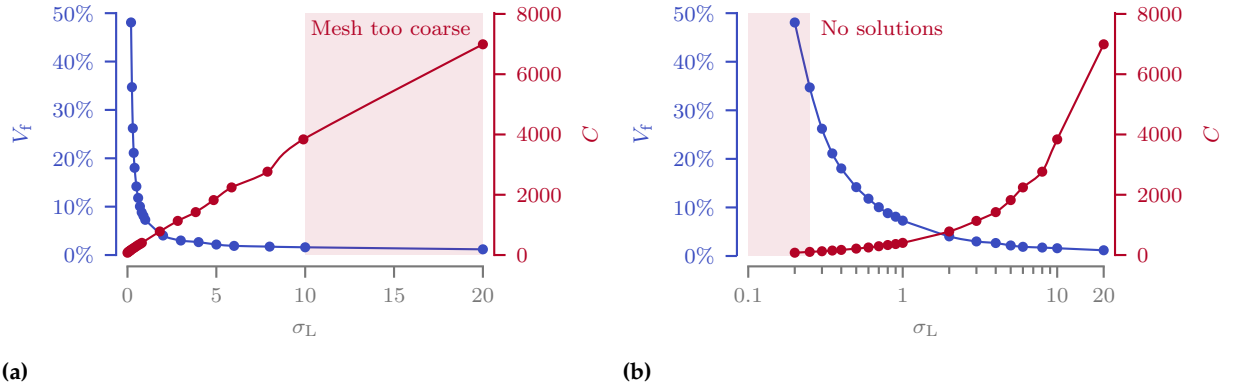


Figure 2.6: Linear (a) and logarithmic (b) plot of the volume fraction V_f and the compliance C with respect to the maximum material allowable σ_L for the continuous mesh structures. Areas in red represent the zones outside the domains of applicability of the applied method.

Finally, in Fig. 2.6 we show the plots summarizing our results, with the method's limits highlighted. To effectively show the different orders of magnitude present in the plot, we have used both linear and logarithmic scales simultaneously. We notice that the volume fraction V_f follows a hyperbolic relationship, while compliance C exhibits a linear correlation with respect to the material allowable σ_L .

TTO OPTIMIZATION RESULTS In this section, we present the optimized structures of the TTO formulation with different values of the material allowable σ_L spanning from 0.2 to 20. Due to the inherent linearity of Formulation \mathbb{P}_0 , the solutions exhibit several intriguing characteristics. Notably, in cases such as the tested L-shaped test case where the structures are not overconstrained and are not subject to asymmetric stress constraints, the formulation aligns with the Michell criteria. Consequently, the topology remains unchanged regardless of the imposed stress limit, and the stress distribution results in a fully stressed structure. Fig. 2.7 provides a visual representation of the optimized topology and the corresponding stress distribution for the different values of the material allowable σ_L . By examining the figure, it is evident that the node positions are constrained by the initial ground structure. The solution resembles half of a spoked wheel, with an irregular distribution of these spokes. One might expect a more evenly distributed arrangement of these spokes. Interestingly, no fillet is formed at the corner of the L-shaped beam. This observation is attributed to the modeling of truss nodes as frictionless joints that do not support moments. However, this aligns with our earlier findings in continuous topology optimization, where the fillet radius diminishes as the volume fraction decreases. Finally, it is crucial to note that in this simple test case with only a single load case, the linear elasticity is inherently considered in the formulation. There is no need to explicitly account for it by imposing kinematic compatibility constraints, as highlighted in previous studies [1, 31, 33].

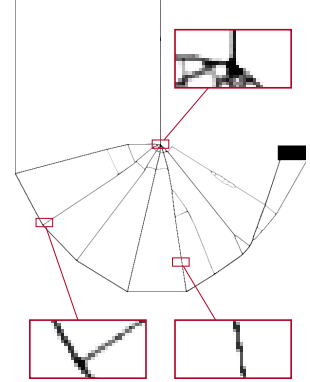


Figure 2.5: The optimized structure for $\sigma_L = 10.0$ with $V_f = 1.60\%$. Some of the structure's features present not even a fully-dense element in their thickness.

1. Bendsøe et al. (2004), 'Topology Optimization'
31. Dorn et al. (1964), 'Automatic design of optimal structures'
33. Hemp (1973), 'Optimum Structures'

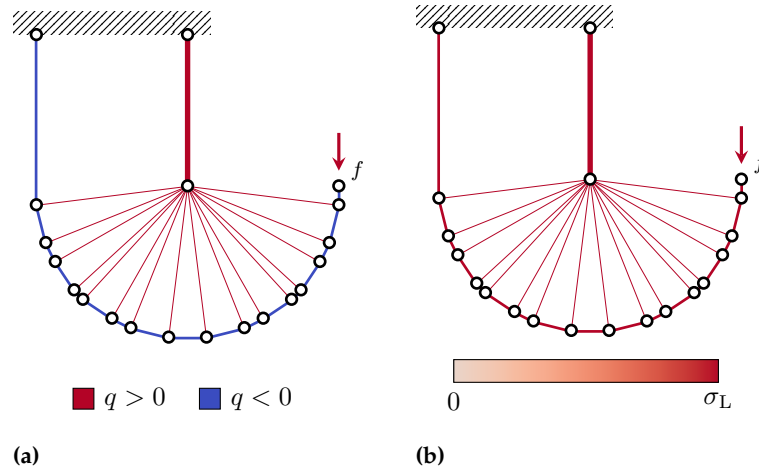


Figure 2.7: Topology (a) and stress distribution (b) plot for the TTO optimized structure of the L-shape beam test case with varying values of the material allowable σ_L on a 33×33 nodes ground structure. The structure topology is invariant with respect to the value of σ_L .

Table 2.3: Numerical results of the TTO method of the L-shape beam test case with varying values of the material allowable σ_L on a 33×33 nodes ground structure. Numbers in red highlight the results that lie outside the domains of applicability of the optimization method.

σ_L	V_f	C	Min λ	Time
50.0	0.12 %	23 282	111.7	1 m 6 s
20.0	0.31 %	9313	70.6	1 m 9 s
10.0	0.62 %	4656	49.9	1 m 18 s
8.0	0.78 %	3725	44.7	1 m 15 s
6.0	1.03 %	2794	38.7	1 m 10 s
5.0	1.24 %	2328	35.3	1 m 24 s
4.0	1.55 %	1863	31.6	1 m 18 s
3.0	2.07 %	1397	27.4	1 m 15 s
2.0	3.10 %	931	22.3	1 m 15 s
1.0	6.21 %	466	15.8	1 m 17 s
0.9	6.90 %	419	15.0	1 m 20 s
0.8	7.76 %	373	14.1	1 m 21 s
0.7	8.87 %	326	13.2	1 m 16 s
0.6	10.35 %	279	12.2	1 m 20 s
0.5	12.42 %	233	11.2	1 m 22 s

The following equation consistently holds for the optimized structures, regardless of the value of σ_L :

$$V^* = \frac{fL}{\sigma_L} \cdot \Gamma, \quad (2.38)$$

where the volume multiplicative constant Γ depends on the load case and the ground structure used to discretize the design space Ω [171]. For this specific test case with the 33×33 nodes ground structure we found $\Gamma = 4.656$. The execution time of the optimization is approximately 90 s and does not change with respect to the maximum stress σ_L . The full numerical results of the multiple optimizations can be found in Table 2.3.

It's worth noting that we have intentionally opted for a dense ground structure here to achieve an element count roughly equivalent to that of the continuous mesh case (305 728 and 270 000 for the TTO and the continuous topology optimization, respectively). We have utilized a fully connected ground structure with 33×33 nodes, but we obtain satisfactory results with just 13×13 nodes (see Fig. 2.8).

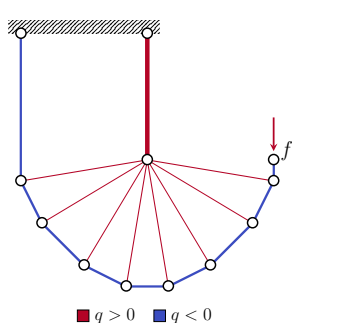


Figure 2.8: Optimized structure obtained using a fully connected ground structure with 13×13 nodes and 7705 candidates.

[171] Lewiński et al. (1994), 'Extended exact solutions for least-weight truss layouts—Part I'

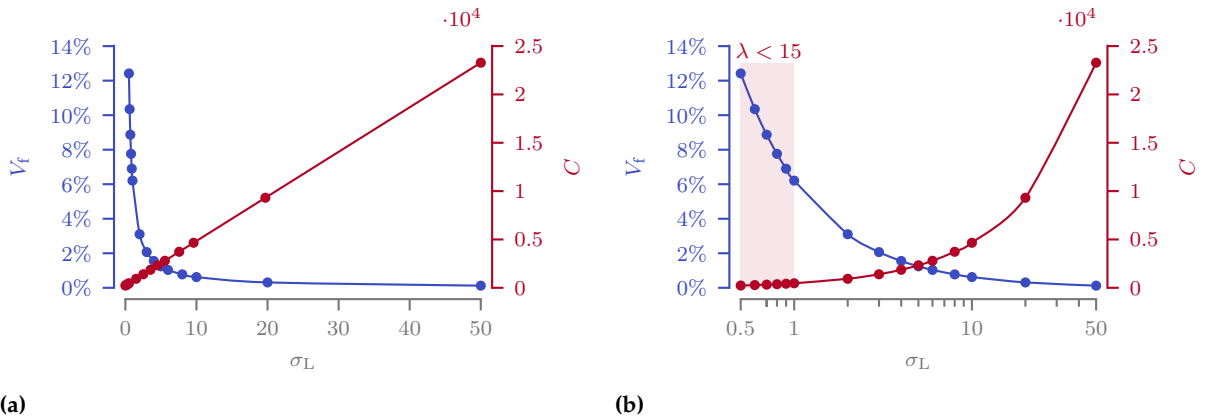


Figure 2.9: Linear (a) and logarithmic (b) plot of the volume fraction V_f and the compliance C with respect to the value of the maximum material allowable σ_L for the TTO optimized structures. Areas in red represent the zones outside the domains of applicability of the truss discretization.

In this case we obtain a volume multiplicative constant $\Gamma = 4.705$, signifying a 1.05 % increase compared to the 33×33 case with $\Gamma = 4.656$. However, the element number is reduced by 97.4 % (305 728 versus 7705 candidates). The computational time for this simplified test case is below one second.

With this example we notice that refining the continuous mesh and refining the ground structure are not equivalent operations. In one case, it allows for representing finer details, while in the other, it permits new shapes for the structure. The choice of the ground structure dictates the final form; it is more restrictive than merely allowing finer details. If bars are missing initially, they will not be added later on.

In assessing solution quality, we employ a distinct metric known as the slenderness ratio, denoted as λ , which represents the ratio between the length and the radius of gyration of the bars of the ground structure. In our specific case, we have established a minimum slenderness ratio of 15. For a bar with a circular cross-sectional area, this corresponds to a radius of R_λ for a bar length of $7.5 R_\lambda$. We highlighted in red the optimized structures that does not respect the minimum slenderness ratio in Table 2.3.

Lastly, Fig. 2.9 provides a visual summary of our findings, emphasizing in red the solutions that do not respect the minimum slenderness ratio $\lambda < 15$. To effectively show the different orders of magnitude present in the plot and how already done for the continuous mesh case, we have used both linear and logarithmic scales simultaneously. In this case, the compliance exhibits a perfectly linear relationship with respect to σ_L , while the volume follows a hyperbolic law in accordance with Equation 2.38.

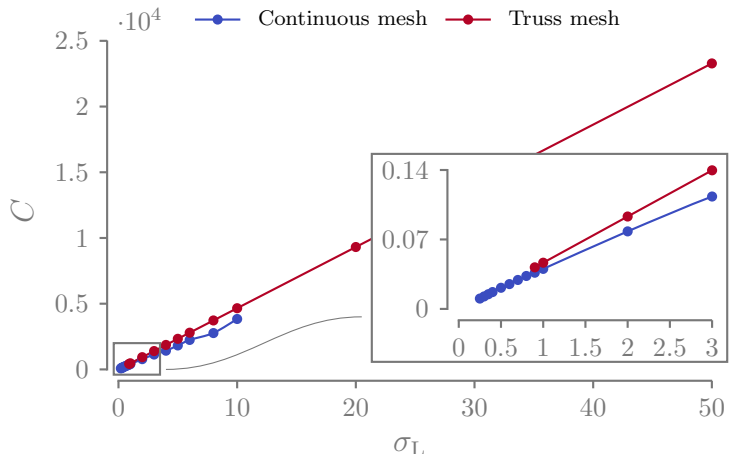


Figure 2.10: Compliance C versus maximum material allowable σ_L plot for the continuous topology optimization and the TTO algorithms.

2.2.3 DISCUSSION

Up until now, we have discussed the results of the continuous topology optimization and the TTO algorithms separately. Here, we provide a comparative analysis by presenting a series of graphs showcasing the key performance indicators considered for both formulations: the maximum material allowable stress σ_L , the compliance C , the volume fraction V_f , and the computational time t . It is important to note that the data presented in these graphs excludes the values that fall outside the methods' limits, highlighted for the two different algorithms in the previous subsections.

Fig. 2.10 depicts the compliance C versus maximum material allowable σ_L graph for the L-shaped beam test case. It is evident that the truss discretization of TTO consistently exhibits lower compliance values for every considered material allowable and maintains a perfectly linear relationship, in contrast to the continuous discretization approach. We speculate that the difference may be attributed to the more complex formulation (non-linearity, use of the filter and projection), potentially causing the continuous approach to converge to a local minimum. It is worth noting that the differences between the two methods reduce for small σ_L values.

In Fig. 2.11 we plot the different volume fractions obtained for a given material allowable (the axis in the graph are swapped as for us the most important figure of merit is the volume fraction). The continuous topology optimization yields structures that are more massive for a given material resistance. This outcome can be attributed not only to the aforementioned non-linearity in the formulation but also to another intriguing phenomenon. When dealing with high volume fractions (see e.g. Fig. 2.3c and d), we observe that the material that compose the “beams” of the structure is distributed across multiple elements, appearing somewhat “smeared”. In contrast, the truss representation concentrates all the structural mass along the line extending from one node to another, putting the material exactly

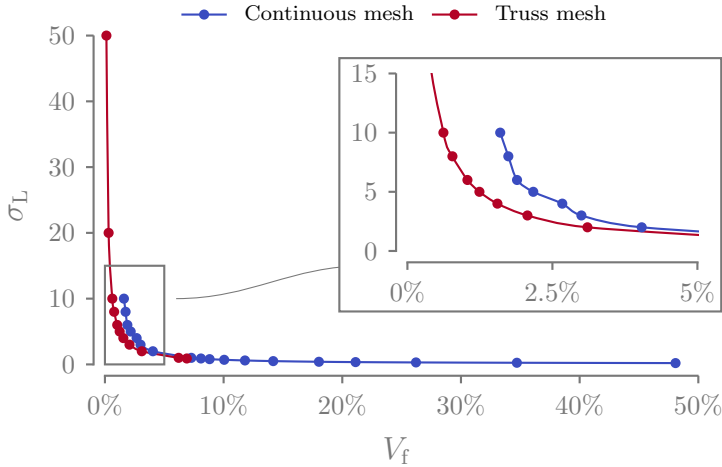


Figure 2.11: Maximum material allowable σ_L versus volume fraction V_f plot for the continuous topology optimization and the TTO algorithms.

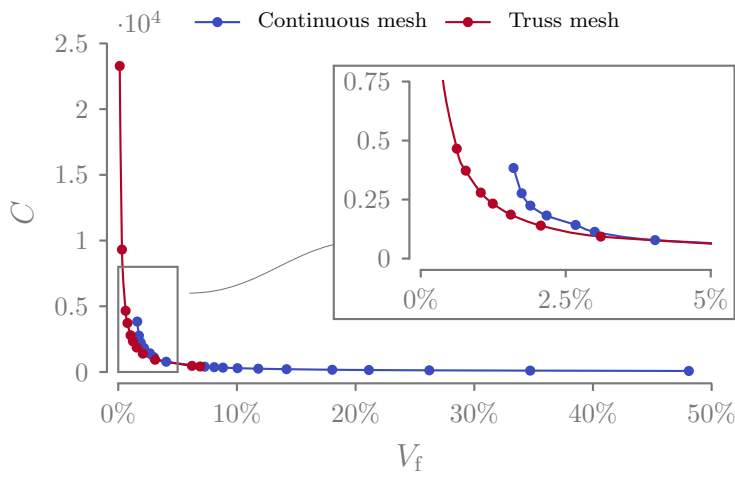


Figure 2.12: Compliance C versus volume fraction V_f plot for the continuous topology optimization and the TTO algorithms.

where needed and being, thus, numerically more efficient. This fact happens because the truss representation is an idealization, and it emphasizes the importance of ensuring that the chosen discretization remains within its applicable domain.

We can also observe that the truss representation serves as the lower limit of the topology optimization. We speculate that improving the convergence of the continuous topology optimization could potentially lead to results approaching those provided by the TTO algorithm. Interestingly, both discretizations follow a similar trend for high-volume fractions, despite the significant disparity in their physical description models. The very same trends can be observed watching the volume-compliance graph of Fig. 2.12.

Finally, in Fig. 2.13 we turn our attention to the computational time comparison between the two optimization methods. It is noteworthy that a consistent three-order of magnitude difference is observed between the two methods (days vs. minutes) for every value of V_f . Additionally, it's worth recalling that for this specific test case, employing an extremely fine ground structure is not always a necessity, as we were able to obtain similar results (slightly more than 1 % volume

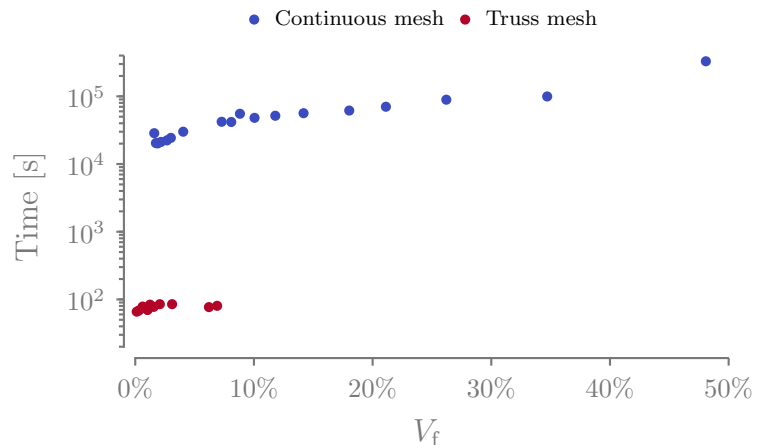


Figure 2.13: Computational time t versus volume fraction V_f plot for the continuous topology optimization and the TTO algorithms.

difference) with coarser ground structures (97 % fewer bars). This fact implies that the calculation time difference between continuous topology optimization and TTO could potentially be even bigger.

The notable difference in computation time for stress-based continuous topology optimization (which is not self-adjoint, in contrast to compliance minimization) points to the potential for exploring SAND approaches for continuous topology optimization. It's worth mentioning that SAND approaches typically lead to a substantial increase in the number of design variables⁴, but could be beneficial when advanced mechanical constraints are used. In TTO problems, this is less of a concern due to the use of the ground structure approach, which results in numerous cross-sectional area design variables and fewer displacement-related ones. This, however, does not hold when dealing with a continuous mesh. While preliminary studies in this direction have been conducted [172], they lie beyond the scope of this thesis and will not be further investigated.

To sum up, the advantages of the TTO optimization algorithm become evident when considering the limitations of continuous discretization for optimizing ultralight structures. The first key drawback of continuous topology optimization is its increasing need for more elements to correctly discretize low-volume fraction structures, substantially augmenting computational time. Additionally, continuous topology optimization faces several numerical challenges, such as the need for constraints aggregation and relaxation. The optimization formulation proposed in this chapter addresses these problems but introduces another drawback: stress limit in optimized structures often exceed the specified allowable limit. To address this challenge, multiple approaches have been proposed within the aggregation framework to accurately account for the true constraint value, like using a set of active stress constraints [173], several aggregation clusters [174] or rectifier functions [175]. However, all of these strategies come at the cost of increased computation time. Furthermore, stress constraints in continuous discretization are often defined for equivalent von Mises

4: In the SAND approach the displacements \mathbf{u} are no more evaluated using the linear Finite Element Method (FEM) equation $\mathbf{K}\mathbf{u} = \mathbf{f}$, but used as design variables of the optimization.

172. Munro et al. (2017), 'Local stress-constrained and slope-constrained SAND topology optimisation'

173. Bruggi et al. (2012), 'Topology optimization for minimum weight with compliance and stress constraints'

174. París et al. (2010), 'Block aggregation of stress constraints in topology optimization of structures'

175. Norato et al. (2022), 'A maximum-rectifier-function approach to stress-constrained topology optimization'

stress, making it more challenging to distinguish between asymmetric bounds for tension and compression. New failure criteria should then be implemented. Finally, the optimization of ultralight structures naturally tends to result in truss-like topologies regardless of the chosen optimization formulation. These structures are naturally subject to local buckling as a mode of failure [66], a phenomenon that is difficult to describe when using continuous elements.

While truss discretization offers advantages in terms of computational efficiency, it does come with certain limitations. In the minimum volume formulation, the problem is linear and cost-effective to solve. However, the linearity is lost when additional constraints, such as local buckling, are introduced. Moreover, as the FEM equation $\mathbf{K}\mathbf{u} = \mathbf{f}$ is never explicitly solved during the optimization, the SAND formulation does not inherently account for the kinematic compatibility of the displacements and the forces of the problem. This limitation restricts its applicability to relatively simple problems, as those presented in this chapter, where kinematic compatibility was inherently satisfied. Issues can arise, however, when dealing with complex scenarios involving multiple loads or constraints that may lead to structures that are statically indeterminate. These limitations are well-known in the literature of TTO and should be taken into account during the optimization if we decide to pursue the development of the optimization algorithm using the TTO framework.

2.3 CONCLUSION

Since the first developments of the topology optimization method, it has been recognized that "For moderately low volume fractions the lay-out of truss-like structures is predicted, but for very low volume fractions it is recommended that the traditional lay-out theory be employed..." [35]. However, the performance gap has never been quantified, nor has the domain of applicability been assessed. Additionally, it's important to note that these assumptions were primarily based on compliance formulations and not on volume minimization formulations, which are more pertinent to the aeronautical context.

In this chapter, we assessed the suitability of employing the TTO algorithm for the optimization of ultralight structures by quantifying the disparities between continuous topology optimization and TTO under the volume minimization under strength constraints formulation. We introduced a standardized two-dimensional test case, the L-shaped beam, commonly utilized in stress-based optimization scenarios. Multiple optimization runs are conducted for both discretization methods, employing various materials, and the results are subsequently compared, with a primary focus on volume fraction, compliance, stress, and computational time in the optimized structures.

⁶⁶. Sigmund et al. (2016), 'On the (non-)optimality of Michell structures'

³⁵. Bendsøe (1989), 'Optimal shape design as a material distribution problem'

The sensitivity calculation is easier, as the different design variables are not explicitly dependent on each other.

Considering the limitations encountered with the continuous approach, particularly at very low volume fractions, we opted to pursue our optimization algorithm development using the Truss Topology Optimization (TTO) framework. The use of a ground structure to discretize the design space is more coherent with the type of structures we are working on, and the use of the SAND approach permits to drastically reduce the computational time and to take into account additional constraints more easily. We also identified certain limitations inherent to truss discretizations, namely the need to take into account the kinematic compatibility of the structure and the local buckling failure mode, which will be addressed in the following chapter.

BIBLIOGRAPHY

- [1] Bendsøe, Martin P. and Sigmund, Ole, 'Topology Optimization'. Berlin, Heidelberg: Springer Berlin Heidelberg, 2004. cited on pages 1, 6, 9, 13, 29, 31, 37
ISBN: [978-3-642-07698-5](#) [978-3-662-05086-6](#)
- [2] Martins, Joaquim R. R. A. and Ning, Andrew, 'Engineering Design Optimization', 1st ed. Cambridge University Press, Nov. 2021. cited on pages 2, 6, 30
ISBN: [978-1-108-98064-7](#) [978-1-108-83341-7](#)
- [3] Prager, W. and Taylor, J. E., 'Problems of Optimal Structural Design', *Journal of Applied Mechanics* 35.1 (Mar. 1968), pp. 102–106. cited on page 3
DOI: [10.1115/1.3601120](#)
- [4] Prager, William, 'Optimality Criteria in Structural Design', *Proceedings of the National Academy of Sciences of the United States of America* 61.3 (1968), Publisher: National Academy of Sciences, pp. 794–796. cited on page 3
- [5] Bendsøe, Martin Philip and Kikuchi, Noboru, 'Generating optimal topologies in structural design using a homogenization method', *Computer Methods in Applied Mechanics and Engineering* 71.2 (Nov. 1988), pp. 197–224. cited on pages 3, 6, 17, 18, 35
DOI: [10.1016/0045-7825\(88\)90086-2](#)
- [6] Bendsøe, Martin P., 'Optimization of Structural Topology, Shape, and Material'. Berlin, Heidelberg: Springer Berlin Heidelberg, 1995. cited on page 3
ISBN: [978-3-662-03117-9](#) [978-3-662-03115-5](#)
- [7] Sigmund, O., 'A 99 line topology optimization code written in Matlab', *Structural and Multidisciplinary Optimization* 21.2 (Apr. 2001), pp. 120–127. cited on page 3
DOI: [10.1007/s001580050176](#)
- [8] Allaire, Grégoire, Belhachmi, Zakaria, and Jouve, François, 'The homogenization method for topology and shape optimization. Single and multiple loads case', *Revue Européenne des Éléments Finis* 5.5-6 (Jan. 1996), pp. 649–672. cited on page 3
DOI: [10.1080/12506559.1996.10511241](#)
- [9] Li, Weichen, Suryanarayana, Phanish, and Paulino, Glaucio H., 'Accelerated fixed-point formulation of topology optimization: Application to compliance minimization problems', *Mechanics Research Communications* 103 (Jan. 2020), p. 103469. cited on page 3
DOI: [10.1016/j.mechrescom.2019.103469](#)

- cited on pages 3, 33
- [10] Ferrari, Federico and Sigmund, Ole, 'A new generation 99 line Matlab code for compliance topology optimization and its extension to 3D', *Structural and Multidisciplinary Optimization* 62.4 (Oct. 2020), pp. 2211–2228.
DOI: [10.1007/s00158-020-02629-w](https://doi.org/10.1007/s00158-020-02629-w)
- cited on page 3
- [11] Anderson, Donald G., 'Iterative Procedures for Nonlinear Integral Equations', *Journal of the ACM* 12.4 (Oct. 1965), pp. 547–560.
DOI: [10.1145/321296.321305](https://doi.org/10.1145/321296.321305)
- cited on page 4
- [12] Conn, Andrew R., Scheinberg, Katya, and Vicente, Luis N., 'Introduction to Derivative-Free Optimization'. Society for Industrial and Applied Mathematics, Jan. 2009.
ISBN: [978-0-89871-668-9](https://doi.org/978-0-89871-668-9) [978-0-89871-876-8](https://doi.org/978-0-89871-876-8)
- cited on page 4
- [13] Audet, Charles and Hare, Warren, 'Derivative-Free and Black-box Optimization', Springer Series in Operations Research and Financial Engineering. Cham: Springer International Publishing, 2017.
ISBN: [978-3-319-68912-8](https://doi.org/978-3-319-68912-8) [978-3-319-68913-5](https://doi.org/978-3-319-68913-5)
- cited on page 4
- [14] Simon, Dan, 'Evolutionary optimization algorithms: biologically-inspired and population-based approaches to computer intelligence', 1. ed. Hoboken, NJ: Wiley, 2013.
ISBN: [978-1-118-65950-2](https://doi.org/978-1-118-65950-2) [978-0-470-93741-9](https://doi.org/978-0-470-93741-9)
- cited on page 4
- [15] Balamurugan, R., Ramakrishnan, C. V., and Swaminathan, N., 'A two phase approach based on skeleton convergence and geometric variables for topology optimization using genetic algorithm', *Structural and Multidisciplinary Optimization* 43.3 (Mar. 2011), pp. 381–404.
DOI: [10.1007/s00158-010-0560-4](https://doi.org/10.1007/s00158-010-0560-4)
- cited on page 4
- [16] Sigmund, Ole, 'On the usefulness of non-gradient approaches in topology optimization', *Structural and Multidisciplinary Optimization* 43.5 (May 2011), pp. 589–596.
DOI: [10.1007/s00158-011-0638-7](https://doi.org/10.1007/s00158-011-0638-7)
- cited on page 4
- [17] Luh, Guan-Chun and Lin, Chun-Yi, 'Structural topology optimization using ant colony optimization algorithm', *Applied Soft Computing* 9.4 (Sept. 2009), pp. 1343–1353.
DOI: [10.1016/j.asoc.2009.06.001](https://doi.org/10.1016/j.asoc.2009.06.001)
- cited on page 4
- [18] Luh, Guan-Chun, Lin, Chun-Yi, and Lin, Yu-Shu, 'A binary particle swarm optimization for continuum structural topology optimization', *Applied Soft Computing*, The Impact of Soft Computing for the Progress of Artificial Intelligence 11.2 (Mar. 2011), pp. 2833–2844.
DOI: [10.1016/j.asoc.2010.11.013](https://doi.org/10.1016/j.asoc.2010.11.013)

- [19] Stolpe, M., 'Global optimization of minimum weight truss topology problems with stress, displacement, and local buckling constraints using branch-and-bound', *International Journal for Numerical Methods in Engineering* 61.8 (2004), pp. 1270–1309.
doi: <https://doi.org/10.1002/nme.1112> cited on page 4
- [20] Mattheck, C. and Burkhardt, S., 'A new method of structural shape optimization based on biological growth', *International Journal of Fatigue* 12.3 (May 1990), pp. 185–190.
doi: [10.1016/0142-1123\(90\)90094-U](https://doi.org/10.1016/0142-1123(90)90094-U) cited on page 4
- [21] Xie, Y. M. and Steven, G. P., 'A simple evolutionary procedure for structural optimization', *Computers & Structures* 49.5 (Dec. 1993), pp. 885–896.
doi: [10.1016/0045-7949\(93\)90035-C](https://doi.org/10.1016/0045-7949(93)90035-C) cited on page 4
- [22] Manickarajah, D, Xie, Y. M, and Steven, G. P., 'An evolutionary method for optimization of plate buckling resistance', *Finite Elements in Analysis and Design* 29.3 (June 1998), pp. 205–230.
doi: [10.1016/S0168-874X\(98\)00012-2](https://doi.org/10.1016/S0168-874X(98)00012-2) cited on page 4
- [23] Young, V., Querin, O. M., Steven, G. P., and Xie, Y. M., '3D and multiple load case bi-directional evolutionary structural optimization (BESO)', *Structural optimization* 18.2 (Oct. 1999), pp. 183–192.
doi: [10.1007/BF01195993](https://doi.org/10.1007/BF01195993) cited on page 4
- [24] Kraft, Dieter, 'A software package for sequential quadratic programming', *Tech. Rep. DFVLR-FB 88-28, DLR German Aerospace Center — Institute for Flight Mechanics, Koln, Germany.* (1988). cited on page 5
- [25] Svanberg, Krister, 'The method of moving asymptotes—a new method for structural optimization', *International Journal for Numerical Methods in Engineering* 24.2 (1987), pp. 359–373.
doi: <https://doi.org/10.1002/nme.1620240207> cited on pages 5, 33
- [26] Svanberg, Krister, 'A Class of Globally Convergent Optimization Methods Based on Conservative Convex Separable Approximations', *SIAM Journal on Optimization* 12.2 (Jan. 2002), Publisher: Society for Industrial and Applied Mathematics, pp. 555–573.
doi: [10.1137/S1052623499362822](https://doi.org/10.1137/S1052623499362822) cited on page 5
- [27] Bruyneel, M., Duysinx, P., and Fleury, C., 'A family of MMA approximations for structural optimization', *Structural and Multidisciplinary Optimization* 24.4 (Oct. 2002), pp. 263–276.
doi: [10.1007/s00158-002-0238-7](https://doi.org/10.1007/s00158-002-0238-7) cited on page 5
- [28] Fleury, Claude and Braibant, Vincent, 'Structural optimization: A new dual method using mixed variables', *International Journal for Numerical Methods in Engineering* 23.3 (1986), pp. 409–428.
doi: [10.1002/nme.1620230307](https://doi.org/10.1002/nme.1620230307) cited on page 5

- cited on page 5
- [29] Wächter, Andreas and Biegler, Lorenz T., 'On the implementation of an interior-point filter line-search algorithm for large-scale nonlinear programming', *Mathematical Programming* 106.1 (Mar. 2006), pp. 25–57.
 DOI: [10.1007/s10107-004-0559-y](https://doi.org/10.1007/s10107-004-0559-y)
- cited on page 5
- [30] Rojas Labanda, Susana and Stolpe, Mathias, 'Benchmarking optimization solvers for structural topology optimization', *Structural and Multidisciplinary Optimization* 52 (Sept. 2015).
 DOI: [10.1007/s00158-015-1250-z](https://doi.org/10.1007/s00158-015-1250-z)
- cited on pages 5, 10, 12, 13, 31, 37
- [31] Dorn, W. S., Gomory, Ralph E., and Greenberg, H., 'Automatic design of optimal structures', *J. Mécanique* (1964).
- cited on pages 5, 12
- [32] Chan, H. S. Y., 'Optimum structural design and linear programming', *College of Aeronautics Report Aero* 175 (1964), Publisher: College of Aeronautics Cranfield.
- cited on pages 5, 10, 12, 37
- [33] Hemp, W. S., 'Optimum Structures'. Clarendon Press, 1973, Google-Books-ID: cJhpAAAAMAAJ.
 ISBN: [978-0-19-856110-1](https://www.googleapis.com/books/v1/info?isbn=9780198561101)
- cited on page 6
- [34] Sankaranarayanan, S., Haftka, Raphael T., and Kapuria, Rakesh K., 'Truss topology optimization with simultaneous analysis and design', *AIAA Journal* 32.2 (Feb. 1994), pp. 420–424.
 DOI: [10.2514/3.12000](https://doi.org/10.2514/3.12000)
- cited on pages 6, 7, 17, 18, 32, 43
- [35] Bendsøe, M. P., 'Optimal shape design as a material distribution problem', *Structural optimization* 1.4 (Dec. 1989), pp. 193–202.
 DOI: [10.1007/BF01650949](https://doi.org/10.1007/BF01650949)
- cited on page 6
- [36] Sigmund, Ole, 'Materials with prescribed constitutive parameters: An inverse homogenization problem', *International Journal of Solids and Structures* 31.17 (Sept. 1994), pp. 2313–2329.
 DOI: [10.1016/0020-7683\(94\)90154-6](https://doi.org/10.1016/0020-7683(94)90154-6)
- cited on pages 6, 20, 21
- [37] Zhang, Weihong and Sun, Shiping, 'Scale-related topology optimization of cellular materials and structures', *International Journal for Numerical Methods in Engineering* 68.9 (2006), pp. 993–1011.
 DOI: [10.1002/nme.1743](https://doi.org/10.1002/nme.1743)
- cited on page 6
- [38] Collet, Maxime, Noël, Lise, Bruggi, Matteo, and Duysinx, Pierre, 'Topology optimization for microstructural design under stress constraints', *Structural and Multidisciplinary Optimization* 58.6 (Dec. 2018), pp. 2677–2695.
 DOI: [10.1007/s00158-018-2045-9](https://doi.org/10.1007/s00158-018-2045-9)
- cited on page 6
- [39] Borrvall, Thomas and Petersson, Joakim, 'Topology optimization of fluids in Stokes flow', *International Journal for Numerical Methods in Fluids* 41.1 (2003), pp. 77–107.
 DOI: [10.1002/fld.426](https://doi.org/10.1002/fld.426)

- [40] Bruyneel, M. and Duysinx, P., 'Note on topology optimization of continuum structures including self-weight', *Structural and Multidisciplinary Optimization* 29.4 (Apr. 2005), pp. 245–256.
DOI: [10.1007/s00158-004-0484-y](https://doi.org/10.1007/s00158-004-0484-y)
- [41] Sigmund, Ole, 'Manufacturing tolerant topology optimization', *Acta Mechanica Sinica* 25.2 (Apr. 2009), pp. 227–239.
DOI: [10.1007/s10409-009-0240-z](https://doi.org/10.1007/s10409-009-0240-z)
- [42] Brackett, D, Ashcroft, I, and Hague, R, 'Topology Optimization for Additive Manufacturing' (2011), p. 15.
DOI: [10.26153/tsw/15300](https://doi.org/10.26153/tsw/15300)
- [43] Sigmund, Ole, 'On the Design of Compliant Mechanisms Using Topology Optimization*', *Mechanics of Structures and Machines* 25.4 (Jan. 1997), Publisher: Taylor & Francis, pp. 493–524.
DOI: [10.1080/08905459708945415](https://doi.org/10.1080/08905459708945415)
- [44] Bruns, Tyler E. and Tortorelli, Daniel A., 'Topology optimization of non-linear elastic structures and compliant mechanisms', *Computer Methods in Applied Mechanics and Engineering* 190.26 (Mar. 2001), pp. 3443–3459.
DOI: [10.1016/S0045-7825\(00\)00278-4](https://doi.org/10.1016/S0045-7825(00)00278-4)
- [45] Wang, Weiming, Munro, Dirk, Wang, Charlie C. L., Keulen, Fred van, and Wu, Jun, 'Space-time topology optimization for additive manufacturing', *Structural and Multidisciplinary Optimization* 61.1 (Jan. 2020), pp. 1–18.
DOI: [10.1007/s00158-019-02420-6](https://doi.org/10.1007/s00158-019-02420-6)
- [46] Allaire, Grégoire, Jouve, François, and Toader, Anca-Maria, 'A level-set method for shape optimization', *Comptes Rendus Mathematique* 334.12 (Jan. 2002), pp. 1125–1130.
DOI: [10.1016/S1631-073X\(02\)02412-3](https://doi.org/10.1016/S1631-073X(02)02412-3)
- [47] Wang, Michael Yu, Wang, Xiaoming, and Guo, Dongming, 'A level set method for structural topology optimization', *Computer Methods in Applied Mechanics and Engineering* 192.1 (Jan. 2003), pp. 227–246.
DOI: [10.1016/S0045-7825\(02\)00559-5](https://doi.org/10.1016/S0045-7825(02)00559-5)
- [48] Allaire, Grégoire, Jouve, François, and Toader, Anca-Maria, 'Structural optimization using sensitivity analysis and a level-set method', *Journal of Computational Physics* 194.1 (Feb. 2004), pp. 363–393.
DOI: [10.1016/j.jcp.2003.09.032](https://doi.org/10.1016/j.jcp.2003.09.032)
- [49] Tortorelli, D. A. and Michaleris, P., 'Design sensitivity analysis: Overview and review', *Inverse Problems in Engineering* 1.1 (Oct. 1994), pp. 71–105.
DOI: [10.1080/174159794088027573](https://doi.org/10.1080/174159794088027573)

cited on pages 7, 9, 33

- [50] Wang, Fengwen, Lazarov, Boyan Stefanov, and Sigmund, Ole, 'On projection methods, convergence and robust formulations in topology optimization', *Structural and Multidisciplinary Optimization* 43.6 (June 2011), pp. 767–784.
 DOI: [10.1007/s00158-010-0602-y](https://doi.org/10.1007/s00158-010-0602-y)

cited on pages 7, 8, 34

- [51] Bendsøe, M. P. and Sigmund, O., 'Material interpolation schemes in topology optimization', *Archive of Applied Mechanics* 69.9 (Nov. 1999), pp. 635–654.
 DOI: [10.1007/s004190050248](https://doi.org/10.1007/s004190050248)

cited on pages 8, 34

- [52] Hashin, Z. and Shtrikman, S., 'A variational approach to the theory of the elastic behaviour of multiphase materials', *Journal of the Mechanics and Physics of Solids* 11.2 (Mar. 1963), pp. 127–140.
 DOI: [10.1016/0022-5096\(63\)90060-7](https://doi.org/10.1016/0022-5096(63)90060-7)

cited on page 8

- [53] Díaz, A. and Sigmund, O., 'Checkerboard patterns in layout optimization', *Structural optimization* 10.1 (Aug. 1995), pp. 40–45.
 DOI: [10.1007/BF01743693](https://doi.org/10.1007/BF01743693)

cited on page 8

- [54] Sigmund, Ole, 'Design of Material Structures using Topology Optimization', PhD thesis, Technical University of Denmark, DK-2800 Lyngby, 1994.

cited on pages 8, 33, 35

- [55] Sigmund, Ole, 'Morphology-based black and white filters for topology optimization', *Structural and Multidisciplinary Optimization* 33.4 (Apr. 2007), pp. 401–424.
 DOI: [10.1007/s00158-006-0087-x](https://doi.org/10.1007/s00158-006-0087-x)

cited on page 9

- [56] Allaire, G. and Francfort, G. A., 'A Numerical Algorithm for Topology and Shape Optimization', *Topology Design of Structures*, NATO ASI Series, ed. by Bendsøe, Martin Philip and Soares, Carlos A. Mota, Dordrecht: Springer Netherlands, 1993, pp. 239–248, ISBN: 978-94-011-1804-0.
 DOI: [10.1007/978-94-011-1804-0_16](https://doi.org/10.1007/978-94-011-1804-0_16)

cited on page 9

- [57] Allaire, G. and Kohn, R. V., 'Topology Optimization and Optimal Shape Design Using Homogenization', *Topology Design of Structures*, NATO ASI Series, ed. by Bendsøe, Martin Philip and Soares, Carlos A. Mota, Dordrecht: Springer Netherlands, 1993, pp. 207–218, ISBN: 978-94-011-1804-0.
 DOI: [10.1007/978-94-011-1804-0_14](https://doi.org/10.1007/978-94-011-1804-0_14)

cited on page 9

- [58] Rozvany, G. I. N., 'A critical review of established methods of structural topology optimization', *Structural and Multidisciplinary Optimization* 37.3 (Jan. 2009), pp. 217–237.
 DOI: [10.1007/s00158-007-0217-0](https://doi.org/10.1007/s00158-007-0217-0)

cited on page 9

- [59] Petersson, Joakim and Sigmund, Ole, 'Slope constrained topology optimization', *International Journal for Numerical Methods in Engineering* 41.8 (1998), _eprint: <https://onlinelibrary.wiley.com/doi/10.100>

- 0207%2819980430%2941%3A8%3C1417%3A%3AAID-NME344%3E3.0.CO%3B2-N, pp. 1417–1434.
 doi: [10.1002/\(SICI\)1097-0207\(19980430\)41:8<1417::AID-NME344>3.0.CO;2-N](#)
- [60] Rojas-Labanda, Susana and Stolpe, Mathias, 'Automatic penalty continuation in structural topology optimization', *Structural and Multidisciplinary Optimization* 52.6 (Dec. 2015), pp. 1205–1221.
 doi: [10.1007/s00158-015-1277-1](#)
- [61] Zhou, Ming, Fleury, Raphael, Shyy, Yaw-Kang, Thomas, Harold, and Brennan, Jeffrey, 'Progress in Topology Optimization with Manufacturing Constraints', *9th AIAA/ISSMO Symposium on Multidisciplinary Analysis and Optimization*, Atlanta, Georgia: American Institute of Aeronautics and Astronautics, Sept. 2002, ISBN: 978-1-62410-120-5.
 doi: [10.2514/6.2002-5614](#)
- [62] Liu, Jikai, Gaynor, Andrew T., Chen, Shikui, Kang, Zhan, Suresh, Krishnan, Takezawa, Akihiro, Li, Lei, Kato, Junji, Tang, Jinyuan, Wang, Charlie C. L., Cheng, Lin, Liang, Xuan, and To, Albert C., 'Current and future trends in topology optimization for additive manufacturing', *Structural and Multidisciplinary Optimization* 57.6 (June 2018), Company: Springer Distributor: Springer Institution: Springer Label: Springer Number: 6 Publisher: Springer Berlin Heidelberg, pp. 2457–2483.
 doi: [10.1007/s00158-018-1994-3](#)
- [63] Aage, Niels, Andreassen, Erik, Lazarov, Boyan S., and Sigmund, Ole, 'Giga-voxel computational morphogenesis for structural design', *Nature* 550.7674 (Oct. 2017), Number: 7674 Publisher: Nature Publishing Group, pp. 84–86.
 doi: [10.1038/nature23911](#)
- [64] Salazar de Troya, Miguel A. and Tortorelli, Daniel A., 'Adaptive mesh refinement in stress-constrained topology optimization', *Structural and Multidisciplinary Optimization* 58.6 (Dec. 2018), pp. 2369–2386.
 doi: [10.1007/s00158-018-2084-2](#)
- [65] Zhang, Shanglong, Gain, Arun L., and Norato, Julián A., 'Adaptive mesh refinement for topology optimization with discrete geometric components', *Computer Methods in Applied Mechanics and Engineering* 364 (June 2020), p. 112930.
 doi: [10.1016/j.cma.2020.112930](#)
- [66] Sigmund, Ole, Aage, Niels, and Andreassen, Erik, 'On the (non-)optimality of Michell structures', *Structural and Multidisciplinary Optimization* 54.2 (Aug. 2016), pp. 361–373.
 doi: [10.1007/s00158-016-1420-7](#)

- cited on page 10
- [67] Wein, Fabian, Dunning, Peter D., and Norato, Julián A., 'A review on feature-mapping methods for structural optimization', *Structural and Multidisciplinary Optimization* 62.4 (Oct. 2020), pp. 1597–1638.
DOI: [10.1007/s00158-020-02649-6](https://doi.org/10.1007/s00158-020-02649-6)
- cited on page 10
- [68] Guo, Xu, Zhang, Weisheng, and Zhong, Wenliang, 'Doing Topology Optimization Explicitly and Geometrically—A New Moving Morphable Components Based Framework', *Journal of Applied Mechanics* 81.8 (May 2014).
DOI: [10.1115/1.4027609](https://doi.org/10.1115/1.4027609)
- cited on page 10
- [69] Zhang, Weisheng, Li, Dong, Yuan, Jie, Song, Junfu, and Guo, Xu, 'A new three-dimensional topology optimization method based on moving morphable components (MMCs)', *Computational Mechanics* 59.4 (Apr. 2017), pp. 647–665.
DOI: [10.1007/s00466-016-1365-0](https://doi.org/10.1007/s00466-016-1365-0)
- cited on page 10
- [70] Norato, J. A., Bell, B. K., and Tortorelli, D. A., 'A geometry projection method for continuum-based topology optimization with discrete elements', *Computer Methods in Applied Mechanics and Engineering* 293 (Aug. 2015), pp. 306–327.
DOI: [10.1016/j.cma.2015.05.005](https://doi.org/10.1016/j.cma.2015.05.005)
- cited on page 10
- [71] Zhang, Shanglong, Norato, Julián A., Gain, Arun L., and Lyu, Naesung, 'A geometry projection method for the topology optimization of plate structures', *Structural and Multidisciplinary Optimization* 54.5 (Nov. 2016), pp. 1173–1190.
DOI: [10.1007/s00158-016-1466-6](https://doi.org/10.1007/s00158-016-1466-6)
- cited on page 10
- [72] Coniglio, Simone, Morlier, Joseph, Gogu, Christian, and Amargier, Rémi, 'Generalized Geometry Projection: A Unified Approach for Geometric Feature Based Topology Optimization', *Archives of Computational Methods in Engineering* 27.5 (Nov. 2020), pp. 1573–1610.
DOI: [10.1007/s11831-019-09362-8](https://doi.org/10.1007/s11831-019-09362-8)
- cited on page 10
- [73] Kazemi, Hesaneh, Vaziri, Ashkan, and Norato, Julián A., 'Multi-material topology optimization of lattice structures using geometry projection', *Computer Methods in Applied Mechanics and Engineering* 363 (May 2020), p. 112895.
DOI: [10.1016/j.cma.2020.112895](https://doi.org/10.1016/j.cma.2020.112895)
- cited on pages 10, 26
- [74] Cheng, G. D. and Guo, X., ' ε -relaxed approach in structural topology optimization', *Structural optimization* 13.4 (June 1997), pp. 258–266.
DOI: [10.1007/BF01197454](https://doi.org/10.1007/BF01197454)
- cited on pages 10, 26
- [75] Rozvany, G.I.N., 'On design-dependent constraints and singular topologies', *Structural and Multidisciplinary Optimization* 21.2 (Apr. 2001), pp. 164–172.
DOI: [10.1007/s001580050181](https://doi.org/10.1007/s001580050181)

- [76] Gao, Xingjun and Ma, Haitao, 'Topology optimization of continuum structures under buckling constraints', *Computers & Structures* 157 (Sept. 2015), pp. 142–152.
DOI: [10.1016/j.comstruc.2015.05.020](https://doi.org/10.1016/j.comstruc.2015.05.020) cited on page 10
- [77] He, Linwei, Gilbert, Matthew, and Song, Xingyi, 'A Python script for adaptive layout optimization of trusses', *Structural and Multidisciplinary Optimization* 60.2 (Aug. 2019), pp. 835–847.
DOI: [10.1007/s00158-019-02226-6](https://doi.org/10.1007/s00158-019-02226-6) cited on page 11
- [78] Kirsch, Uri, 'Optimal topologies of truss structures', *Computer Methods in Applied Mechanics and Engineering* 72.1 (Jan. 1989), pp. 15–28.
DOI: [10.1016/0045-7825\(89\)90119-9](https://doi.org/10.1016/0045-7825(89)90119-9) cited on pages 11, 31
- [79] Rozvany, G. I. N., Bendsøe, M. P., and Kirsch, U., 'Layout Optimization of Structures', *Applied Mechanics Reviews* 48.2 (Feb. 1995), pp. 41–119.
DOI: [10.1115/1.3005097](https://doi.org/10.1115/1.3005097) cited on pages 11, 31
- [80] Kirsch, Uri, 'Optimal design of trusses by approximate compatibility', *Computers & Structures* 12.1 (July 1980), pp. 93–98.
DOI: [10.1016/0045-7949\(80\)90097-8](https://doi.org/10.1016/0045-7949(80)90097-8) cited on page 11
- [81] Cheng, G., 'Some aspects of truss topology optimization', *Structural Optimization* 10.3-4 (Dec. 1995), pp. 173–179.
DOI: [10.1007/BF01742589](https://doi.org/10.1007/BF01742589) cited on page 11
- [82] Achitziger, W., 'Local stability of trusses in the context of topology optimization Part I: Exact modelling', *Structural Optimization* 17.4 (Dec. 1999), pp. 235–246.
DOI: [10.1007/BF01206999](https://doi.org/10.1007/BF01206999) cited on page 11
- [83] Maxwell, J. Clerk, 'I.—On Reciprocal Figures, Frames, and Diagrams of Forces', *Earth and Environmental Science Transactions of The Royal Society of Edinburgh* 26.1 (1870), Publisher: Royal Society of Edinburgh Scotland Foundation, pp. 1–40.
DOI: [10.1017/S0080456800026351](https://doi.org/10.1017/S0080456800026351) cited on page 11
- [84] Michell, A. G. M., 'The limits of economy of material in frame-structures', *The London, Edinburgh, and Dublin Philosophical Magazine and Journal of Science* 8.47 (Nov. 1904), pp. 589–597.
DOI: [10.1080/14786440409463229](https://doi.org/10.1080/14786440409463229) cited on pages 11, 13, 36
- [85] Gilbert, Matthew and Tyas, Andrew, 'Layout optimization of large-scale pin-jointed frames', *Engineering Computations* 20.8 (Dec. 2003), pp. 1044–1064.
DOI: [10.1108/02644400310503017](https://doi.org/10.1108/02644400310503017) cited on page 13
- [86] Pedersen, Pauli, 'Optimal Joint Positions for Space Trusses', *Journal of the Structural Division* 99.12 (Dec. 1973), Publisher: American Society of Civil Engineers, pp. 2459–2476.
DOI: [10.1061/\(JSDEAG.0003669](https://doi.org/10.1061/(JSDEAG.0003669) cited on page 13

- cited on page 13
- [87] Achtziger, Wolfgang, 'On simultaneous optimization of truss geometry and topology', *Structural and Multidisciplinary Optimization* 33.4 (Apr. 2007), pp. 285–304.
DOI: [10.1007/s00158-006-0092-0](https://doi.org/10.1007/s00158-006-0092-0)
- cited on page 13
- [88] Descamps, Benoît and Filomeno Coelho, Rajan, 'A lower-bound formulation for the geometry and topology optimization of truss structures under multiple loading', *Structural and Multidisciplinary Optimization* 48.1 (July 2013), pp. 49–58.
DOI: [10.1007/s00158-012-0876-3](https://doi.org/10.1007/s00158-012-0876-3)
- cited on page 13
- [89] He, L. and Gilbert, M., 'Rationalization of trusses generated via layout optimization', *Structural and Multidisciplinary Optimization* 52.4 (Oct. 2015), pp. 677–694.
DOI: [10.1007/s00158-015-1260-x](https://doi.org/10.1007/s00158-015-1260-x)
- cited on page 13
- [90] Lu, Hongjia and Xie, Yi Min, 'Reducing the number of different members in truss layout optimization', *Structural and Multidisciplinary Optimization* 66.3 (Feb. 2023), p. 52.
DOI: [10.1007/s00158-023-03514-y](https://doi.org/10.1007/s00158-023-03514-y)
- cited on page 13
- [91] Savine, Florent, Irisarri, François-Xavier, Julien, Cédric, Vincenti, Angela, and Guerin, Yannick, 'A component-based method for the optimization of stiffener layout on large cylindrical rib-stiffened shell structures', *Structural and Multidisciplinary Optimization* 64.4 (Oct. 2021), pp. 1843–1861.
DOI: [10.1007/s00158-021-02945-9](https://doi.org/10.1007/s00158-021-02945-9)
- cited on pages 13, 31
- [92] Parkes, E.W., 'Joints in optimum frameworks', *International Journal of Solids and Structures* 11.9 (Sept. 1975), pp. 1017–1022.
DOI: [10.1016/0020-7683\(75\)90044-X](https://doi.org/10.1016/0020-7683(75)90044-X)
- cited on pages 14, 15, 17
- [93] Schaedler, Tobias A. and Carter, William B., 'Architected Cellular Materials', *Annual Review of Materials Research* 46.1 (July 2016), pp. 187–210.
DOI: [10.1146/annurev-matsci-070115-031624](https://doi.org/10.1146/annurev-matsci-070115-031624)
- cited on pages 14, 17, 18
- [94] Kohn, Robert V. and Strang, Gilbert, 'Optimal design and relaxation of variational problems', *Communications on Pure and Applied Mathematics* 39.1 (1986), pp. 113–137.
DOI: [10.1002/cpa.3160390107](https://doi.org/10.1002/cpa.3160390107)
- cited on pages 14, 17, 18
- [95] Allaire, G. and Aubry, S., 'On optimal microstructures for a plane shape optimization problem', *Structural optimization* 17.2 (Apr. 1999), pp. 86–94.
DOI: [10.1007/BF01195933](https://doi.org/10.1007/BF01195933)
- cited on page 14
- [96] Fleck, N. A., Deshpande, V. S., and Ashby, M. F., 'Micro-architected materials: past, present and future', *Proceedings of the Royal Society A: Mathematical, Physical and Engineering Sciences* 466.2121 (Sept. 2010), Publisher: Royal Society, pp. 2495–2516.
DOI: [10.1098/rspa.2010.0215](https://doi.org/10.1098/rspa.2010.0215)

- [97] NZ, Bernard Spragg, 'Hypholoma fasciculare,' Apr. 2023. cited on page 14
URL: <https://www.flickr.com/photos/volvob12b/52833345708/>
- [98] LIBRARY, STEVE GSCHMEISSNER/SCIENCE PHOTO, 'Leaf structure, SEM'. cited on page 14
URL: <https://www.sciencephoto.com/media/30288/view/leaf-structure-sem>
- [99] gripspix (mostly off, health issues), 'Wing of a dragonfly, detail', Aug. 2007. cited on page 14
URL: <https://www.flickr.com/photos/gripspix/1233292309/>
- [100], 'bone_03'. cited on page 14
URL: https://archimorph.files.wordpress.com/2010/01/bone_03.jpg
- [101] Ashby, M. F., 'Materials selection in mechanical design', 2nd ed. Oxford, OX ; Boston, MA: Butterworth-Heinemann, 1999. ISBN: 978-0-7506-4357-3 cited on page 14
- [102] Bensoussan, Alain, Lions, J.-L., and Papanicolaou, George, 'Asymptotic analysis for periodic structures', Studies in mathematics and its applications v. 5. Amsterdam ; New York : New York: North-Holland Pub. Co. ; sole distributors for the U.S.A. and Canada, Elsevier North-Holland, 1978. ISBN: 978-0-444-85172-7 cited on pages 15, 20
- [103] Dai, G. M. and Zhang, W. H., 'Size effects of basic cell in static analysis of sandwich beams', *International Journal of Solids and Structures* 45.9 (May 2008), pp. 2512–2533. doi: [10.1016/j.ijsolstr.2007.12.007](https://doi.org/10.1016/j.ijsolstr.2007.12.007) cited on page 15
- [104] Kalamkarov, Alexander L., Andrianov, Igor V., and Dani-shevs'kyy, Vladyslav V., 'Asymptotic Homogenization of Composite Materials and Structures', *Applied Mechanics Reviews* 62.3 (Mar. 2009). doi: [10.1115/1.3090830](https://doi.org/10.1115/1.3090830) cited on pages 15, 20
- [105] Coelho, P. G., Amiano, L. D., Guedes, J. M., and Rodrigues, H. C., 'Scale-size effects analysis of optimal periodic material microstructures designed by the inverse homogenization method', *Computers & Structures*, CIVIL-COMP 174 (Oct. 2016), pp. 21–32. doi: [10.1016/j.compstruc.2015.10.001](https://doi.org/10.1016/j.compstruc.2015.10.001) cited on pages 15, 20
- [106] Zhang, Yan, Xiao, Mi, Li, Hao, Gao, Liang, and Chu, Sheng, 'Multiscale concurrent topology optimization for cellular structures with multiple microstructures based on ordered SIMP interpolation', *Computational Materials Science* 155 (Dec. 2018), pp. 74–91. doi: [10.1016/j.commatsci.2018.08.030](https://doi.org/10.1016/j.commatsci.2018.08.030) cited on pages 15, 19

- cited on pages 15–17
- [107] Cramer, Nicholas B., Cellucci, Daniel W., Formoso, Olivia B., Gregg, Christine E., Jenett, Benjamin E., Kim, Joseph H., Lendraitis, Martynas, Swei, Sean S., Trinh, Greenfield T., Trinh, Khanh V., and Cheung, Kenneth C., 'Elastic shape morphing of ultralight structures by programmable assembly', *Smart Materials and Structures* 28.5 (Apr. 2019), p. 055006.
 doi: [10.1088/1361-665X/ab0ea2](https://doi.org/10.1088/1361-665X/ab0ea2)
- cited on pages 15, 16
- [108] Evans, A. G., He, M. Y., Deshpande, V. S., Hutchinson, John W., Jacobsen, A. J., and Barvosa-Carter, W., 'Concepts for Enhanced Energy Absorption Using Hollow Micro-Lattices', *International Journal of Impact Engineering* (2010).
 doi: [10.1016/j.ijimpeng.2010.03.007](https://doi.org/10.1016/j.ijimpeng.2010.03.007)
- cited on pages 15, 16
- [109] Schaedler, Tobias A., Ro, Christopher J., Sorensen, Adam E., Eckel, Zak, Yang, Sophia S., Carter, William B., and Jacobsen, Alan J., 'Designing Metallic Microlattices for Energy Absorber Applications', *Advanced Engineering Materials* 16.3 (2014), pp. 276–283.
 doi: [10.1002/adem.201300206](https://doi.org/10.1002/adem.201300206)
- cited on pages 15, 16
- [110] Ozdemir, Zuhal, Hernandez-Nava, Everth, Tyas, Andrew, Warren, James A., Fay, Stephen D., Goodall, Russell, Todd, Iain, and Askes, Harm, 'Energy absorption in lattice structures in dynamics: Experiments', *International Journal of Impact Engineering* 89 (Mar. 2016), pp. 49–61.
 doi: [10.1016/j.ijimpeng.2015.10.007](https://doi.org/10.1016/j.ijimpeng.2015.10.007)
- cited on page 16
- [111] Opgenoord, Max M. and Willcox, Karen E., 'Aeroelastic Tailoring using Additively Manufactured Lattice Structures', 2018 *Multidisciplinary Analysis and Optimization Conference*, Atlanta, Georgia: American Institute of Aeronautics and Astronautics, June 2018.
 doi: [10.2514/6.2018-4055](https://doi.org/10.2514/6.2018-4055)
- cited on page 16
- [112] Hutmacher, Dietmar W., 'Scaffolds in tissue engineering bone and cartilage', *Biomaterials, Orthopaedic Polymeric Biomaterials: Applications of Biodegradables* 21.24 (Dec. 2000), pp. 2529–2543.
 doi: [10.1016/S0142-9612\(00\)00121-6](https://doi.org/10.1016/S0142-9612(00)00121-6)
- cited on page 16
- [113] Mota, Carlos, Puppi, Dario, Chiellini, Federica, and Chiellini, Emo, 'Additive manufacturing techniques for the production of tissue engineering constructs', *Journal of Tissue Engineering and Regenerative Medicine* 9.3 (Mar. 2015), pp. 174–190.
 doi: [10.1002/tterm.1635](https://doi.org/10.1002/tterm.1635)
- cited on page 16
- [114] Nikolova, Maria P. and Chavali, Murthy S., 'Recent advances in biomaterials for 3D scaffolds: A review', *Bioactive Materials* 4 (Oct. 2019), pp. 271–292.
 doi: [10.1016/j.bioactmat.2019.10.005](https://doi.org/10.1016/j.bioactmat.2019.10.005)

- [115] Lu, T. J., Stone, Howard A., and Ashby, M. F., 'Heat transfer in open-cell metal foams', *Acta Materialia* 46.10 (June 1998), Publisher: Elsevier Limited, pp. 3619–3635.
DOI: [10.1016/S1359-6454\(98\)00031-7](https://doi.org/10.1016/S1359-6454(98)00031-7) cited on page 16
- [116] Wadley, Haydn N. G. and Queheillalt, Douglas T., 'Thermal Applications of Cellular Lattice Structures', *Materials Science Forum* 539-543 (2007), Conference Name: THERMEC 2006, pp. 242–247.
DOI: [10.4028/www.scientific.net/MSF.539-543.242](https://doi.org/10.4028/www.scientific.net/MSF.539-543.242) cited on page 16
- [117] AirShowConsultants, 'The REAL monster from Loch Ness – Vickers Wellington', June 2013.
URL: <https://shortfinals.org/2013/06/15/the-real-monster-from-loch-ness-vickers-wellington-r-for-robert/> cited on page 16
- [118] Cheung, Kenneth C. and Gershenfeld, Neil, 'Reversibly Assembled Cellular Composite Materials', *Science* 341.6151 (Sept. 2013), Publisher: American Association for the Advancement of Science Section: Report, pp. 1219–1221.
DOI: [10.1126/science.1240889](https://doi.org/10.1126/science.1240889) cited on pages 16, 17
- [119] Jenett, Benjamin, Calisch, Sam, Cellucci, Daniel, Cramer, Nick, Gershenfeld, Neil, Swei, Sean, and Cheung, Kenneth C., 'Digital Morphing Wing: Active Wing Shaping Concept Using Composite Lattice-Based Cellular Structures', *Soft Robotics* 4.1 (Mar. 2017), pp. 33–48.
DOI: [10.1089/soro.2016.0032](https://doi.org/10.1089/soro.2016.0032) cited on pages 16, 17
- [120] Dong, Liang, Deshpande, Vikram, and Wadley, Haydn, 'Mechanical response of Ti–6Al–4V octet-truss lattice structures', *International Journal of Solids and Structures* 60-61 (May 2015), pp. 107–124.
DOI: [10.1016/j.ijsolstr.2015.02.020](https://doi.org/10.1016/j.ijsolstr.2015.02.020) cited on pages 16, 17
- [121] Stolpe, Mathias, 'Fail-safe truss topology optimization', *Structural and Multidisciplinary Optimization* 60.4 (Oct. 2019), pp. 1605–1618.
DOI: [10.1007/s00158-019-02295-7](https://doi.org/10.1007/s00158-019-02295-7) cited on pages 16, 17
- [122] Wu, Jun, Sigmund, Ole, and Groen, Jeroen P., 'Topology optimization of multi-scale structures: a review', *Structural and Multidisciplinary Optimization* (Mar. 2021).
DOI: [10.1007/s00158-021-02881-8](https://doi.org/10.1007/s00158-021-02881-8) cited on pages 16–20
- [123] Hunt, Christopher J., Wisnom, Michael R., and Woods, Benjamin K. S., 'WrapToR composite truss structures: Improved process and structural efficiency', *Composite Structures* 230 (Dec. 2019), p. 111467.
DOI: [10.1016/j.compstruct.2019.111467](https://doi.org/10.1016/j.compstruct.2019.111467) cited on pages 16, 17

- cited on pages 16, 18
- [124] Gershenfeld, Neil, Carney, Matthew, Jenett, Benjamin, Calisch, Sam, and Wilson, Spencer, 'Macrofabrication with Digital Materials: Robotic Assembly', *Architectural Design* 85.5 (2015), pp. 122–127.
 DOI: [10.1002/ad.1964](https://doi.org/10.1002/ad.1964)
- cited on pages 16, 18
- [125] Jenett, Ben and Cheung, Kenneth, 'BILL-E: Robotic Platform for Locomotion and Manipulation of Lightweight Space Structures', *25th AIAA/AHS Adaptive Structures Conference*, Grapevine, Texas: American Institute of Aeronautics and Astronautics, Jan. 2017.
 DOI: [10.2514/6.2017-1876](https://doi.org/10.2514/6.2017-1876)
- cited on pages 16, 18
- [126] Costa, Allan, Jenett, Benjamin, Kostitsyna, Irina, Abdel-Rahman, Amira, Gershenfeld, Neil, and Cheung, Kenneth, 'Algorithmic Approaches to Reconfigurable Assembly Systems', *arXiv:2008.11925 [cs]* (Aug. 2020), arXiv: 2008.11925.
 DOI: [10.1109/AERO.2019.8741572](https://doi.org/10.1109/AERO.2019.8741572)
- cited on pages 16, 18
- [127] Niehs, Eike, Schmidt, Arne, Scheffer, Christian, Biediger, Daniel E., Yannuzzi, Michael, Jenett, Benjamin, Abdel-Rahman, Amira, Cheung, Kenneth C., Becker, Aaron T., and Fekete, Sándor P., 'Recognition and Reconfiguration of Lattice-Based Cellular Structures by Simple Robots', *2020 IEEE International Conference on Robotics and Automation (ICRA)*, ISSN: 2577-087X, May 2020, pp. 8252–8259.
 DOI: [10.1109/ICRA40945.2020.9196700](https://doi.org/10.1109/ICRA40945.2020.9196700)
- cited on pages 16–18
- [128] Deshpande, V. S., Ashby, M. F., and Fleck, N. A., 'Foam topology: bending versus stretching dominated architectures', *Acta Materialia* 49.6 (Apr. 2001), pp. 1035–1040.
 DOI: [10.1016/S1359-6454\(00\)00379-7](https://doi.org/10.1016/S1359-6454(00)00379-7)
- cited on pages 17, 18
- [129] Ashby, M.f, 'The properties of foams and lattices', *Philosophical Transactions of the Royal Society A: Mathematical, Physical and Engineering Sciences* 364.1838 (Jan. 2006), Publisher: Royal Society, pp. 15–30.
 DOI: [10.1098/rsta.2005.1678](https://doi.org/10.1098/rsta.2005.1678)
- cited on pages 17, 18
- [130] Zhou, M. and Rozvany, G. I. N., 'The COC algorithm, Part II: Topological, geometrical and generalized shape optimization', *Computer Methods in Applied Mechanics and Engineering*, Second World Congress on Computational Mechanics 89.1 (Aug. 1991), pp. 309–336.
 DOI: [10.1016/0045-7825\(91\)90046-9](https://doi.org/10.1016/0045-7825(91)90046-9)
- cited on page 18
- [131] Rodrigues, H., Guedes, J.M., and Bendsoe, M.P., 'Hierarchical optimization of material and structure', *Structural and Multi-disciplinary Optimization* 24.1 (Aug. 2002), pp. 1–10.
 DOI: [10.1007/s00158-002-0209-z](https://doi.org/10.1007/s00158-002-0209-z)

- [132] Pantz, O. and Trabelsi, K., 'A Post-Treatment of the Homogenization Method for Shape Optimization', *SIAM Journal on Control and Optimization* 47.3 (Jan. 2008), Publisher: Society for Industrial and Applied Mathematics, pp. 1380–1398.
doi: [10.1137/070688900](https://doi.org/10.1137/070688900) cited on page 18
- [133] Groen, Jeroen P. and Sigmund, Ole, 'Homogenization-based topology optimization for high-resolution manufacturable microstructures', *International Journal for Numerical Methods in Engineering* 113.8 (2018), _eprint: <https://onlinelibrary.wiley.com/doi/pdf/10.1002/nme.5575>, pp. 1148–1163.
doi: [10.1002/nme.5575](https://doi.org/10.1002/nme.5575) cited on pages 18–20
- [134] Wang, Chuang, Gu, Xiaojun, Zhu, Jihong, Zhou, Han, Li, Shaoying, and Zhang, Weihong, 'Concurrent design of hierarchical structures with three-dimensional parameterized lattice microstructures for additive manufacturing', *Structural and Multidisciplinary Optimization* 61.3 (Mar. 2020), pp. 869–894.
doi: [10.1007/s00158-019-02408-2](https://doi.org/10.1007/s00158-019-02408-2) cited on page 18
- [135] Guedes, JoséMiranda and Kikuchi, Noboru, 'Preprocessing and postprocessing for materials based on the homogenization method with adaptive finite element methods', *Computer Methods in Applied Mechanics and Engineering* 83.2 (Oct. 1990), pp. 143–198.
doi: [10.1016/0045-7825\(90\)90148-F](https://doi.org/10.1016/0045-7825(90)90148-F) cited on pages 18, 19
- [136] Allaire, Grégoire, Geoffroy-Donders, Perle, and Pantz, Olivier, 'Topology optimization of modulated and oriented periodic microstructures by the homogenization method', *Computers & Mathematics with Applications, Simulation for Additive Manufacturing* 78.7 (Oct. 2019), pp. 2197–2229.
doi: [10.1016/j.camwa.2018.08.007](https://doi.org/10.1016/j.camwa.2018.08.007) cited on page 19
- [137] Geoffroy-Donders, Perle, Allaire, Grégoire, and Pantz, Olivier, '3-d topology optimization of modulated and oriented periodic microstructures by the homogenization method', *Journal of Computational Physics* 401 (Jan. 2020), p. 108994.
doi: [10.1016/j.jcp.2019.108994](https://doi.org/10.1016/j.jcp.2019.108994) cited on page 19
- [138] Kumar, Tej and Suresh, Krishnan, 'A density-and-strain-based K-clustering approach to microstructural topology optimization', *Structural and Multidisciplinary Optimization* 61.4 (Apr. 2020), pp. 1399–1415.
doi: [10.1007/s00158-019-02422-4](https://doi.org/10.1007/s00158-019-02422-4) cited on page 19
- [139] Xia, Liang and Breitkopf, Piotr, 'Multiscale structural topology optimization with an approximate constitutive model for local material microstructure', *Computer Methods in Applied Mechanics and Engineering* 286 (Apr. 2015), pp. 147–167.
doi: [10.1016/j.cma.2014.12.018](https://doi.org/10.1016/j.cma.2014.12.018) cited on page 19

- cited on page 19
- [140] Wang, Chuang, Zhu, Ji Hong, Zhang, Wei Hong, Li, Shao Ying, and Kong, Jie, 'Concurrent topology optimization design of structures and non-uniform parameterized lattice microstructures', *Structural and Multidisciplinary Optimization* 58.1 (July 2018), pp. 35–50.
 DOI: [10.1007/s00158-018-2009-0](https://doi.org/10.1007/s00158-018-2009-0)
- cited on page 19
- [141] Imediegwu, Chikwesiri, Murphy, Ryan, Hewson, Robert, and Santer, Matthew, 'Multiscale structural optimization towards three-dimensional printable structures', *Structural and Multidisciplinary Optimization* 60.2 (Aug. 2019), pp. 513–525.
 DOI: [10.1007/s00158-019-02220-y](https://doi.org/10.1007/s00158-019-02220-y)
- cited on pages 19, 20
- [142] Kim, Cheolwoong, Lee, Jaewook, and Yoo, Jeonghoon, 'Machine learning-combined topology optimization for functionary graded composite structure design', *Computer Methods in Applied Mechanics and Engineering* 387 (Dec. 2021), p. 114158.
 DOI: [10.1016/j.cma.2021.114158](https://doi.org/10.1016/j.cma.2021.114158)
- cited on pages 19, 20
- [143] White, Daniel A., Arrighi, William J., Kudo, Jun, and Watts, Seth E., 'Multiscale topology optimization using neural network surrogate models', *Computer Methods in Applied Mechanics and Engineering* 346 (Apr. 2019), pp. 1118–1135.
 DOI: [10.1016/j.cma.2018.09.007](https://doi.org/10.1016/j.cma.2018.09.007)
- cited on pages 19, 20
- [144] Chandrasekhar, Aaditya and Suresh, Krishnan, 'Multi-Material Topology Optimization Using Neural Networks', *Computer-Aided Design* 136 (July 2021), p. 103017.
 DOI: [10.1016/j.cad.2021.103017](https://doi.org/10.1016/j.cad.2021.103017)
- cited on pages 19, 20
- [145] Wang, Liwei, Liu, Zhao, Da, Daicong, Chan, Yu-Chin, Chen, Wei, and Zhu, Ping, 'Enhancing Data-driven Multiscale Topology Optimization with Generalized De-homogenization', Dec. 2021.
 URL: <https://arxiv.org/abs/2112.02506v2>
- cited on pages 19, 20
- [146] Duriez, Edouard, Morlier, Joseph, Charlotte, Miguel, and Azzaro-Pantel, Catherine, 'A well connected, locally-oriented and efficient multi-scale topology optimization (EMTO) strategy', *Structural and Multidisciplinary Optimization* 64.6 (Dec. 2021), pp. 3705–3728.
 DOI: [10.1007/s00158-021-03048-1](https://doi.org/10.1007/s00158-021-03048-1)
- cited on pages 19, 20
- [147] Sigmund, Ole, 'On benchmarking and good scientific practise in topology optimization', *Structural and Multidisciplinary Optimization* 65.11 (Oct. 2022), p. 315.
 DOI: [10.1007/s00158-022-03427-2](https://doi.org/10.1007/s00158-022-03427-2)
- cited on page 20
- [148] Cheng, Lin, Bai, Jiaxi, and To, Albert C., 'Functionally graded lattice structure topology optimization for the design of additive manufactured components with stress constraints', *Computer Methods in Applied Mechanics and Engineering* 344 (Feb. 2019), pp. 334–359.

- DOI: [10.1016/j.cma.2018.10.010](https://doi.org/10.1016/j.cma.2018.10.010)
- [149] Huang, X. and Xie, Y. M., 'Optimal design of periodic structures using evolutionary topology optimization', *Structural and Multidisciplinary Optimization* 36.6 (Nov. 2008), pp. 597–606.
DOI: [10.1007/s00158-007-0196-1](https://doi.org/10.1007/s00158-007-0196-1) cited on pages 20, 21
- [150] Tugilimana, Alexis, Coelho, Rajan Filomeno, and Thrall, Ashley P., 'An integrated design methodology for modular trusses including dynamic grouping, module spatial orientation, and topology optimization', *Structural and Multidisciplinary Optimization* 60.2 (Aug. 2019), pp. 613–638.
DOI: [10.1007/s00158-019-02230-w](https://doi.org/10.1007/s00158-019-02230-w) cited on pages 20, 21
- [151] Bakker, Coen, Zhang, Lidan, Higginson, Kristie, and Keulen, Fred van, 'Simultaneous optimization of topology and layout of modular stiffeners on shells and plates', *Structural and Multidisciplinary Optimization* 64.5 (Nov. 2021), pp. 3147–3161.
DOI: [10.1007/s00158-021-03081-0](https://doi.org/10.1007/s00158-021-03081-0) cited on pages 20, 21
- [152] Tugilimana, Alexis, Thrall, Ashley P., Descamps, Benoît, and Coelho, Rajan Filomeno, 'Spatial orientation and topology optimization of modular trusses', *Structural and Multidisciplinary Optimization* 55.2 (Feb. 2017), pp. 459–476.
DOI: [10.1007/s00158-016-1501-7](https://doi.org/10.1007/s00158-016-1501-7) cited on pages 20, 21
- [153] Stromberg, Lauren L., Beghini, Alessandro, Baker, William F., and Paulino, Glaucio H., 'Application of layout and topology optimization using pattern gradation for the conceptual design of buildings', *Structural and Multidisciplinary Optimization* 43.2 (Feb. 2011), pp. 165–180.
DOI: [10.1007/s00158-010-0563-1](https://doi.org/10.1007/s00158-010-0563-1) cited on page 21
- [154] Wu, Jun, Dick, Christian, and Westermann, Rüdiger, 'A System for High-Resolution Topology Optimization', *IEEE Transactions on Visualization and Computer Graphics* 22.3 (Mar. 2016), Conference Name: IEEE Transactions on Visualization and Computer Graphics, pp. 1195–1208.
DOI: [10.1109/TVCG.2015.2502588](https://doi.org/10.1109/TVCG.2015.2502588) cited on page 21
- [155] Stragiotti, Enrico, Irisarri, François-Xavier, Julien, Cédric, and Morlier, Joseph, 'Towards manufactured lattice structures: a comparison between layout and topology optimization', *AeroBest 2021 International Conference on Multidisciplinary Design Optimization of Aerospace Systems. Book of proceedings*, Lisbon, Portugal: ECCOMAS, July 2021, pp. 229–244. cited on page 23
- [156] Achtziger, Wolfgang and Kanzow, Christian, 'Mathematical programs with vanishing constraints: optimality conditions and constraint qualifications', *Mathematical Programming* 114.1 (July 2008), pp. 69–99.
DOI: [10.1007/s10107-006-0083-3](https://doi.org/10.1007/s10107-006-0083-3) cited on page 24

- cited on page 24
- [157] Cheng, Gengdong and Jiang, Zheng, 'Study on Topology Optimization with Stress Constraints', *Engineering Optimization* 20.2 (Nov. 1992), pp. 129–148.
 doi: [10.1080/03052159208941276](https://doi.org/10.1080/03052159208941276)
- cited on pages 25–27, 33
- [158] Verbart, Alexander, Langelaar, Matthijs, and Keulen, Fred van, 'A unified aggregation and relaxation approach for stress-constrained topology optimization', *Structural and Multidisciplinary Optimization* 55.2 (Feb. 2017), pp. 663–679.
 doi: [10.1007/s00158-016-1524-0](https://doi.org/10.1007/s00158-016-1524-0)
- cited on pages 25, 32
- [159] Duysinx, P. and Bendsøe, M. P., 'Topology optimization of continuum structures with local stress constraints', *International Journal for Numerical Methods in Engineering* 43.8 (1998), pp. 1453–1478.
 doi: [10.1002/\(SICI\)1097-0207\(19981230\)43:8<1453::AID-NME480>3.0.CO;2-2](https://doi.org/10.1002/(SICI)1097-0207(19981230)43:8<1453::AID-NME480>3.0.CO;2-2)
- cited on pages 25, 26, 32
- [160] Le, Chau, Norato, Julian, Bruns, Tyler, Ha, Christopher, and Tortorelli, Daniel, 'Stress-based topology optimization for continua', *Structural and Multidisciplinary Optimization* 41.4 (Apr. 2010), pp. 605–620.
 doi: [10.1007/s00158-009-0440-y](https://doi.org/10.1007/s00158-009-0440-y)
- cited on page 26
- [161] Holmberg, Erik, Torstenfelt, Bo, and Klarbring, Anders, 'Stress constrained topology optimization', *Structural and Multidisciplinary Optimization* 48.1 (2013), pp. 33–47.
 doi: [10.1007/s00158-012-0880-7](https://doi.org/10.1007/s00158-012-0880-7)
- cited on page 26
- [162] Silva, Gustavo Assis da, Beck, André Teófilo, and Sigmund, Ole, 'Stress-constrained topology optimization considering uniform manufacturing uncertainties', *Computer Methods in Applied Mechanics and Engineering* 344 (Feb. 2019), pp. 512–537.
 doi: [10.1016/j.cma.2018.10.020](https://doi.org/10.1016/j.cma.2018.10.020)
- cited on page 26
- [163] Stolpe, Mathias, 'On Models and Methods for Global Optimization of Structural Topology', Publisher: Matematik, PhD thesis, 2003.
- cited on page 26
- [164] Sved, G. and Ginos, Z., 'Structural optimization under multiple loading', *International Journal of Mechanical Sciences* 10.10 (Oct. 1968), pp. 803–805.
 doi: [10.1016/0020-7403\(68\)90021-0](https://doi.org/10.1016/0020-7403(68)90021-0)
- cited on page 27
- [165] Silva, Gustavo Assis da, Aage, Niels, Beck, André Teófilo, and Sigmund, Ole, 'Local versus global stress constraint strategies in topology optimization: A comparative study', *International Journal for Numerical Methods in Engineering* 122.21 (2021), pp. 6003–6036.
 doi: [10.1002/nme.6781](https://doi.org/10.1002/nme.6781)

- [166] Kreisselmeier, G. and Steinhauser, R., 'Systematic Control Design by Optimizing a Vector Performance Index', *IFAC Proceedings Volumes*, IFAC Symposium on computer Aided Design of Control Systems, Zurich, Switzerland, 29-31 August 12.7 (Sept. 1979), pp. 113–117.
DOI: [10.1016/S1474-6670\(17\)65584-8](https://doi.org/10.1016/S1474-6670(17)65584-8)
- [167] Watts, Seth, Arrighi, William, Kudo, Jun, Tortorelli, Daniel A., and White, Daniel A., 'Simple, accurate surrogate models of the elastic response of three-dimensional open truss micro-architectures with applications to multiscale topology design', *Structural and Multidisciplinary Optimization* 60.5 (Nov. 2019), pp. 1887–1920.
DOI: [10.1007/s00158-019-02297-5](https://doi.org/10.1007/s00158-019-02297-5)
- [168] Johnson, Steven G., 'The NLOpt nonlinear-optimization package', <https://github.com/stevengj/nlopt>, 2007.
- [169] Diamond, Steven and Boyd, Stephen, 'CVXPY: A Python-Embedded Modeling Language for Convex Optimization', 2016.
- [170] Domahidi, Alexander, Chu, Eric, and Boyd, Stephen, 'ECOS: An SOCP solver for embedded systems', 2013 *European Control Conference (ECC)*, Zurich: IEEE, July 2013, pp. 3071–3076, ISBN: 978-3-033-03962-9.
DOI: [10.23919/ECC.2013.6669541](https://doi.org/10.23919/ECC.2013.6669541)
- [171] Lewiński, T., Zhou, M., and Rozvany, G. I. N., 'Extended exact solutions for least-weight truss layouts—Part I: Cantilever with a horizontal axis of symmetry', *International Journal of Mechanical Sciences* 36.5 (1994), pp. 375–398.
DOI: [10.1016/0020-7403\(94\)90043-4](https://doi.org/10.1016/0020-7403(94)90043-4)
- [172] Munro, Dirk and Groenwold, Albert, 'Local stress-constrained and slope-constrained SAND topology optimisation', *International Journal for Numerical Methods in Engineering* 110.5 (May 2017), pp. 420–439.
DOI: [10.1002/nme.5360](https://doi.org/10.1002/nme.5360)
- [173] Bruggi, Matteo and Duysinx, Pierre, 'Topology optimization for minimum weight with compliance and stress constraints', *Structural and Multidisciplinary Optimization* 46.3 (Sept. 2012), pp. 369–384.
DOI: [10.1007/s00158-012-0759-7](https://doi.org/10.1007/s00158-012-0759-7)
- [174] París, J., Navarrina, F., Colominas, I., and Casteleiro, M., 'Block aggregation of stress constraints in topology optimization of structures', *Advances in Engineering Software*, Advances in optimum engineering design 41.3 (Mar. 2010), pp. 433–441.
DOI: [10.1016/j.advengsoft.2009.03.006](https://doi.org/10.1016/j.advengsoft.2009.03.006)

cited on page 42

- [175] Norato, Julián A., Smith, Hollis A., Deaton, Joshua D., and Kolonay, Raymond M., 'A maximum-rectifier-function approach to stress-constrained topology optimization', *Structural and Multidisciplinary Optimization* 65.10 (Sept. 2022), p. 286.
DOI: [10.1007/s00158-022-03357-z](https://doi.org/10.1007/s00158-022-03357-z)